Available online at www.sciencedirect.com
ScienceDirect
Coordination Chemistry Reviews 253 (2009) 291–324
COORDINATION CHEMISTRY REVIEWS
www.elsevier.com/locate/ccr

Review

Transition metal complexes with bulky 4,6-di-*tert*-butyl-*N*-aryl(alkyl)-*o*-iminobenzoquinonato ligands: Structure, EPR and magnetism

Andrey I. Poddel'sky *, Vladimir K. Cherkasov, Gleb A. Abakumov

G.A. Razuvaev Institute of Organometallic Chemistry, Russian Academy of Sciences, 49 Tropinina Street, 603950 Nizhny Novgorod, Russia

Received 17 October 2006; accepted 11 February 2008
Available online 16 February 2008

Contents

Abstract

Coordination compounds based on the substituted *o*-iminoquinonato, *o*-iminosemiquinonato and *o*-amidophenolato ligands with transition metal ions are described from the viewpoint of their structural and magnetic properties. The present review summarizes data on homoleptic transition metal

Abbreviations[1]*:* Q, quinone; SQ, semiquinone; Cat, catecholate; 3,5-DBBQ, 3,5-di-*tert*-butyl-*o*-benzoquinone; 3,5-DBSQ and 3,5-DBCat, its semiquinone and catecholate forms respectively; 3,6-DBBQ, 3,6-di-*tert*-butyl-*o*-benzoquinone; 3,6-DBSQ and 3,6-DBCat, its semiquinone and catecholate forms respectively; 9,10-PhenQ, 9,10-phenanthrenequinone; 9,10-PhenSQ and 9,10-PhenCat, its semiquinone and catecholate forms respectively; *o*-Cl_4BQ, tetrachloro-*o*-benzoquinone; *o*-Cl_4SQ and *o*-Cl_4Cat, its semiquinone and catecholate forms respectively; IBQ, *o*-iminobenzoquinone; ISQ, *o*-iminobenzosemiquinonato radical–anion; AP, *o*-amidophenolato dianion; APH, *o*-aminophenolato anion; APH_2, *o*-aminophenol.

* Corresponding author.
E-mail address: aip@iomc.ras.ru (A.I. Poddel'sky).

0010-8545/$ – see front matter
doi:10.1016/j.ccr.2008.02.004

complexes of bulky bidentate *N*-aryl-*o*-iminoquinonato type ligands involving comparison with *o*-quinonato analogues; penta- and hexacoordinate bis-*o*-iminobenzoquinonato complexes of ML_2X, ML_2X_2 and ML_2L' types; mono-*o*-iminobenzoquinonato complexes and complexes based on three-, tetra- and pentadentate bis-*o*-iminobenzoquinones. Synthetic aspects are also included.

Keywords: *o*-Iminobenzoquinone; *o*-Iminobenzosemiquinone; *o*-Amidophenolate; Transition metal; Complexes; O,N-ligands; X-ray structure; EPR; Magnetochemistry

1. Introduction

Significant progress has been made in recent years in the field of complexes with redox-active *o*-quinonato, *o*-iminoquinonato and related ligands. The extensive data on complexes of these ligands types have been collected [1–25]. The investigation of metal complexes with *o*-iminobenzoquinonato ligands has attracted attention in view of their distinctive features. The presence of nitrogen (its main isotope ^{14}N is magnetic) in *o*-iminoquinones reveals additional information on the spin density distribution in chelate ring. The application of *o*-iminosemiquinone (as well as *o*-semiquinone) as a spin label in metal complexes allows one to monitor complex composition, structure and dynamic processes simply by means of EPR spectroscopy [8,26–31].

On the other hand, *o*-iminosemiquinones contain an unpaired electron similar to the *o*-semiquinones. Hence these ligands in complexes can be considered as magnetic centers. From this point of view the investigation of magnetic exchange interactions between ligands and/or between ligand and metal is important. The redox-potentials of *o*-iminoquinones are shifted to more negative range compared to the redox-potentials of *o*-quinones. This also allows the synthesis of transition metal complexes containing the *o*-iminobenzosemiquinone – radical–anion form of *o*-iminoquinone. The variation of substituents at the nitrogen atom of *o*-iminobenzoquinone leads to a widening of the range of steric hindrance near the metallic center.

This review highlights the versatility of *o*-iminobenzoquinone ligands in structural and magnetic engineering aspects. We will begin with a review of mono-*o*-iminobenzoquinonato systems, followed by the description of bis-ligand systems of $M(ISQ)_2X$/$M(ISQ)_2L$ and $M(ISQ)_2X_2$/$M(ISQ)_2L_2$ types, and then homoleptic multiligand systems will be discussed. Other *o*-iminobenzoquinonato species will be described in the final section of the review.

The complexes can be synthesized by several approaches using different forms of ligands as starting reagents: corresponding *o*-iminobenzoquinones (IBQ), *o*-iminobenzosemiquinones (ISQ) or *o*-aminophenols (APH_2). Scheme 1 displays *o*-aminophenols which are the most used as ligands in *o*-iminobenzoquinonato type complexes reported in literature.

2. General remarks

The detailed analysis of X-ray data on transition metals *o*-quinono (Q), *o*-semiquinonato (SQ) and catecholate (Cat) complexes has shown that lengths of C–O and C–C bonds of the chelate ring are sensitive to the oxidation level of ligand [1,2,4,5,13,15,19,32,33]. The C–O distance in catecholate complexes varies in the range of 1.32–1.39 Å, while the C–C bond of the hexatomic carbon ring is close to aromatic one and has an average value of 1.39–1.41 Å; for semiquinonato complexes these values are: C–O 1.28–1.31 Å, C–C 1.42–1.45 Å; for complexes with neutral quinones [33] the C–O bond lengths is ∼1.23 Å, and C–C is ∼1.53 Å. These parameters are helpful in the determination of electronic configuration of high-spin complexes containing one or more *o*-quinone ligands.

In the case of low-spin systems, EPR spectroscopy is also a useful tool to obtain additional information on the unpaired electron localization. Variable-temperature magnetic susceptibility measurements are applied to determine a number of unpaired electrons, the character and the exchange interaction energy of the unpaired electrons on π^*_{SQ}-MO and non-bonding AO of metal center.

o-Iminobenzoquinone (like *o*-quinone) undergoes a series of redox transitions. Scheme 2 shows neutral *o*-iminobenzoquinone and its mono- and doubly reduced forms (*o*-iminobenzosemiquinone ISQ^- and *o*-amidophenolate AP^{2-}, respectively) connected by one-electron redox-steps and the further protonation of dianion AP^{2-} with the formation of *o*-aminophenolate anion APH^- and *o*-aminophenol APH_2.

Redox processes in complexes with these ligands are accompanied by changes in the geometrical parameters of the *o*-iminoquinonato groups. X-ray data on *o*-iminoquinone complexes provide important information on the compounds' composition and structure, and oxidation level. However, in some cases when strong antiferromagnetic coupling is present in the complex, the iminobenzosemiquinone bond lengths (as well as *o*-semiquinone) can provide misleading information about the oxidation level of ligands and, consequently, central metal.

The investigation of magnetic properties coupled with spectroscopic and X-ray data allows one to make some important conclusions about the electronic structure of complexes and the character of the electronic interactions.

3. Mono-*o*-iminobenzoquinonato complexes

Among transition metal complexes containing one 4,6-di-*tert*-butyl-*N*-aryl-*o*-iminobenzoquinonato ligand and another neutral donor and/or valence-bound ligand are complexes of copper, nickel, palladium, platinum, cobalt, iron, ruthenium and osmium with $ISQ^{L1\text{-}L4,L7}$ type ligands.

3.1. Synthesis

(i) A common way to prepare mono-*o*-iminobenzoquinonato complex is the exchange reaction between the equivalent

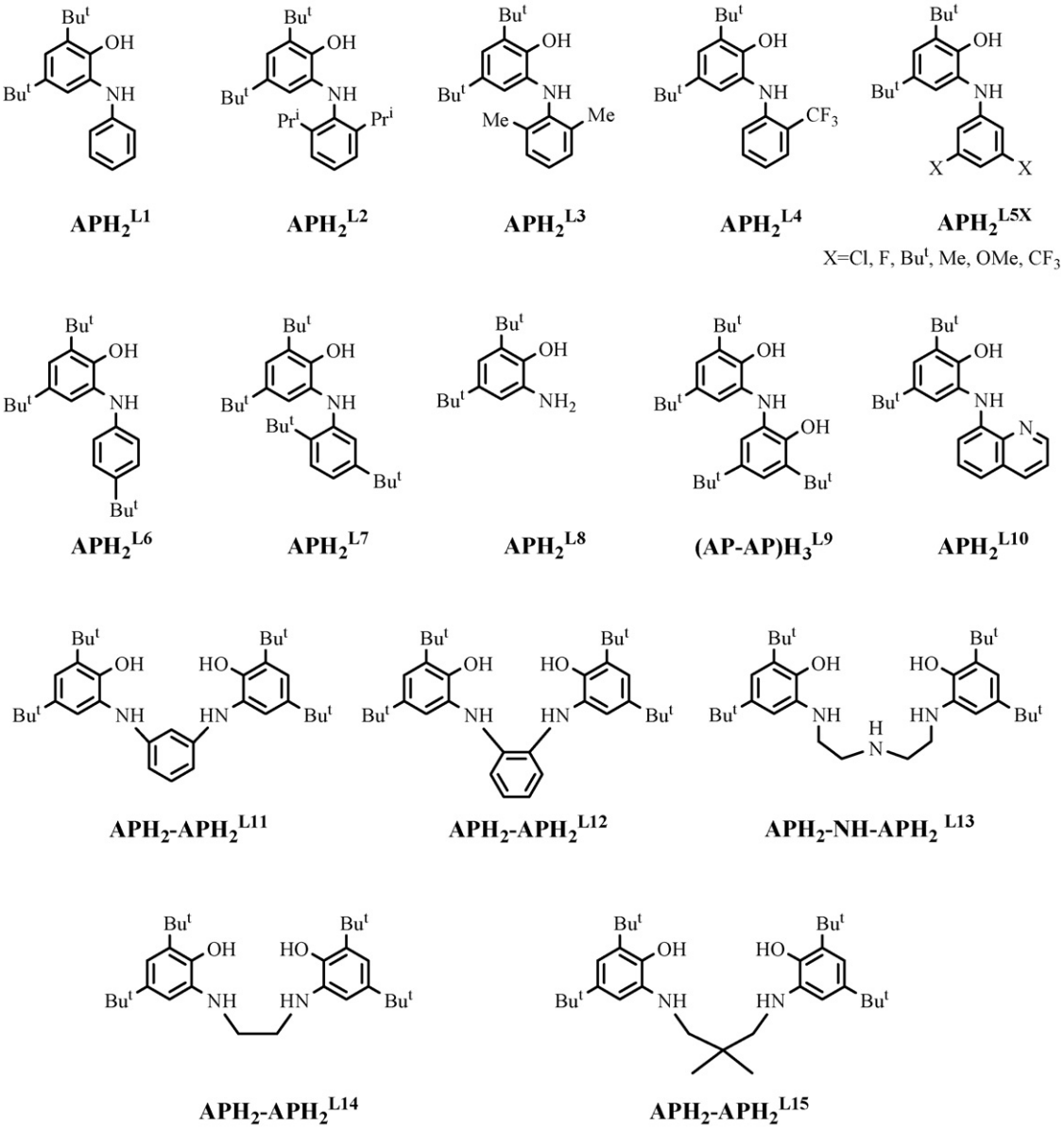

Scheme 1. Types of *o*-aminophenols used as ligands for *o*-iminobenzoquinonato complexes. Superscript L numbers identify species cited in the text.

amounts of *o*-aminophenol APH_2 and a corresponding metal salt (Eqs. (1) and (2) in Scheme 3). The insertion of neutral donor ligands allows one to complete the coordination sphere of a central metal. An acid residue (for example, HCl, HBr, CH_3COOH etc.) is usually neutralized by some base (Et_3N, NaOEt, etc.). Subsequent oxidation of the *o*-amidophenolato product leads to *o*-iminobenzosemiquinonato or *o*-iminobenzoquinonato complexes.

For instance, complex $[Cu(dmtacn)ISQ^{L1}]PF_6$ (**1**), shown in Scheme 4, was synthesized by the reaction of $CuCl_2{\cdot}6H_2O$ with 4,6-di-*tert*-butyl-*N*-phenyl-

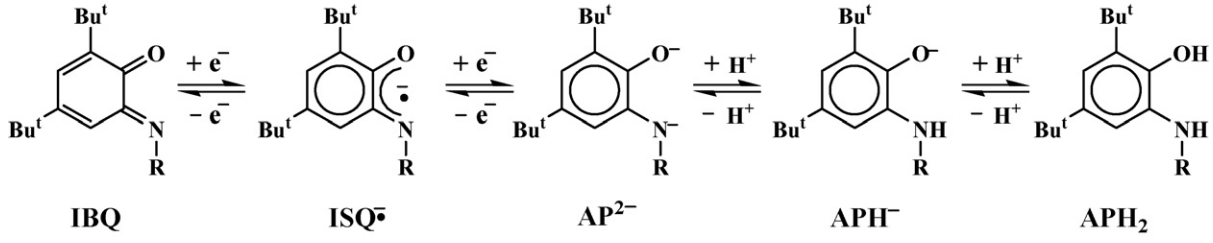

Scheme 2. Forms of the *o*-iminobenzoquinonato type ligand connected by one-electron redox and protonation steps.

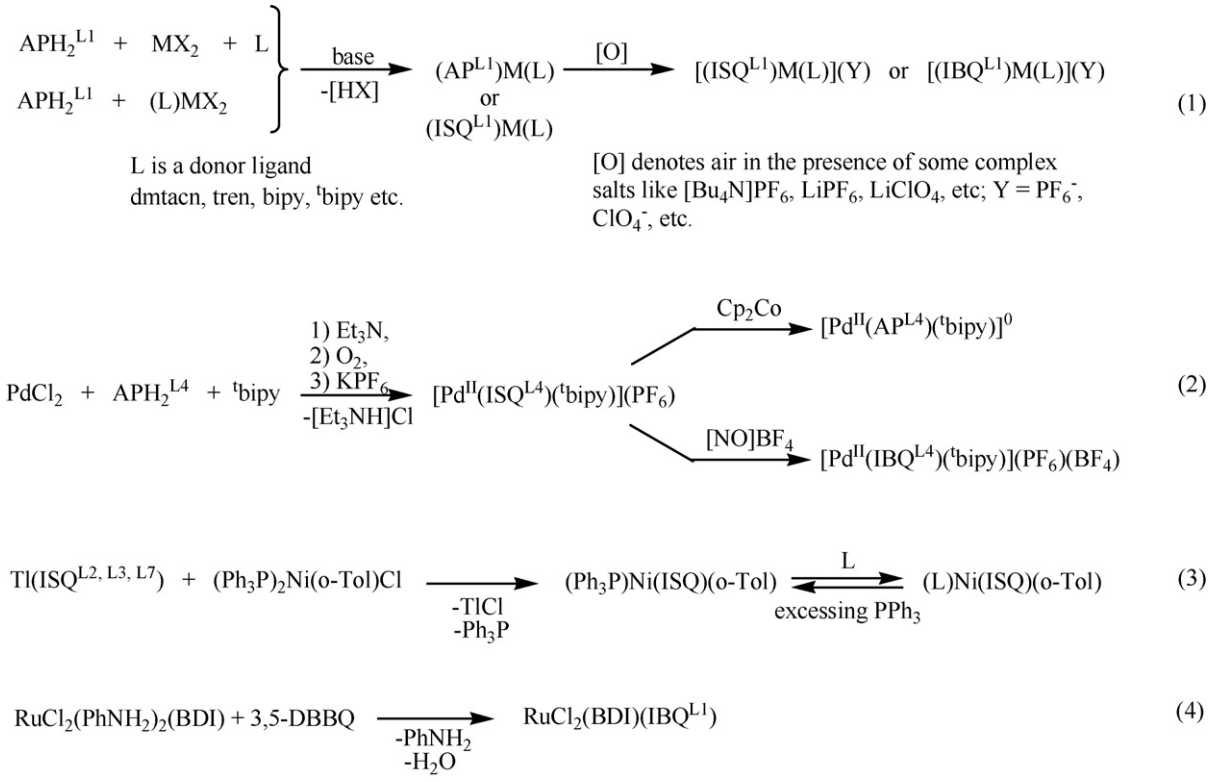

Scheme 3. Synthetic ways to mono-*o*-iminobenzoquinonato type complexes.

o-aminophenol and 1,4-dimethyl-1,4,7-triazacyclononane (dmtacn) in the presence of air and Et_3N with subsequent addition of $[n\text{-}Bu_4N]PF_6$ [6].

A common synthetic route to hexacoordinate mono-*o*-iminobenzoquinonato nickel(II), cobalt(III) and iron(III) complexes (Scheme 4) with tetradentate tris-(2-aminoethyl)amine (tren) $[Ni^{II}(tren)(IBQ^{L1})](PF_6)_2$ (**2**), $[Ni^{II}(tren)(ISQ^{L1})](ClO_4)$ (**3**), $[Co^{III}(tren)(ISQ^{L1})](ClO_4)_2{\cdot}0.5CH_3OH{\cdot}0.5H_2O$ (**4**) and $[Fe^{III}(tren)(ISQ^{L1})](ClO_4)_2{\cdot}0.5CH_3OH{\cdot}0.5H_2O$ (**5**) is the interaction of equivalent amounts of a neutral tetradentate ligand tren, 4,6-di-*tert*-butyl-*N*-phenyl-*o*-aminophenol $APH_2{}^{L1}$ with nickel or cobalt acetates $M(CH_3COO)_2{\cdot}4H_2O$ (M = Ni, Co), or iron(II) chloride $FeCl_2{\cdot}4H_2O$ in methanol solution in the presence of air, two molar equivalent of Et_3N, and $LiPF_6$ or $LiClO_4$ salts [34]. To prepare complex with neutral *o*-iminobenzoquinone $[Ni^{II}(tren)(IBQ^{L1})](PF_6)_2$ (**2**), a strong current of air was passed through the reaction mixture at room temperature. On the other hand, the *o*-iminobenzosemiquinonato complex $[Ni^{II}(tren)(ISQ^{L1})](ClO_4)$ (**3**) was prepared by heating the reaction mixture for 30 min in the presence of air but without specifically passing air through the solution.

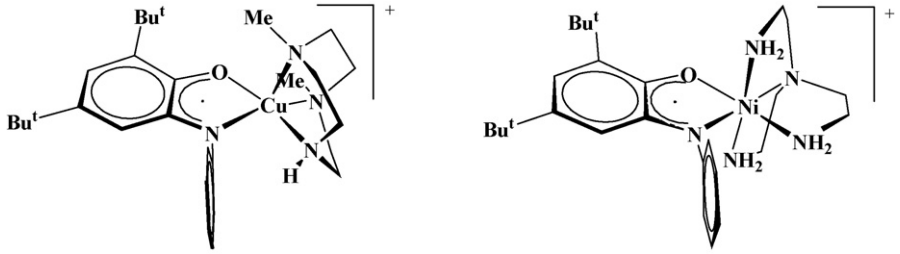

$[Cu(dmtacn)ISQ^{L1}]^+$ cation in $[Cu(dmtacn)ISQ^{L1}]PF_6$ (**1**)

$[Ni^{II}(tren)(ISQ^{L1})]^+$ cation in **3**

analogues:

$[Ni^{II}(tren)(IBQ^{L1})](PF_6)_2$	**2**
$[Ni^{II}(tren)(ISQ^{L1})](ClO_4)$	**3**
$[Co^{III}(tren)(ISQ^{L1})](ClO_4)_2{\cdot}0.5CH_3OH{\cdot}0.5H_2O$	**4**
$[Fe^{III}(tren)(ISQ)^{L1}](ClO_4)_2{\cdot}0.5CH_3OH{\cdot}0.5H_2O$	**5**

Scheme 4. The structure of complex cations $[Cu(dmtacn)ISQ^{L1}]^+$ and $[Ni^{II}(tren)(ISQ^{L1})]^+$ in crystals of **1** [6] and **3** [34] respectively.

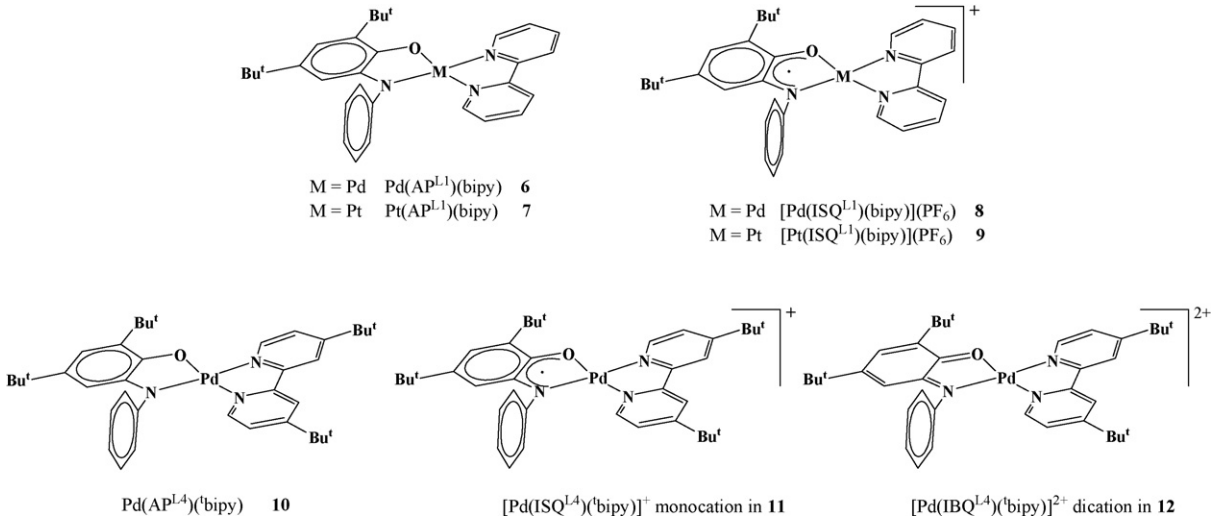

Scheme 5. Structures of palladium and platinum complexes **6–12** [35,36].

The mono-*o*-amidophenolato complexes of $[M^{II}(AP^{L1})(bipy)]$ type (Scheme 5), where M = Pd (**6**), Pt (**7**), (formed from APH_2^{L1} and $M(bipy)Cl_2$ in the presence of NaOMe and the absence of air) give complex cations $[M^{II}(ISQ^{L1})(bipy)](PF_6)$, where M = Pd (**8**), Pt (**9**), after oxidation by ferrocenium hexafluorophosphate [35].

A palladium complex, similar to **6**, is $[Pd^{II}(AP^{L4})(^tbipy)]^0$ (**10**), where ^{t}bipy is 4,4′-di-*tert*-butyl-2,2′-dipyridyl [36] is a product of the one-electron reduction of *o*-iminobenzosemiquinonato palladium(II) complex $[Pd^{II}(ISQ^{L4})(^tbipy)](PF_6)$ (**11**) (prepared according to Eq. (2) shown in Scheme 3) by a cobaltocene. On the other hand, $[Pd^{II}(IBQ^{L4})(^tbipy)](PF_6)(BF_4)\cdot 2CH_2Cl_2$ (**12**), a complex with O,N-coordinated neutral *o*-iminobenzoquinone IBQ^{L4}, is an one-electron oxidized derivative of the *o*-iminobenzosemiquinonato complex **11** [36].

Mono-(*N*-phenyl-*o*-iminobenzosemiquinonato) ruthenium and osmium complexes of $[M(ISQ^{L1})(bipy)_2](PF_6)$ type (M = Ru, **13**; Os, **14**), Scheme 6, are also products of exchange reaction of *o*-aminophenols with appropriate metal salt in the presence of base and air [11,37].

(ii) In some cases, when the *o*-iminobenzoquinone form of the ligand is stable, it is possible to perform the exchange reaction between metal salt and *o*-iminobenzosemiquinone thallium derivative which can easily be synthesized from thallium amalgam and the corresponding *o*-iminobenzoquinone [38]. This method allows one to avoid the presence of any base and air in the reaction mixture. Eq. (3) in Scheme 3 exhibits the synthesis of mono-*o*-iminobenzosemiquinonato nickel complexes of $(Ph_3P)Ni(ISQ)(o\text{-Tol})$ type (ISQ is ISQ^{L2}, **15**; ISQ^{L3}, **16**; ISQ^{L7}, **17**) with Ni–C σ-bond [39].

(iii) One can use exchange reactions of the neutral ligand (e.g. exchange of PPh_3 with $AsEt_3$, Py, Pyz, Et_3N, isonitriles RNC, Me_3P etc.). They do not affect the *o*-iminobenzosemiquinonato ligand in coordination sphere [39] (Eq. (3) in Scheme 3).

(iv) Template synthesis. There is only one example of *o*-iminobenzoquinone synthesis within the coordination

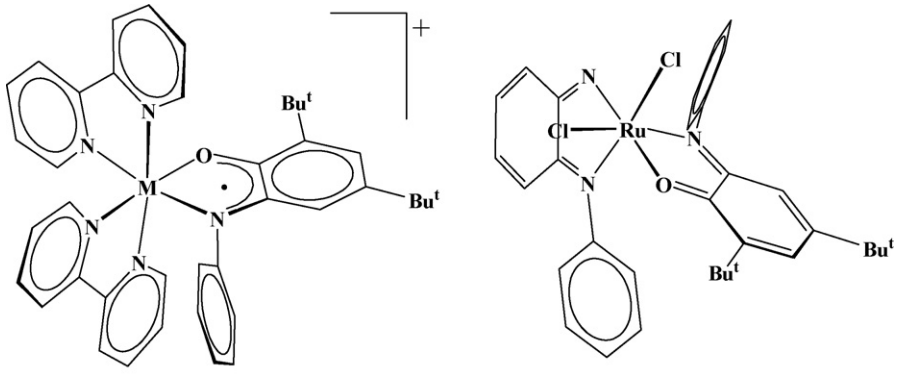

Scheme 6. Ruthenium and osmium mono-*o*-iminobenzosemiquinonato complexes **13, 14** and **18** [11,40].

sphere of the central metal. The ruthenium complex $RuCl_2(BDI)(IBQ^{L1})$ (**18**) is a product of the reaction of $RuCl_2(PhNH_2)_2(BDI)$ and 3,5-di-*tert*-butylcatechol in methanol at room temperature (Eq. (4) in Scheme 3) [40].

3.2. Structure and magnetism

The bulky *N*-aryl-substituted 4,6-di-*tert*-butyl-*o*-iminobenzoquinone forms a copper complex $[Cu(dmtacn)ISQ^{L1}]PF_6$ (**1**) [6] whose crystals consist of $[Cu(dmtacn)ISQ^{L1}]^+$ cations and PF_6^- anions (Scheme 4). The C–N, C–O, C–C distances (X-ray) (see Table 1) suggest the radical–anion form ISQ of O,N-coordinated ligand to be present. Copper(II) ion lies in pentacoordinate square–pyramidal environment where the ISQ^{L1} ligand occupies two places in pyramid base and one of nitrogen atoms of dmtacn is in the apical site.

The low-temperature value of μ_{eff} (see Table S1 of Supplementary information) is close to the spin-only value for systems with $S = 1$. Therefore the authors conclude this complex **1** consists of intramolecularly ferromagnetically coupled Cu(II) ion ($S_{Cu} = 1/2$) and radical–anion ISQ^{L1} ($S_{rad} = 1/2$). Ferromagnetic coupling arises between the half-occupied d_{x2-y2} copper AO and π*-MO of ISQ radical ligand; the symmetry of the interacting orbitals requires ferromagnetic exchange only. The behavior of μ_{eff} at different temperatures is typical for multispin systems with triplet ground state and thermal population of an excited state with lower spin multiplicity.

Hexacoordinate mono-*o*-iminobenzoquinonato nickel(II), cobalt(III) and iron(III) complexes with the tetradentate ligand tris-(2-aminoethyl)amine (tren) were reported in ref. [34]. All the compounds are salts containing complex cations: $[Ni^{II}(tren)(IBQ^{L1})](PF_6)_2$ (**2**), $[Ni^{II}(tren)(ISQ^{L1})](ClO_4)$ (**3**), $[Co^{III}(tren)(ISQ^{L1})](ClO_4)_2{\cdot}0.5CH_3OH{\cdot}0.5H_2O$ (**4**) and $[Fe^{III}(tren)(ISQ^{L1})](ClO_4)_2{\cdot}0.5CH_3OH{\cdot}0.5H_2O$ (**5**).

The structurally characterized complexes of the neutral O,N-coordinated *o*-iminobenzoquinone were not reported in the literature prior to the publication [34]. Only data on O,N-coordinated *o*-iminodenzoquinonato complexes generated electrochemically in solution have been presented [6,7].

All compounds contain the octahedral cation $[M(tren)(IBQ^{L1}$ or $ISQ^{L1})]^{n+}$. Geometrical characteristics of O,N-coordinated ligands in **2–5** confirm the oxidation level of ligand: for IBQ^{L1} ligand in $[Ni^{II}(tren)(IBQ^{L1})]^{2+}$ distances C–O and C–N are shorter (up to 0.08 and 0.05 Å respectively) than those in ISQ^{L1} ligands of the other three complex cations (namely, $[Ni^{II}(tren)(ISQ^{L1})]^+$ (Scheme 4), $[Co^{III}(tren)(ISQ^{L1})]^{2+}$ and $[Fe^{III}(tren)(ISQ^{L1})]^{2+}$).

The UV–visible spectra of the compounds described are also helpful for determining the oxidation level of the O,N-coordinated ligands. Radical–anionic *o*-iminobenzosemiquinonato complexes (**3–5** as well as **1**) display a number of intense intraligand charge transfer absorptions with maxima in the range 450–950 nm and extinction coefficients of $\sim 10^3\ M^{-1}\ cm^{-1}$. These absorptions, which are connected with transitions in the ISQ ligand(s), are absent in complexes of neutral *o*-iminobenzoquinone or dianionic *o*-amidophenolato species [34]. For IBQ-complexes maxima at 400–500 nm are

Table 1
Selected bond lengths (Å) of mono-*o*-iminobenzoquinonato type transition metal complexes

N	Complex	C_1–O	C_2–N	C_1–C_2	C_2–C_3	C_3–C_4	C_4–C_5	C_5–C_6	C_1–C_6	M–O	M–N	Reference
1	$[Cu(dmtacn)ISQ^{L1}]PF_6$	1.301	1.343	1.442	1.428	1.357	1.428	1.376	1.434	1.935	1.973	[6]
2	$[Ni^{II}(tren)(IBQ^{L1})](PF_6)_2$	1.234	1.301	1.519	1.432	1.352	1.467	1.349	1.463	2.119	2.054	[34]
3	$[Ni^{II}(tren)(ISQ^{L1})](ClO_4)$	1.294	1.348	1.465	1.430	1.370	1.427	1.374	1.435	2.053	2.033	[34]
4	$[Co^{III}(tren)(ISQ^{L1})](ClO_4)_2{\cdot}0.5CH_3OH{\cdot}0.5H_2O$	1.323	1.349	1.436	1.421	1.367	1.430	1.376	1.418	1.885	1.921	[34]
5	$[Fe^{III}(tren)(ISQ^{L1})](ClO_4)_2{\cdot}0.5CH_3OH{\cdot}0.5H_2O$	1.296	1.345	1.442	1.425	1.371	1.443	1.373	1.431	1.910	1.859	[34]
6	$[Pd^{II}(AP^{L1})bipy]$	1.348	1.387	1.421	1.395	1.402	1.398	1.405	1.406	1.968	1.974	[35]
7	$[Pt^{II}(AP^{L1})bipy]$	1.357	1.390	1.417	1.401	1.405	1.394	1.404	1.397	1.980	1.985	[35]
8	$[Pd^{II}(ISQ^{L1})bipy]PF_6$	1.309	1.346	1.450	1.420	1.366	1.437	1.382	1.428	1.989	2.014	[35]
9	$[Pt^{II}(ISQ^{L1})bipy]PF_6$	1.317	1.350	1.429	1.416	1.376	1.430	1.394	1.429	1.996	2.011	[35]
10	$[Pd^{II}(AP^{L4})(^tbpy)]$	1.353	1.387	1.415	1.396	1.399	1.395	1.413	1.404	1.969	1.981	[36]
11	$[Pd^{II}(ISQ^{L4})(^tbpy)](PF_6)$	1.307	1.360	1.439	1.422	1.355	1.439	1.381	1.422	1.983	2.021	[36]
12	$[Pd^{II}(IBQ^{L4})(^tbpy)](PF_6)(BF_4){\cdot}2CH_2Cl_2$	1.242	1.306	1.499	1.428	1.345	1.466	1.354	1.458	2.024	2.050	[36]
18	$RuCl_2(BDI)(IBQ^{L1})$	1.280	1.339	1.439	1.420	1.355	1.441	1.355	1.439	2.022	1.974	[40]

For **3–5** the data are given for the single independent cations only [34]. The experimental error was not greater than ± 0.005 Å.

typical. For example, $[Ni^{II}(tren)(IBQ^{L1})](PF_6)_2$, **2**, has bands at 411 and 488 nm with ε of ~3–4 × 10^3 M^{-1} cm^{-1} and has no absorption above 500 nm. The same spectroscopic features are shown by M(IBQ) species generated electrochemically from **1**, **3** and **4**. For AP-complexes, the most intense absorptions are usually observed below 400 nm.

The M–O and M–N bond lengths in **2**–**5** are typical for the corresponding metal: octahedral Ni(II) in **2** and **3** {Ni–O are 2.119 and 2.053 Å, Ni–N are 2.054 and 2.033 Å in complexes $[Ni^{II}(tren)(IBQ^{L1})](PF_6)_2$ (**2**) and $[Ni^{II}(tren)(ISQ^{L1})](ClO_4)$ (**3**), respectively}; low-spin Co(III) (d^6, $S_{Co} = 0$) in **4** {Co–O, 1.885 Å; Co–N, 1.921 Å in $[Co^{III}(tren)(ISQ^{L1})](ClO_4)_2$ (**4**)} and low-spin Fe(III) (d^5, $S_{Fe} = 1/2$) in **5** {Fe–O, 1.910 Å; Fe–N, 1.859 Å in $[Fe^{III}(tren)(ISQ^{L1})](ClO_4)_2$ (**5**)} also in an octahedral environment.

Magnetochemical data are in accordance with X-ray results. The ground state of *o*-iminobenzoquinone complex $[Ni^{II}(tren)(IBQ^{L1})](PF_6)_2$ (**2**) is $S = 1$, which is usual for hexacoordinate Ni(II) (d^8, $S_{Ni} = 1$) complexes. The ground state of the *o*-iminobenzosemiquinonato analogue $[Ni^{II}(tren)(ISQ^{L1})](ClO_4)$ (**3**) is $S = 3/2$ (Table S1) attained via strong, symmetry required, intramolecular ferromagnetic coupling between the e_g subshell of nickel(II) (d^8, $S_{Ni} = 1$) and π*-MO of ISQ ($S_{rad} = 1/2$) [34].

The complex $[Co^{III}(tren)(ISQ^{L1})](ClO_4)_2{\cdot}0.5CH_3OH{\cdot}0.5H_2O$ (**4**) possesses an $S = 1/2$ ground state. The EPR spectrum, in CH_2Cl_2 solution (g = 1.997) exhibits HFS on cobalt ^{59}Co and one nitrogen with HFS constants 14.0 G and 8.8 G respectively. The unpaired electron is localized on organic ligand MO with a weak contribution of metal orbitals. These data agree with the description of this complex **4** as diamagnetic low-spin cobalt(III) with the *o*-iminobenzosemiquinone radical–anion [34].

In the dication $[Fe^{III}(tren)(ISQ^{L1})]^{2+}$ **5**, strong metal – ligand antiferromagnetic exchange from the coupling of low-spin iron(III) (d^5, $S_{Fe} = 1/2$), connected with tetradentate ligand "tren", and radical–anion *o*-iminobenzosemiquinone causes diamagnetism [34].

Mono-*o*-amidophenolato complexes of $[M^{II}(AP^{L1})bipy]$ type (where M = Pd (**6**), Pt (**7**)) give complex cations $[M^{II}(ISQ^{L1})bipy](PF_6)$ (M = Pd (**8**), Pt (**9**)) under oxidation by ferrocenium hexafluorophosphate (Scheme 5) [35]. Table 1 presents selected bond distances in complexes **6**–**9**. C–O and C–N bonds of chelate ring in *o*-iminobenzosemiquinonato complexes **8** and **9** are 0.04–0.05 Å shorter than those bonds in *o*-amidophenolato complexes **6** and **7**. The oxidation of **6** and **7** results in the elongation of M–O and M–N bonds with O,N-chelated ligands of about 0.02 and 0.03–0.04 Å respectively. The C–C distances in the quinone part of the ISQ ligands, for **8** and **9**, display a quinonoid type pattern.

The UV–visible spectra of *o*-amidophenolato complexes **6** and **7**, display very intense broad absorption bands at 745 and 780 nm ($\varepsilon \sim 10^3$–10^4 M^{-1} cm^{-1}). These were assigned to a spin and dipole allowed LLCT (ligand-to-ligand charge transition) between AP and bipy ligands. As will be shown below, these LLCT bands are typical for square-planar complexes with *o*-iminosemiquinone and another bidentate ligand; they are only weakly dependent on the nature of the metal. The ISQ-complexes **8** and **9** have absorption bands of in the 600–1000 nm range with intensities ~10^3 M^{-1} cm^{-1} indicating a radical–anion O,N-coordinated ligand; there is no very intense LLCT band.

Complexes **8**, **9** possess an $S = 1/2$ ground state while **6** and **7** are, of course, diamagnetic. The EPR parameters of **8**, **9** (Table S2 of Supplementary information) show localization of the unpaired electron on the organic ligand: for $[Pd^{II}(ISQ^{L1})bipy](PF_6)$ (**8**) $g_{iso} = 2.002$, for $[Pt^{II}(ISQ^{L1})bipy](PF_6)$ (**9**) $g_{iso} = 2.00$; HFS constants $A(^{14}N) = 7.71$ and 7.1 G; A(H) = 4.6 and 4.67 G for Pd and Pt complexes respectively. These results are typical of square-planar complexes of diamagnetic metals with one organic radical ligand.

An interesting series of palladium complexes is described in ref. [36]. Complexes $[Pd^{II}(AP^{L4})(^tbipy)]^0$ (**10**), $[Pd^{II}(ISQ^{L4})(^tbipy)](PF_6)$ (**11**), and $[Pd^{II}(IBQ^{L4})(^tbipy)](PF_6)(BF_4){\cdot}2CH_2Cl_2$ (**12**) represent the redox-series of the O,N-chelating ligand (Scheme 5). Here ^{t}bipy is 4,4′-di-*tert*-butyl-2,2′-dipyridyl. The first compound, **10**, is a neutral diamagnetic palladium(II) complex with *o*-amidophenolato dianion. It is a product of one-electron reduction of **11** – a paramagnetic *o*-iminobenzosemiquinonato palladium(II) complex. On the other hand, **12**, a complex with O,N-coordinated neutral *o*-iminobenzoquinone IBQ^{L4}, is an one-electron oxidized derivative of *o*-iminobenzosemiquinonato complex **11**.

The AP-complex **10** shows a very intense broad LLCT absorption at 708 nm (~10^4 M^{-1} cm^{-1}), the ISQ-complex **11** has two intense bands at 436 and 460 nm with $\varepsilon \sim 5 \times 10^3$ M^{-1} cm^{-1} and a number of bands in the range 700–1000 nm with $\varepsilon \sim 0.5$–0.7×10^3 M^{-1} cm^{-1} while for IBQ-complex **12** absorption above 550 nm is not observed but there is an intense band at 385 nm ($\varepsilon \sim 7 \times 10^3$ M^{-1} cm^{-1}). All complexes were characterized by X-ray crystallography. Geometrical characteristics of O,N-chelated ligands are given in Table 1. They clearly show the differences in structures of neutral IBQ^0, radical–anion ISQ^- and dianion AP^{2-} forms of O,N-coordinated ligand.

Paramagnetic complex **11** has the expected $S = 1/2$ ground state with an X-band EPR spectrum, in CH_2Cl_2 solution at 298 K, (Table S2) typical for a ligand-centered radical in *o*-iminobenzosemiquinonato complexes.

Mono-(*N*-phenyl-*o*-iminobenzosemiquinonato) ruthenium and osmium complexes of $[M(ISQ^{L1})(bipy)_2](PF_6)$ type (M = Ru, **13**; Os, **14**), Scheme 6, have been investigated by spectroelectrochemistry and X- and W-band EPR [11] and also studied in ref. [37] with similar results. A large difference in *g*-anisotropy was observed. Ruthenium complex **13** has a value of $g = 2.0049$ at 298 K with hyperfine coupling of the unpaired electron with both the nitrogen atom of *o*-iminobenzosemiquinone ligand and the ruthenium (Table S2). The value $A(^{14}N) = 7.8$ G is typical for ISQ complexes [34,35,39] but $A(^{99}Ru) = 10.1$ G, $A(^{101}Ru) = 11.3$ G are greater than those observed for other Ru-complexes (4–8 G for $A(^{99}Ru)$ and 4.4–8.6 G for (^{101}Ru)). This was rationalized in

terms of a large ligand-to-metal spin transfer [11]. An isotropic g value indicates a ligand-centered (*o*-iminobenzosemiquinone) unpaired electron, but g-anisotropy (evaluated from W-band EPR at 5 K, $\Delta g = g_1 - g_3 = 0.0665$) reflects a remarkable contribution of the metal to SOMO in $[Ru^{II}(ISQ^{L1})(bipy)_2](PF_6)$ (**13**). The assignment of **13** as $[Ru^{II}(ISQ^{L1})(bipy)_2](PF_6)$ specie is preferable to $[Ru^{III}(AP^{L1})(bipy)_2](PF_6)$ based on the comparison of Δg in ruthenium(II) and ruthenium(III) complexes. The value of Δg for different ruthenium(III) dioxolene and related complexes varies in the range of 0.2–0.8 depending on the degree of metal/ligand orbital mixing (e.g., $\Delta g = 0.833$ for $[(4\text{-OOC-CH}_2\text{-Cat})Ru(NH_3)_4]$, 4-OOC-$CH_2$-Cat = 4-(carboxylatomethyl)catecholate trianion [41]; 0.54 for $[(acac)_2Ru^{III}(\mu\text{-}Q^2)Ru^{III}(acac)_2]$, Q^2 = dianion of 1,10-phenanthroline-5,6-diimine [10], 0.19–0.30 for a series of monocations/monoanions $[LRu(acac)_2]^{+/-}$ complexes, L is the derivative of *o*-aminophenol or *o*-aminothiophenol [42]). On the other hand, ruthenium(II) complexes reported in the literature reveal g-anisotropy values of $0.008 < \Delta g < 0.08$ (e.g. 0.082 for $[(3,5\text{-DBSQ})Ru(bipy)_2]^+$ [43], 0.0083 for [(4-oxo-5-methyl-SQ)Ru(bipy)$_2$] [44] 0.036 for $[(4,7\text{-NN-phenSQ})Ru(bipy)_2]^+$, 4,7-NN-phenSQ = 4,7-phenanthroline-5,6-semiquinolate [45]). The significant metal–ligand orbital mixing for ruthenium complexes with *o*-quinones, *o*-iminoquinones, *o*-diimines and its derivatives is quite common [15,17,45–50].

The UV–visible spectrum of **13** allows one to corroborate assignment of complex as an ISQ-specie due to a number of intense bands in the range 500–1000 nm with $\varepsilon \sim 10^3$–10^4 M^{-1} cm^{-1} where bands at ~500 and 690 nm were assigned to a MLCT (metal-to-ligand charge transfer) [11,16]. The osmium analogue **14** is characterized by absorption bands at about 530 and 690 nm with the same assignment.

With respect to the EPR spectrum of the osmium complex **14**, the HFC of ^{189}Os was not observed because of the large line width, the g-anisotropy ($\Delta g = 0.370$, Table S2) is much higher than in ruthenium analogue **13**. This illustrates a large contribution of a metal-centered state $[Os^{III}(AP^{L1})(bipy)](PF_6)$. The heavier osmium stabilizes the higher oxidation state relative to the ruthenium homologue [13,51]. For comparison, the *o*-iminobenzosemiquinonato osmium(III) complexes $Os^{III}(PPh_3)(ap\text{-}R)(ISQ^{Me})$, where ap-R is tridentate dianionic ligands derived from 2-arylazo-4-methylphenol (aryl is *p*-methoxyphenyl, *p*-tolyl, phenyl, *p*-chlorophenyl and *p*-nitrophenyl), ISQ^{Me} is radical–anion 4-methyl-*o*-iminobenzosemiquinone, were reported to be diamagnetic due to antiferromagnetic coupling of the low-spin osmium(III) (d^5, $S = 1/2$) with the *o*-iminobenzosemiquinonato unpaired electron [52].

Four-coordinate nickel complexes of $(Ph_3P)Ni(ISQ)(o\text{-Tol})$ type simultaneously containing a *o*-iminobenzosemiquinone radical–anion and *o*-tolyl σ-bound to nickel have been reported in ref. [39]. EPR spectroscopic data are given in Table S2. EPR investigations indicate a strongly distorted geometry divergent from square planar to tetrahedral. The geometry distortion is explained by the steric repulsion of ligands. In the series of complexes $(Ph_3P)Ni(ISQ^{L2})(o\text{-Tol})$ (**15**), $(Ph_3P)Ni(ISQ^{L3})(o\text{-Tol})$ (**16**), $(Ph_3P)Ni(ISQ^{L7})(o\text{-Tol})$ (**17**) (Scheme 7), the decrease

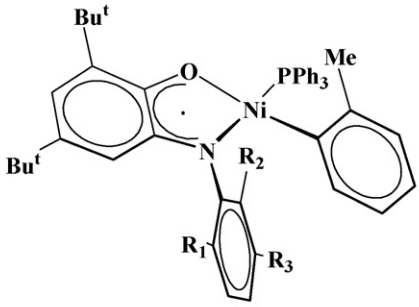

$R_1 = R_2 = Pr^i$, $R_3 = H$ $(Ph_3P)Ni(ISQ^{L2})(o\text{-Tol})$ **15**
$R_1 = R_2 = Me$, $R_3 = H$ $(Ph_3P)Ni(ISQ^{L3})(o\text{-Tol})$ **16**
$R_1 = R_3 = Bu^t$, $R_2 = H$ $(Ph_3P)Ni(ISQ^{L7})(o\text{-Tol})$ **17**

Scheme 7. *o*-Iminobenzosemiquinonato nickel complexes **15**–**17** [39].

of *N*-aryl hindrance leads to a decrease of steric repulsion. Consequently, the geometry of complex tends to be square planar. Complexes are able to ligand exchange: neutral Ph_3P ligand can be substituted with such ligands as Et_3As, Py, Pyz, Et_3N, RNC, Me_3P. At the same time, more bulky ligands (Ph_3As, Bu_3^tP, bidentate ligand bipy) fail to substitute the Ph_3P ligand in the coordination sphere.

The next remarkable ruthenium complex $RuCl_2(BDI)(IBQ^{L1})$ (**18**) is a product of oxidative coupling of ruthenated aniline with 3,5-di-*tert*-butyl-catechol [40]. According to X-ray, it is a ruthenium(II) complex of neutral *N*-phenyl-1,2-phenylenediimine (BDI) and *o*-iminobenzoquinone IBQ^{L1} (Scheme 6, Table 1).

4. Pentacoordinate bis-*o*-iminobenzoquinonato complexes of $M(ISQ)_2X$/$M(ISQ)_2L$ types

The bis-*o*-iminoquinonato complexes of ML_2X and ML_2L' species, where X is halogen or other anionic ligand, L′ is a neutral ligand, L the *o*-iminobenzosemiquinone radical–anion or *o*-amidophenolate dianion, are an interesting group (Scheme 8). Such complexes include the possibility to find: (i) heteroligand systems containing different types of radicals and (ii) linear molecular chains where X will be the connecting bridge between ML_2 fragments. Halogen-containing species ML_2Hal are represented in the literature by cobalt, iron and manganese complexes [53–56].

4.1. Synthesis

Synthetic methods to $M(ISQ)_2X$ type compounds (Scheme 9) depend on the nature of the metal and possible steric hindrance of the *o*-iminobenzoquinonato ligand. Cobalt complexes $Co(ISQ^{L1})_2Cl$ (**19**) and $Co(ISQ^{L1})_2I$ (**20**) were prepared by the treatment of 2-anilino-4,6-di-*tert*-butylphenol APH_2^{L1} with inorganic cobalt(II) salt ($[Co(H_2O)_6](BF_4)_2$ for **19** and CoI_2 for **20**) in CH_3CN solutions in the presence of air and Et_3N [54]. A 1:1 molar ratio of cobalt salt to ligand was employed for **19** and 1:1.56 for **20** (but not as 1:2) to avoid the formation of tris-ligand specie $Co(ISQ^{L1})_3$ (**54**, see Section 6.5). Notewor-

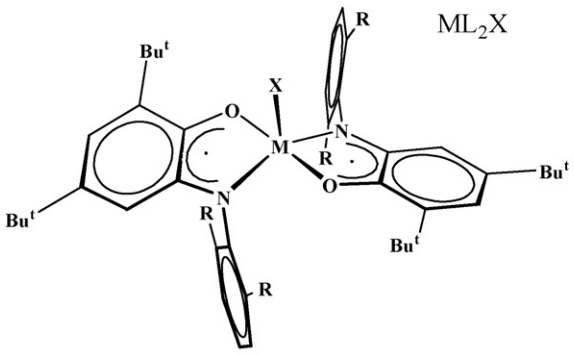

M = Co
X = Cl, R = H **19**
X = I, R = H **20**
X = Cl, R = Me **21**
X = Cl, R = Pr^i **22**
X = I, R = Me **23**

M = Fe
X = Cl, R = H **24**
X = Br, R = H **25**
X = I, R = H **26**
X = Br, R = Me **27**

M = Mn, X = Cl, R = Pr^i **28**
M = Fe, X = N_3, R = H **29**
M = Fe, X = SCN, R = H **30**
M = Co, X = SCN, R = Me **31**

M = Co, X = CH_2CN,
$R_{(under\ ligand\ plane)}$ = CF_3, $R_{(above\ ligand\ plane)}$ = H **32**

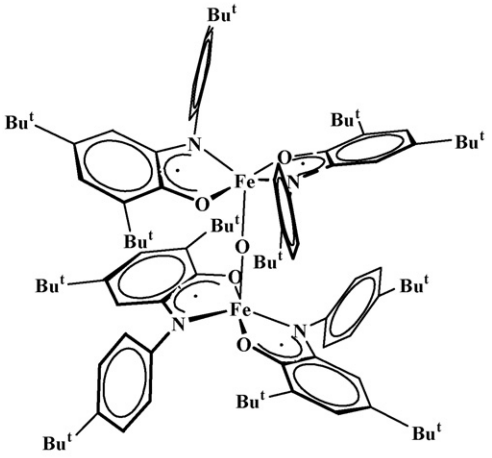

$(ISQ^{L6})_2$Fe-O-Fe$(ISQ^{L6})_2$ **33**

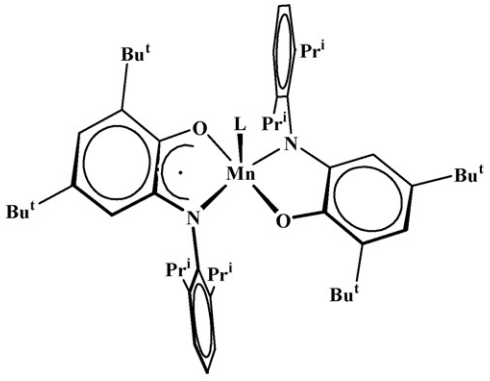

$Mn(ISQ^{L2})(AP^{L2})L$
L = THF **34**
L = CH_3OH **35**

Scheme 8. Complexes of ML_2X and ML_2L' types [53–61].

thy, the chlorine atom for **19** was taken away from $CHCl_3$ used as component of solvent mixture ($CH_3CN/CHCl_3$) to isolate **19**. Yields were ~10% for **19** and 43% for **20** (calculated per initial *o*-aminophenol). Pentacoordinate species $Co(ISQ^{L3})_2Cl$ (**21**) and $Co(ISQ^{L2})_2Cl$ (**22**) were synthesized by different methods. $Co(ISQ^{L3})_2Cl$ (**21**) was formed as a product of reaction between bis-ligand specie $Co(ISQ^{L3})_2$ (**56**, Section 6.5) and CH_2Cl_2 [53]. Note, chlorine atom in **21** was also abstracted from the chlorine-containing solvent. However $Co(ISQ^{L2})_2$ (**55**, Section 6.5) does not react with CH_2Cl_2 [53].

$MX_2 + APH_2 \xrightarrow[-[HX]]{base,\ O_2} M(ISQ)_2X$ (1)
molar ratio M/L ~ 1 : 1-1.5

$MX_2 + IBQ + Tl(ISQ) \xrightarrow[-TlX]{} M(ISQ)_2X$ (2)
molar ratio 1 : 1 : 1

$Co(ISQ^{L3})_2 + CH_2Cl_2 \xrightarrow[(solvent)]{} Co(ISQ^{L3})_2Cl$ (3)

$CoCl_2 + IBQ^{L2} \longrightarrow Co(ISQ^{L2})_2Cl$ (4)
molar ratio 1 : 2

$Co(ISQ^{L3})_2 + I_2 \longrightarrow Co(ISQ^{L2})_2I$ (5)
molar ratio 2 : 1

Scheme 9. Preparation of ML_2X type complexes.

Another way to prepare **21** is the interaction of anhydrous $CoCl_2$ with thallium *o*-iminobenzosemiquinone and neutral *o*-iminobenzoquinone in a 1:1:1 molar ratio. This synthetic method applied to prepare **22** gives the hard to separate mixture of desired product **22** and four-coordinate complex **55**. Therefore a pure sample of $Co(ISQ^{L2})_2Cl$ (**22**) was prepared using the reaction of dry $CoCl_2$ with neutral *o*-iminobenzoquinone IBQ^{L2} (molar ratio 1:2) with yield ~60% [55]. The iodide complex $Co(ISQ^{L3})_2I$ (**23**) – analogue of **20** – was easily prepared by the oxidation of $Co(ISQ^{L3})_2$ (**56**, Section 6.5) by iodine I_2 in toluene solution with yield 42% [55].

The iron species $Fe(ISQ^{L1})_2Hal$ [56], Hal = Cl (**24**), Br (**25**), I (**26**), were synthesized using a method similar to that for preparation of cobalt complexes **29** and **20**: from iron(II) salts and 2-anilino-4,6-di-*tert*-butylphenol in presence of Et_3N (molar ratio was 1:1.5:3) and air.

$$[Fe^{III}(dmfa)_6](ClO_4)_3 + NaN_3 + APH_2{}^{L1} \xrightarrow[\text{methanol}]{O_2} Fe(ISQ^{L1})_2(N_3) \quad (1)$$

$$[Fe^{III}(dmfa)_6](ClO_4)_3 + KSCN + APH_2{}^{L1} \xrightarrow[\text{methanol}]{O_2} Fe(ISQ^{L1})_2(NCS) \quad (2)$$

$$Co(ISQ^{L3})_2Cl + KSCN \xrightarrow{\text{THF-methanol}} Co(ISQ^{L3})_2(SCN) \quad (3)$$

Scheme 10. Preparation of ML_2X type complexes **29–31**.

More bulky iron and manganese complexes $Fe(ISQ^{L3})_2Br$ (**27**) and $Mn(ISQ^{L2})_2Cl$ (**28**) were prepared from the corresponding metal halides ($FeBr_2$, $MnCl_2$), corresponding thallium *o*-iminobenzosemiquinones and *o*-iminobenzoquinone in molar ratio 1:1:1 [55].

Besides halogen-containing complexes, other ML_2X complexes were reported in literature: $Fe^{III}(ISQ^{L1})_2(N_3)$ (**29**) and $Fe^{III}(ISQ^{L1})_2(NCS)$ (**30**) [57], $Co(ISQ^{L3})_2(SCN)$ (**31**) [55] and $Co(ISQ^{L4})_2(CH_2CN)$ (**32**) [60] (Scheme 8). Complex **32** was prepared when the synthesis of **57** was carried out in acetonitrile instead of methanol in the presence of air. The iron–azide complex **29** was synthesized from *o*-aminophenol $APH_2{}^{L1}$, iron salt $[Fe^{III}(dmfa)_6](ClO_4)_3$ (dmfa = dimethylformamide) and sodium azide (molar ratio is 2:1:4) on air in methanol solution (Scheme 10, Eq. (1)). Complex **30** was prepared in an analogous way using potassium thiocyanate instead of sodium azide (Scheme 10, Eq. (2)). The SCN-group was inserted into cobalt complex **31** by the exchange reaction between chloride complex $Co(ISQ^{L3})_2Cl$ (**21**) and KSCN (Scheme 10, Eq. (3)).

An unusual *o*-iminobenzosemiquinonato complex – binuclear iron complex containing μ-oxo-bridge, $(ISQ^{L6})_2Fe–O–Fe(ISQ^{L6})_2$ (**33**), was described in ref. [58] (Scheme 8). Complex **33** was synthesized by the reaction of $[Fe(H_2O)_6](ClO_4)_2$ with *o*-aminophenol $APH_2{}^{L6}$ in the presence of Et_3N and air.

The pentacoordinate manganese(III) complexes $Mn(ISQ^{L2})(AP^{L2})L$ (L is THF (**34**) or CH_3OH (**35**)) were synthesized from four-coordinate $Mn(ISQ^{L2})(AP^{L2})$ (**69**, see Section 6.8) by dilution of this compound in corresponding solvent [61] or from manganese(II) salt and *o*-iminobenzosemiquinonato thallium salt (molar ratio is 1:2) in a suitable solvent medium [59].

4.2. Structure and magnetism

Selected structural data on $M(ISQ)_2X$ and $M(ISQ)_2L$ types complexes are shown in Table 2. All the complexes adopt a distorted square–pyramidal geometry. In all cases, O,N-chelating ligands form the pyramid base while X (L) substituent is axial. The geometric characteristics undoubtedly indicate radical–anionic *o*-iminobenzosemiquinone ligands in **19–21**, **24–30**, **32** and **33** (C–O, 1.29–1.31 Å, C–N, 1.34–1.36 Å, typical quinoid type distortion of C–C rings in quinonic part), while the manganese complex **34** contains ligands in different oxidation levels: *o*-iminobenzosemiquinone and *o*-amidophenolate.

Increasing steric hindrance near the metallic center (due to *N*-aryl substituents) heightens the distortion of the pyramid (Scheme 11). The N–M–N bond angle tends to be reduced in comparison with O–M–O (Table 2): in **19**, **20**, **24–26**, **29–32** the difference ∠(O–M–O)–∠(N–M–N) is not more than ~6.2°, while in **21**, **27** and **28** it achieves 22–25.8°. The situation is reversed in the binuclear iron complex **33** where ∠(O–M–O) is at about 13° less than ∠(N–M–N) due to steric repulsion of two $M(ISQ)_2$ components.

The electronic spectra of all $M(ISQ)_2X$ type complexes (**19–32**) are characterized by a very intense broad absorption with maximum in the range 700–850 nm (with $\varepsilon \sim 0.3–1.2 \times 10^4\ M^{-1}\ cm^{-1}$) and another in the range 450–700 nm (with $\varepsilon \sim 0.8–1.5 \times 10^4\ M^{-1}\ cm^{-1}$). There have been no detailed assignment of these bands. Usually they are interpreted as a LLCT between π-orbitals of ISQ ligands or as a LMCT [54,56,57,60]. Similar bands are observed in the spectra of bis-ligand square-planar complexes of $M(ISQ)_2$ type, for which a more detailed analysis of the electronic structure was performed (see Section 6.2).

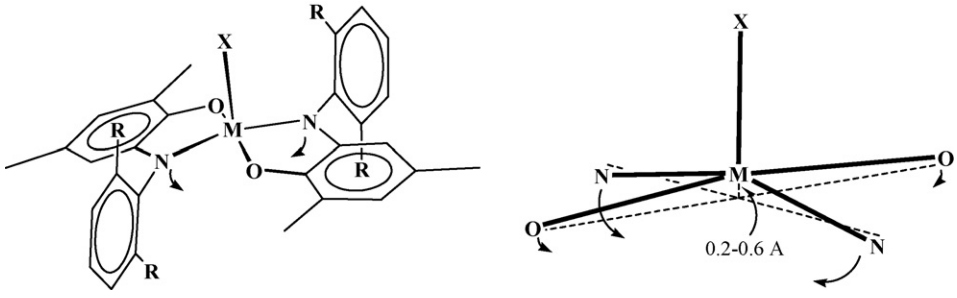

Scheme 11. Angle reducing in ML_2X type complexes with the growth of R substituents.

Table 2
Structural data on ML_2X and ML_2L' type complexes

N	Complex	Bond length (Å)					Angle (°)		Reference
		M–O, av.	M–N, av.	C–O, av.	C–N, av.	M–X (L′)	O–M–O	N–M–N	
19	$Co(ISQ^{L1})_2Cl$	1.863	1.876	1.302	1.345	2.265	163.57	161.57	[54]
20	$Co(ISQ^{L1})_2I$	1.868	1.861	1.297	1.352	2.578	162.89	162.59	[54]
21	$Co(ISQ^{L3})_2Cl$	1.862	1.863	1.292	1.346	2.255	172.34	149.17	[53]
24	$Fe(ISQ^{L1})_2Cl$	1.963	2.041	1.292	1.344	2.220	146.04	139.90	[56,57]
25	$Fe(ISQ^{L1})_2Br$, 1st polymorph **25a/25b**[a]	1.873/1.951	1.892/2.047	1.308/1.291	1.357/1.347	2.366/2.369	157.72/141.97	155.95/150.40	[56,57]
25	$Fe(ISQ^{L1})_2Br$, 2nd polymorph **25b**[a]	1.957	2.045	1.293	1.343	2.371	146.68	140.63	[57]
26	$Fe(ISQ^{L1})_2I$[a]	1.875/1.901	1.885/1.923	1.310/1.304	1.357/1.348	2.591/2.591	157.31/154.50	158.59/156.50	[56,57]
27	$Fe(ISQ^{L3})_2Br$	1.946	1.998	1.297	1.341	2.376	162.57	136.79	[55]
28	$Mn(ISQ^{L2})_2Cl$	1.874	1.947	1.313	1.355	2.273	165.43	143.65	[55]
29	$Fe(ISQ^{L1})_2(N_3)$[a]	1.876/1.910	1.883/1.933	1.309/1.302	1.358/1.350	1.958/1.948	159.13/156.36	155.74/153.03	[57]
30	$Fe(ISQ^{L1})_2(NCS)$	1.942	2.008	1.286	1.345	1.952	151.38	145.69	[57]
32	$Co(ISQ^{L4})_2(CH_2CN)$	1.850	1.857	1.305	1.352	2.004	170.07	165.97	[60]
33	$(ISQ^{L6})_2Fe–O–Fe(ISQ^{L6})_2$[b]	1.964	2.061	1.297	1.346	1.775	av. 136.57	av. 149.61	[58]
34	$Mn(ISQ^{L2})(AP^{L2})THF$	1.865	1.911	1.346	1.387	2.231	172.93	160.27	[59]
		1.879	1.929	1.329	1.378				

[a] For complexes **25**, **26**, **29**, there are two values of av. lengths for each bond given in the table. For **25**, left/right value relates to first/second polymorph form of **25** (at 100 K). For **26** and **29** – to 100 and 295 K respectively. See explanations in text.
[b] Average data are given over four ligands.

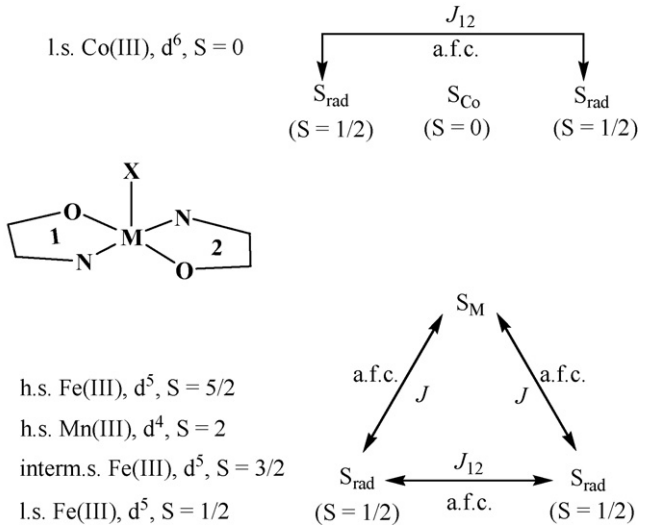

Chart 1. The qualitative scheme of magnetic exchange interactions in ML_2X complexes. Here and in other Charts: a.f.c. is antiferromagnetic coupling, f.c. is ferromagnetic coupling.

The electronic spectrum of the binuclear iron complex **33** resembles closely the spectra of these $M(ISQ)_2X$ complexes and reveals the presence of this type of core [58].

The magnetic behavior of these complexes is rather interesting (Table S3 of Supplementary information). All the cobalt complexes **19**–**23** [54,55] are diamagnetic (ground state $S = 0$) in spite of the presence of two radical ISQ ligands. Authors have shown that the electronic structures of these complexes may be correctly described as singlet diradical containing a diamagnetic low-spin cobalt(III), d^6, and two *o*-iminobenzosemiquinonato radical–anions which are strongly antiferromagnetically coupled. Complex **32** is also diamagnetic ($S = 0$) and contains a carbon-coordinated anion $(CH_2CN)^-$ [60]. The manganese complex **28** possesses a triplet ground state which is attained through strong antiferromagnetic coupling of two (among four) unpaired electrons (d^1_{xz}, d^1_{yz}) of high-spin manganese(III), d^4 ($S_{Mn} = 2$), with two unpaired electrons on π*-MO of the ISQ radical ligands [55]. It is remarkable that the replacement of an anionic apical substituent (Cl in **28**) with a neutral donor group (THF in **34**) with conservation of oxidation state Mn(III) stabilizes a different ground state for the complex, namely an $S = 3/2$ ground state in $Mn^{III}(ISQ^{L2})(AP^{L2})THF$ (**34**) [59].

The most interesting magnetochemical behavior of these ML_2X complexes was observed with the iron complexes. The complex $Fe(ISQ^{L1})_2Cl$ (**24**) has an $S = 3/2$ ground state while $Fe(ISQ^{L1})_2I$ (**26**) – an $S = 1/2$ state at low temperature [56]. High-spin iron(III), d^5, $S_{Fe} = 5/2$, in **24** or intermediate-spin iron(III), d^5, $S_{Fe} = 3/2$, in **26** is coupled antiferromagnetically with two radical ISQ ligands causing the resultant ground states of these complexes (Chart 1).

The unit cells in crystals of $Fe(ISQ^{L1})_2Br$ (**25**) contain two different structural forms (it is the first polymorph – an 1:1 mixture of **25a** and **25b** at temperature below 120 K) [56]. These two forms reveal different states of iron(III): ground state of **25a** is an $S = 1/2$ while **25b** possesses an $S = 3/2$ ground state [57]. The difference in spin states of central ion in two

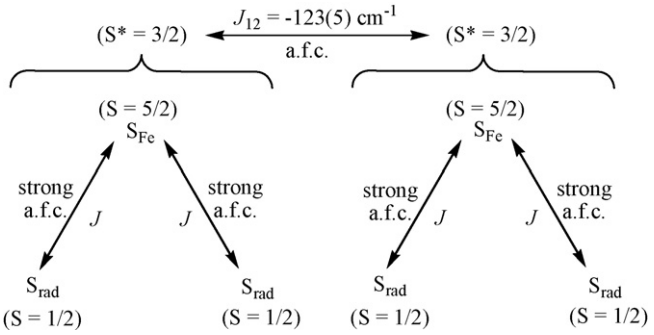

Chart 2. The qualitative scheme of magnetic exchange interactions in binuclear iron complex **33**.

species **25a** and **25b** is embodied in structural features as well as in Mössbauer spectroscopy and magnetochemistry. Note that the second polymorph containing only **25b** [57] was also prepared using a procedure which differs slightly from that one for first polymorph containing both forms (**25a** and **25b**): $NaOCH_3$ was applied as the base instead of Et_3N and molar ratio $FeBr_2$ to *o*-aminophenol was 1:1 [57] contrary to 1:1.5 [56]. Moreover, Ph_3P was added to promote the crystallization of the product in the case of first polymorph (**25a** and **25b**). This step was omitted in the synthesis of the second polymorph (**25b**).

Iodide $Fe(ISQ^{L1})_2I$ (**26**) and azide $Fe(ISQ^{L1})_2(N_3)$ (**29**) complexes possess the pure $S = 1/2$ ground state in the range of 4–130 K and 4–49 K respectively. At higher temperature, spin crossover to $S = 3/2$ form is observed [57]. Molecules of **25a** in first polymorph form of **25** undergo spin crossover above 150 K. Spin crossover $S = 1/2 \leftrightarrow S = 3/2$ is accompanied by structural changes of the metal–chelate units. In the $S = 1/2$ form, the Fe–O bonds (1.87–1.88 Å) and Fe–N (1.88–1.89 Å) are short. Upon spin crossover to $S = 3/2$ state, the Fe–O and Fe–N distances become longer achieving values of 1.94–1.96 and 2.01–2.05 Å (Table 2) while the axial Fe–X bond length is nearly constant. In fact, the *o*-iminobenzosemiquinonato ligands also remain unchanged within experimental error. Magnetochemical studies of $Fe(ISQ^{L1})_2I$ (**26**) have shown the presence of 63% of $S = 1/2$ form and 37% of $S = 3/2$ form at 295K [57]. The first polymorph of **25** contains 18.5% of the $S = 1/2$ form (**25a**) and 81.5% of the $S = 3/2$ form (**25b**) at 295 K. These results are in agreement with crystallographic data on $S = 3/2$ and 1/2 forms. Estimated ratio of $S = 1/2$ to $S = 3/2$ forms based on X-ray determinations is 84:16 for **26**, 42:58 for **25a** in first polymorph, while **25b** is in $S = 3/2$ form only; and 80:20 for **29**. Compound $Fe(ISQ^{L1})_2(SCN)$ (**30**) has a temperature independent $S = 3/2$ ground state. Based on our unpublished data, the iron complex $Fe(ISQ^{L3})_2Br$ (**27**) has an $S = 1/2$ ground state. In this complex, antiferromagnetic coupling metal–ligand takes place between intermediate spin iron(III), d^5 ($S_{Fe} = 3/2$), and radical ligand with exchange parameters J(Fe-ISQ) = $J = -66(7)$ cm^{-1} and J(ISQ-ISQ) = $J_{12} = -106(19)$ cm^{-1} (Chart 1).

The binuclear iron complex **33** has an $S = 0$ ground state. The strong antiferromagnetic coupling between high-spin iron(III), d^5 ($S_{Fe} = 5/2$), and two ISQ^{L6} radical ligands leads to $S^* = 3/2$ state for each half of molecule. The observed singlet ground state of **33** is attained through the strong antiferromagnetic coupling between the two halves through the μ-oxo group [58] (Chart 2).

5. Hexacoordinate bis-*o*-iminobenzoquinonato complexes of $M(ISQ)_2X_2$/$M(ISQ)_2L_2$ types

Hexacoordinate bis-*o*-iminobenzoquinonato complexes, of $M(ISQ)_2X_2$/$M(ISQ)_2L_2$ are still rare. We have found only seven examples of such complexes in the literature. There is a nickel complex $[Ni^{II}(IBQ^{L4})_2(OClO_3)_2]$ (**36**) [62], rhenium complex $Re^{II}(ISQ^{L2})_2(CO)_2$ (**37**) [61] and a number of zirconium complexes $Zr^{IV}(AP^{tBu})_2(THF)_2$ (**38**), $Zr^{IV}(ISQ^{tBu})_2Cl_2$ (**39**), $[Li(Et_2O)]_2[Zr^{IV}(AP^{tBu})_2Ph_2]$ (**40**), $[Li(Et_2O)]_2[Zr^{IV}(AP^{tBu})_2(p\text{-Tol})_2]$ (**41**), $[Li(Et_2O)]_2[Zr^{IV}(AP^{tBu})_2Me_2]$ (**42**), where $[AP^{tBu}]^{2-}$ and $[ISQ^{tBu}]^{\bullet -}$ are the 4,6-di-*tert*-butyl-*N*-*tert*-butyl-*o*-amidophenolate dianion and 4,6-di-*tert*-butyl-*N*-*tert*-butyl-*o*-iminobenzosemiquinonato radical–anion respectively [63,64] (Scheme 12).

5.1. Synthesis

The nickel complex **36** is a product of the oxidation of bis-*o*-iminobenzosemiquinonato nickel(II) complex $Ni(ISQ^{L4})_2$ (**45**, see Section 6.2) with two equivalents of $AgClO_4{\cdot}H_2O$ [62] while the rhenium complex $Re^{II}(ISQ^{L2})_2(CO)_2$ (**37**) was prepared from rhenium carbonyl and *o*-iminobenzoquinone IBQ^{L2} under UV in toluene [61]. This synthetic method will also be considered in Section 6.1.

The exchange reaction of double equivalent of lithium *o*-amidophenolate with zirconium(IV) chloride $ZrCl_4(THF)_2$ affords zirconium bis-*o*-amidophenolate $Zr^{IV}(AP^{tBu})_2(THF)_2$ (**38**). Oxidation of **38** by gaseous chlorine at −78 °C leads to the bis-*o*-iminobenzosemiquinonato product $Zr^{IV}(ISQ^{tBu})_2Cl_2$ (**39**) [63]. The latter complex was also prepared by the oxidation of bis-*o*-amidophenolate complex **38** with $PhICl_2$ at low temperature and from $ZrCl_4$ and two equivalents of lithium *o*-iminobenzosemiquinone (ISQ^{tBu})Li. In all cases the yield was not greater than 55%. Aryl/alkyl derivatives $[Li(Et_2O)]_2[Zr^{IV}(AP^{tBu})_2Ph_2]$ (**40**), $[Li(Et_2O)]_2[Zr^{IV}(AP^{tBu})_2(p\text{-Tol})_2]$ (**41**), $[Li(Et_2O)]_2[Zr^{IV}(AP^{tBu})_2Me_2]$ (**42**) were prepared from a freshly prepared *in situ* bis-*o*-amidophenolate complex $Zr^{IV}(AP^{tBu})_2(Et_2O)_2$ which is the closest analogue of **38** and corresponding aryl/alkyllithium in diethyl ether. The preparative yield was less 37%.

5.2. Structure and magnetism

Complex **36** adopts a hexacoordinate octahedral geometry where neutral O,N-coordinated *o*-iminobenzoquinones form the equatorial plane being *trans* to each other. The ligand characteristics are typical for neutral IBQ (C–O is 1.239(2) Å, C–N is 1.296(2) Å, formally double C–C are 1.352(2) and 1.357(2) Å [62]) and close to the corresponding characteristics of IBQ ligands in palladium complexes **49** and **51** (see Section 6.3) [62]. Complex **36** possesses the expected triplet ground state ($S = 1$) for nickel(II) complexes of octahedral geometry.

The rhenium(II) complex **37** was prepared by the oxidative addition of *o*-iminobenzoquinone IBQ^{L2} to rhenium car-

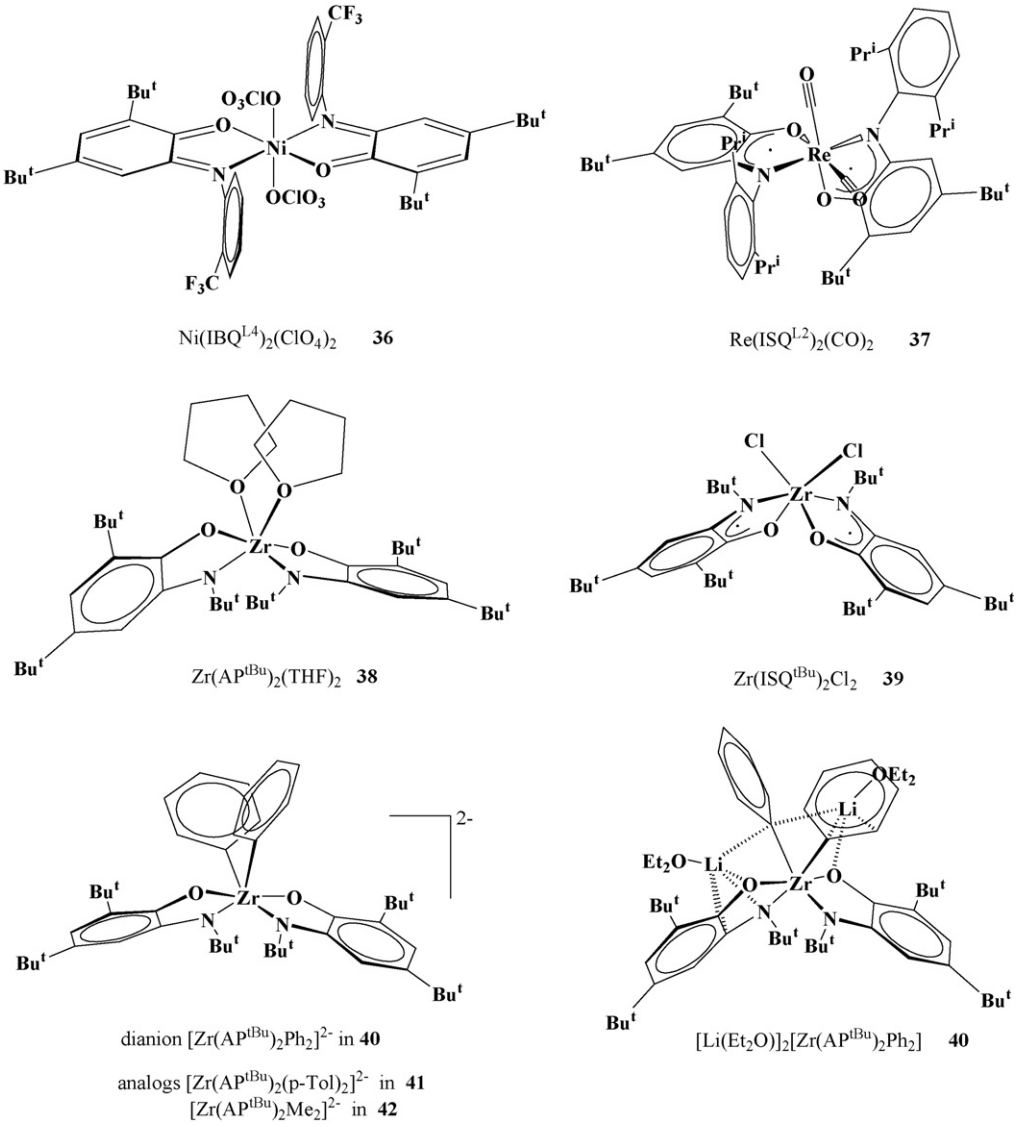

Scheme 12. Complexes **36** [62], **37** [61], **38**, **39**, **40**, and complex anions in **40**–**42** [63,64].

bonyl [61]. Noteworthy is the significant difference between reactivity of manganese and rhenium carbonyls toward *o*-iminobenzoquinone: the reaction of $Mn_2(CO)_{10}$ with IBQ^{L2} under the same conditions leads to complete elimination of CO groups yielding four-coordinate manganese(III) complex **64** (see Section 6.8). Complex **37** has a distorted octahedral geometry. However, here the CO groups are in the *cis*-position (in contrast to *trans*-location of $OClO_3^-$-groups in **36**). In rhenium complex **37**, O,N-coordinated ligands adopt a geometry with *trans* nitrogen atoms (N–Re–N is 163.85(6)°). The bond lengths C–O (1.311(2), 1.305(2) Å), C–N (both 1.360(2) Å) and other characteristics of O,N-coordinated ligands clearly reveal radical–anionic ISQ^- coordination mode. Antiferromagnetic exchange between t_{2g} unpaired electron of low-spin rhenium(II) (d^5, $S = 1/2$) and one unpaired electron on ligand π*-MO of one ISQ ligand causes an observed doublet ground state of **37** that is supported by X-band EPR spectrum of toluene solution of **37** exhibiting HFC with rhenium nuclei of 37 G with $g_{iso} = 1.982$.

X-ray crystallography was used to determine the molecular structure of the zirconium complexes **38**, **39**, **40** and **42**. Noticeably, the solid zirconium complexes adopt quite different geometries. While $Zr^{IV}(AP^{tBu})_2(THF)_2$ (**38**) has hexacoordinate trigonal antiprism geometry and $Zr^{IV}(ISQ^{tBu})_2Cl_2$ (**39**) has intermediate conformation between trigonal antiprism and prism, complex dianions $[Zr^{IV}(AP^{tBu})_2Ph_2]^{2-}$ in **40** and $[Zr^{IV}(AP^{tBu})_2Me_2]^{2-}$ in **42** adopt a slightly distorted octahedral geometry. In all cases the geometric features are rationalized by the small chelating O–Zr–N angle of the O,N-ligands (av. over both ligands: 76.0° in **38**, 72.6° in **39**, 72.0° in **40**, 71.2° in **42**).

In complexes **38**, **40** and **42**, the bond lengths in O,N-chelating ligands support the dianionic nature of the *o*-amidophenolate ligands [63,64]. The chloride complex **39** has radical–anionic *o*-iminobenzosemiquinones with C–O and C–N distances of 1.316(3) and 1.339(3) Å in contrast with those distances in **38**, **40**, **42** (av. 1.358(5) and 1.413(6) Å in **48**, 1.366(5) and 1.403(5) Å in **40**, 1.369(3) and 1.398(3) Å in **42**).

As one can expect, the bis-*o*-iminobenzosemiquinonato zirconium complex **39** should be a diradical complex. The magnetic data (μ_{eff} is 0.12 μ_B at 4 K and 1.25 μ_B at 400 K) and EPR lead to the supposition of spin-pairing in this diradical complex to create a singlet ground state with the thermally accessible triplet excited state [63].

6. Homoleptic transition metal complexes with bidentate *N*-aryl-*o*-iminoquinone ligands. Comparison with *o*-quinone analogues

Here, we will consider homoleptic complexes of transition metals V, Cr, Mn, Fe, Co, Ni, Pd, Pt, Cu with different substituted *o*-iminoquinonato ligands and compare with their *o*-quinone analogues. The selected bond lengths of some *o*-iminobenzoquinonato transition metal complexes are listed in Table 3. Tables S4 and S5 of supplementary information contain the EPR spectroscopic data and magnetic data on complexes, respectively.

6.1. Synthetic methods

There are three principal methods to prepare homoleptic *o*-iminobenzoquinonato transition metal complexes.

(i) The first is the reaction of corresponding *o*-aminophenols with transition metal salts in the presence of stoichiometric amounts of base (e.g. Et_3N) and air (or without the latter) (Scheme 13). This method was used for the syntheses of the overwhelming majority of complexes reported. There are complexes of cobalt [53,60,65], nickel [6,60], iron [7,66], chromium [7], manganese [67,68], vanadium [7]. However, different conditions and limitations take place in this method. On the one hand, this method requires the use of a polar solvent and this can complicate the product by solvation. On the other hand, air imposes a limitation on the stability of the product.

(ii) The second method is exchange reaction of transition metal salts with an alkali or thallium salt of *o*-iminobenzosemiquinone. Thus method does not require air oxygen as external oxidant. Applicability of this method was shown in [53].

(iii) The third method consists in the interaction of free *o*-iminobenzoquinones with metal carbonyls. Only this third method is applicable for the preparation of the square planar bis-ligand manganese complex [61]. Some cobalt complexes were also prepared by third method [53]. In this method, an inert solvent medium may be chosen (hexane, toluene etc.). But the main limitation of this method is the stability of free neutral *o*-iminobenzoquinone. The free *o*-iminobenzoquinone form of the ligands APH_2^{L1}, APH_2^{L4} – APH_2^{L7}, $(AP\text{-}AP)H_3^{L9}$, APH_2^{L10}, APH_2-$APH_2^{L11,L12,L14,L15}$, APH_2-NH-APH_2^{L13} is not very stable because of the absence of substituents in the two and six positions of the *N*-aryl fragment (i.e. when α- or β-carbon atoms have hydrogen atoms). This form undergoes rearrangement by intramolecular cyclization to phenoxazine species. Therefore syntheses in most of these cases proceed

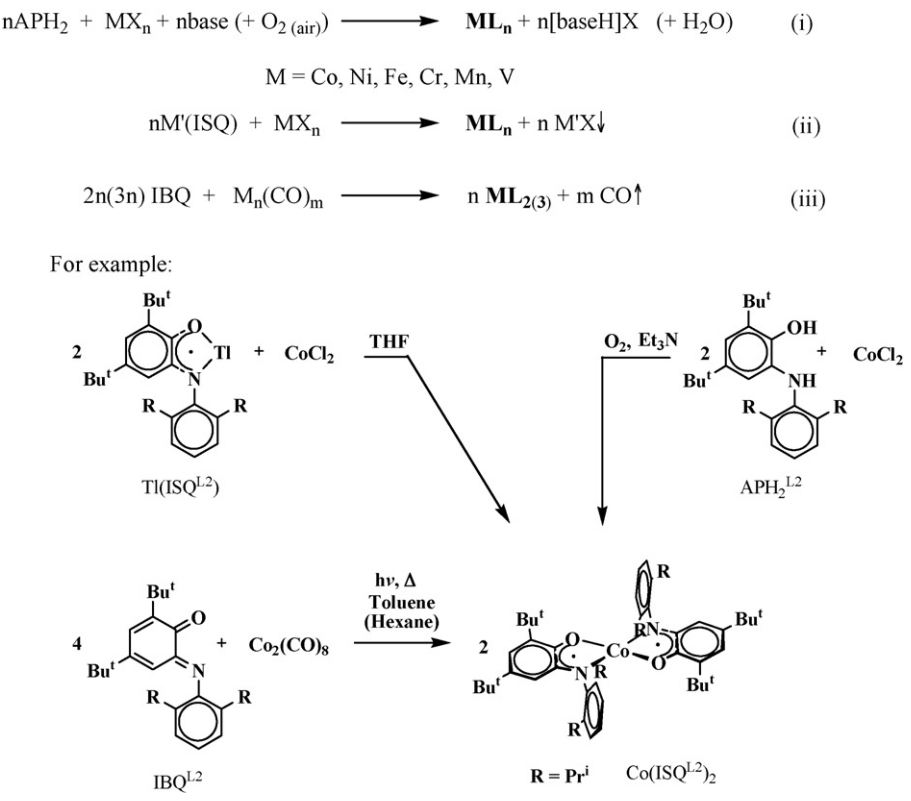

Scheme 13. Synthetic ways to homoleptic *o*-iminobenzoquinonato complexes.

Table 3
Selected bond lengths (Å) of *o*-iminosemiquinonato (ISQ), *o*-aminophenolato (APH) and *o*-amidophenolato (AP) ligands in transition metal complexes

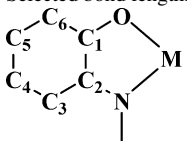

N	Complex		C_1–O	C_2–N	C_1–C_2	C_2–C_3	C_3–C_4	C_4–C_5	C_5–C_6	C_1–C_6	M–O	M–N	Reference
44	$Ni^{II}(ISQ^{L5Cl})_2$[a]		1.333	1.370	1.427	1.430	1.384	1.430	1.396	1.429	av. 1.827	av. 1.859	[6]
45	$Ni^{II}(ISQ^{L4})_2$[a]		1.315	1.355	1.432	1.418	1.376	1.430	1.385	1.425	av. 1.836	av. 1.844	[60]
45a	$[Ni^{II}(ISQ^{L4})(AP^{L4})]^-[CoCp_2]^+$	ISQ	1.329	1.378	1.407	1.410	1.386	1.407	1.384	1.428	1.844	1.831	[60]
		AP	1.345	1.382	1.422	1.394	1.401	1.386	1.411	1.403	1.846	1.843	
46	$Pd^{II}(ISQ^{L1})_2$[a]		1.314	1.352	1.430	1.425	1.374	1.431	1.375	1.430	1.977	1.959	[6]
47	$Pt^{II}(ISQ^{L1})_2$[a]		1.317	1.372	1.419	1.414	1.373	1.430	1.376	1.427	1.977	1.946	[35]
48	$Pd^{II}(ISQ^{L4})_2$		1.341	1.354	1.437	1.413	1.377	1.421	1.377	1.427	1.975	1.963	[62]
49	$[Pd^{II}(ISQ^{L4})(IBQ^{L4})][BF_4]$	IBQ	1.255	1.316	1.491	1.424	1.353	1.478	1.350	1.450	1.997	2.011	[62]
		ISQ	1.313	1.345	1.443	1.417	1.362	1.445	1.376	1.427	1.974	1.966	
50	$[Cp_2Co][Pd^{II}(ISQ^{L4})(AP^{L4})]$	ISQ	1.329	1.377	1.422	1.406	1.388	1.401	1.403	1.426	2.001	1.960	[62]
		AP	1.341	1.378	1.426	1.406	1.391	1.400	1.396	1.405	1.984	1.996	
51	$[Pd^{II}(IBQ^{L4})_2]_3(BF_4)_4\{(BF_4)_2H\}_2$		av. 1.252	av. 1.301	av. 1.506	av. 1.430	av. 1.350	av. 1.472	av. 1.353	av. 1.447	av. 2.005	av. 1.996	[62]
52	$Cu^{II}(ISQ^{L1})_2$		1.290	1.335	1.454	1.425	1.369	1.432	1.376	1.436	av. 1.912	av. 1.936	[6]
53	$Cu^{II}(ISQ^{SMe})_2$		av. 1.294	av. 1.353	av. 1.454	av. 1.420	av. 1.369	av. 1.433	av. 1.376	av. 1.430	av. 1.923	av. 1.937	[78]
54	$Co^{III}(ISQ^{L1})_3$		av. 1.304	av. 1.347	av. 1.438	av. 1.428	av. 1.369	av. 1.433	av. 1.380	av. 1.427	av. 1.888	av. 1.934	[65]
55	$Co^{II}(ISQ^{L2})_2$		av. 1.327	av. 1.368	av. 1.418	av. 1.413	av. 1.378	av. 1.419	av. 1.382	av. 1.413	av. 1.822	av. 1.840	[53]
57	$Co^{III}(ISQ^{L4})(AP^{L4})$		av. 1.328	av. 1.373	av. 1.422	av. 1.406	av. 1.380	av. 1.420	av. 1.385	av. 1.417	av. 1.823	av. 1.936	[60]
57a	$[Co^{III}(AP^{L4})_2]^-[CoCp_2]^+$[a]		1.339	1.388	1.402	1.393	1.394	1.397	1.402	1.404	av. 1.830	av. 1.837	[60]
58	$Fe^{III}(ISQ^{L1})_3$		av. 1.303	av. 1.343	av. 1.453	av. 1.423	av. 1.357	av. 1.432	av. 1.380	av. 1.432	av. 2.014	av. 2.099	[7]
59	$Fe^{III}(ISQ^{L5F})_3$		av. 1.284	av. 1.339	av. 1.456	av.1.423	av. 1.369	av. 1.434	av. 1.375	av. 1.437	av. 2.010	av. 2.086	[66]
60	$Fe^{III}(ISQ^{L5Bu-t})_3$[b]		av. 1.295	av. 1.352	av. 1.442	av. 1.421	av. 1.373	av. 1.426	av. 1.381	av. 1.429	av.1.904/1.996	av.1.922/2.075	[66]
61	$Cr^{III}(ISQ^{L1})_3$		av. 1.304	av. 1.358	av. 1.437	av. 1.420	av. 1.373	av. 1.427	av. 1.379	av. 1.427	av. 1.954	av. 2.001	[7]
62	$Mn^{III}(ISQ^{L1})_2(APH^{L1})$	ISQ	av. 1.306 1.339	av. 1.352	av. 1.442	av. 1.412	av. 1.359	av. 1.422	av. 1.378	av. 1.428	av. 1. 916	av. 2.016	[92]
	APH			1.422	1.399	1.383	1.382	1.387	1.388	1.409	1.896	2.345	
63	$Mn^{IV}(ISQ^{L1})_2(AP^{L1})$	ISQ	av. 1.301	av. 1.353	av. 1.435	av. 1.426	av. 1.362	av. 1.436	av. 1.373	av. 1.425	av. 1.908	av. 1.976	[92]
		AP	1.342	1.395	1.421	1.402	1.383	1.412	1.389	1.411	1.873	1.963	
64	$Mn^{IV}(ISQ^{L5But})_2(AP^{L5But})$	ISQ	av. 1.300	av. 1.350	av. 1.434	av. 1.416	av. 1.371	av. 1.427	av. 1.377	av. 1.427	av. 1.922	av. 1.959	[68]
		AP	1.330	1.384	1.413	1.404	1.385	1.411	1.390	1.412	1.868	1.919	
69	$Mn^{III}(ISQ^{L2})(AP^{L2})$[a]		1.326	1.368	1.412	1.401	1.383	1.407	1.387	1.421	1.859	1.896	[61]
70	$V^{V}(AP^{L1})_2(ISQ^{L1})$	ISQ	1.317	1.344	1.423	1.427	1.378	1.421	1.385	1.412	1.945	2.079	[7]
		AP	av. 1.323	av. 1.362	av. 1.422	av. 1.407	av. 1.379	av. 1.416	av. 1.373	av. 1.418	av. 1.916	av. 1.990	
71	$V^{V}(AP^{L1})_2(APH^{L1})$[c]	APH	av. 1.354	av. 1.472	av. 1.398	av. 1.382	av. 1.389	av. 1.397	av. 1.395	av. 1.415	av. 1.893	av. 2.230	[7]
		AP	av. 1.333	av. 1.386	av. 1.413	av. 1.403	av. 1.389	av. 1.409	av. 1.385	av. 1.413	av. 1.915	av. 1.975	

[a] For **57a**, **69** the two ligands in the neutral molecules are crystallographically identical.
[b] Fe–O and Fe–N bonds are given at two temperatures (100 and 293 K).
[c] For **71** average values of distances are calculated per both crystallographically independent molecules in the unit cell.

from the *o*-aminophenol form of the ligands (first method) to prepare *o*-iminobenzoquinonato complexes.

6.2. Nickel

Bis-ligand *o*-benzoquinonato and *o*-iminobenzoquinonato nickel complexes are similar in their structure as well as in their magnetic properties in most cases [6,60,69].

o-Iminoquinonato nickel(II) complexes $Ni(ISQ^{L1})_2$ (**43**) and $Ni(ISQ^{L5Cl})_2$ (**44**), where ISQ^{L5Cl} is 4,6-di-*tert*-butyl-*N*-(3,5-dichlorophenyl)-*o*-iminobenzosemiquinone, were reported in [6]. Complex $Ni(ISQ^{L4})_2$ (**45**) which is analogue of cobalt complex **7** was characterized in [60].

X-ray data are available for $Ni(ISQ^{L5Cl})_2$ (**44**) and $Ni(ISQ^{L4})_2$ (**45**) (Scheme 14). Complexes **44** and **45** are square planar, and centrosymmetric, as are all bis-*o*-semiquinone nickel complexes. The Ni–O and Ni–N, C–O, C–N bond distances (Table 3) indicate the radical–anion form of the ligands. Worthy of note is that the C–O and C–N distances in **44** and **45** tend to values intermediate between those usual for ISQ and AP ligands. They are about 0.01–0.02 Å longer than the usual bond lengths in ISQ complexes. It is a common situation in square-planar complexes (Ni, Pd, Pt, Co etc.) with very strong antiferromagnetic exchange ligand–ligand and is rationalized by the formation of molecular orbital over both ligands (see below).

Complexes **43**–**45** are diamagnetic, the ^{1}H NMR spectra of **43** and **44**, recorded at 298 K, showed no line broadening, being evidence of an $S = 0$ ground state. The strong antiferromagnetic ligand–ligand exchange takes place in all monomeric square-planar nickel(II) complexes with two radical–anion ligands (either *o*-benzosemiquinone or *o*-iminobenzosemiquinone). The reduction of **45** with cobaltocene yields the paramagnetic ionic complex $[Ni^{II}(ISQ^{L4})(AP^{L4})]^-[CoCp_2]^+$ (**45a**) where the anion possesses an $S = 1/2$ ground state (Table S5) [60].

The electronic spectra of complexes **43**–**45** contain intraligand transition bands of $\varepsilon \sim 10^3\ M^{-1}\ cm^{-1}$ in the range 400–700 nm indicative for ISQ ligands, and a very intense ($\varepsilon \sim 3$–$5 \times 10^4\ M^{-1}\ cm^{-1}$) absorption maximum in the range 800–900 nm. A number of studies include the calculations of electronic structures of bis-ligand nickel, cobalt, palladium, platinum, iron etc. complexes with *o*-benzoquinonediimine and *o*-benzoquinonedithiolate ligands [60,62,70–73] in order to understand their structural and spectroscopic properties. The electronic spectra of the neutral complexes and their monocations and monoanions can be considered using a model which involves two redox-active molecular orbitals shown in Chart 3. Depending on the complex symmetry, authors have chosen D_{2h} or C_{2h} point groups. In the first case, the $1b_{1u}$ and $2b_{2g}$ MOs are the positive and negative combinations of the SOMO of two radical ligands. (In ML_2 complexes of O,N-ligands, the complex symmetry is reduced from D_{2h} to C_{2h} and the redox-active MOs are a_u and b_g).

The symmetry of the $1b_{1u}$ MO does not allow the interaction with the d-AOs of the central transition metal, while the $2b_{2g}$ MO can interact with the d_{xz},d_{yz}-AO. The degree of this orbital mixing depends on the relative energies of orbitals.

For neutral ML_2 species the $1b_{1u}$ MO is HOMO and the $2b_{2g}$ MO is LUMO. In general, the electronic spectra of such complexes are dominated by the $1b_{1u} \rightarrow 2b_{2g}$ transitions which are LLCT or LMCT in origin depending on the metal contribution to the $2b_{2g}$ orbital which can be different for various metals and ligands. For instance, in the case of nickel complex Ni(*o*-benzosemiquinonediinine)$_2$, the $1b_{1u} \rightarrow 2b_{2g}$ transition is LLCT in origin because of the weak interaction of $2b_{2g}$ with low-lying Ni $3d_{xz,yz}$ orbitals [60,72].

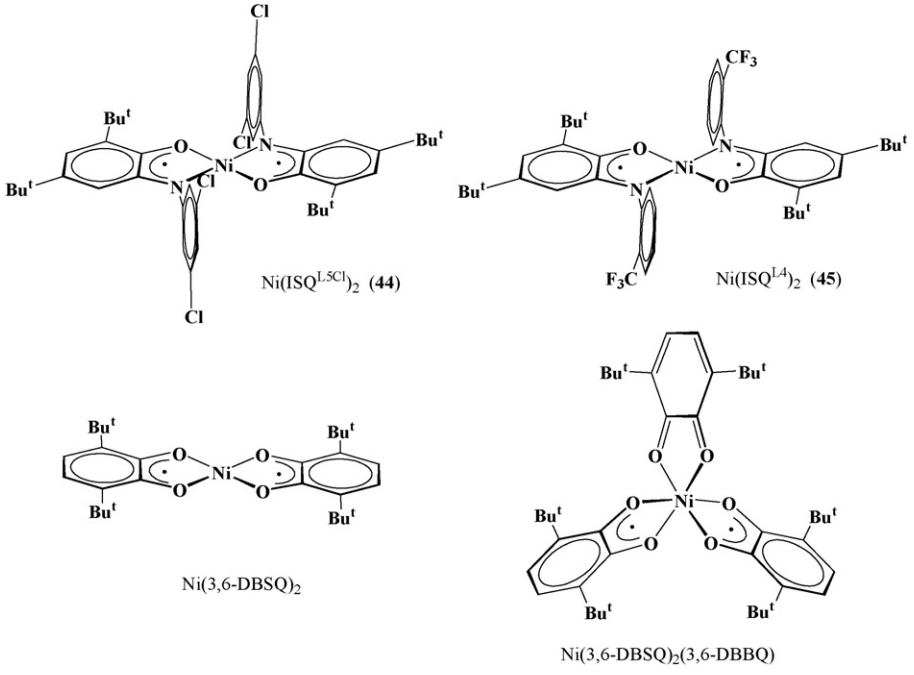

Scheme 14. The structures of *o*-iminobenzosemiquinonato **44**, **45** and o-benzosemiquinonato nickel complexes [6,60,69,76].

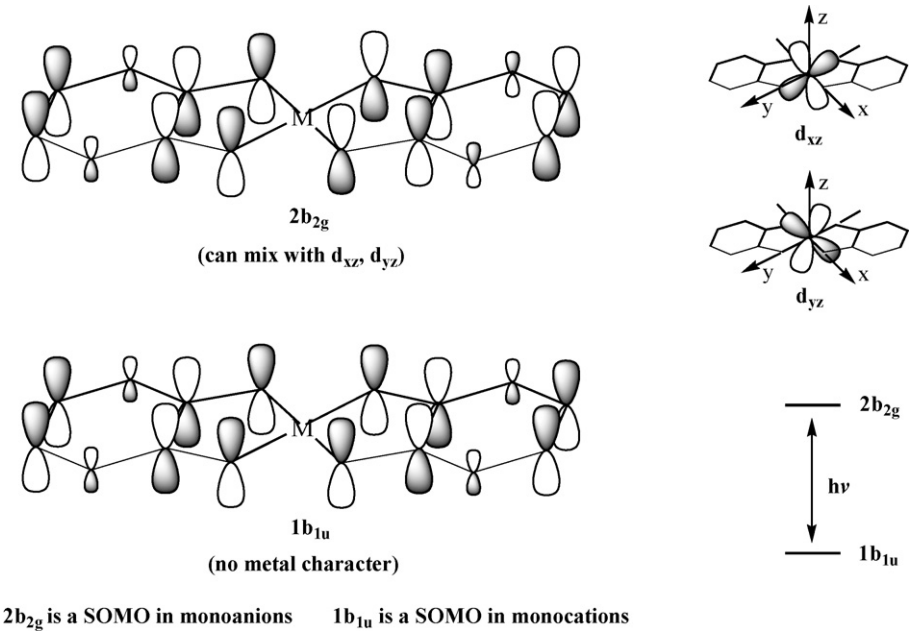

Chart 3. The two redox-active MOs of square-planar complexes ML_2.

For dithiolato complexes M(*o*-benzosemiquinonedithiolate)$_2$, M = Ni, Pd, Pt, the $2b_{2g}$ MO has 16–26% of metal d-character [73] and the $1b_{1u} \rightarrow 2b_{2g}$ transition can also be considered as LLCT. However, the reduction of these complexes to dianions $[M(o\text{-benzene-dithiolate})_2]^{2-}$ leads to increased metal character in $2b_{2g}$ MO up to 52% [73]. In dianionic $[Fe(o\text{-benzene-dithiolate})_2]^{2-}$ the $2b_{2g}$ orbital is predominantly metal in character (82% of d_{xz}) and $1b_{1u} \rightarrow 2b_{2g}$ transition is now LMCT transition [71]. Detailed calculations taking into account configuration interactions show, however, that some of low-lying bands can be composed of double and triple excitations involving lower occupied and higher vacant orbitals [60].

In the monocations $[ML_2]^+$ the $1b_{1u}$ orbital is SOMO, while in the monoanions $[ML_2]^-$, the $1b_{1u}$ orbital is doubly occupied and the $2b_{2g}$ orbital is now the SOMO. The change in the orbital occupations as compared to that of the neutral species causes a shift of the $1b_{1u} \rightarrow 2b_{2g}$ transition to the near-infrared region. Noteworthy, the spectra of monocations and monoanions show very intense absorption in 1200–1800 nm. The corresponding transition was considered as ligand-to-ligand intervalence charge transfer (LLIVCT), since the complexes contain ligands in different oxidation states (i.e. SQ and Q; SQ and Cat) [74].

For instance, the reduction of **45** to **45a** leads to a bathochromic shift (from 900 to 1340 nm) and LLCT is formally LLIVCT [60].

In Ni(3,6-DBSQ)$_2$ [69], the Ni–O (1.825(2) and 1.824(2) Å) distances are significantly shorter than analogous distances in previously reported nickel complexes: (Py)$_2$Ni(9,10-phenSQ)$_2$ (2.022, 2.028, 2.082, 2.100 Å) [4]; (CTH)Ni(3,5-DBSQ)[PF_6] (2.06 Å) [75]. The C–O (1.309 and 1.304 Å), and C–C bonds of the chelate ring (1.435 Å) lie in ranges characteristic for these types of bonds in SQ ligands (1.27–1.31 Å for C–O and 1.42–1.45 Å for C–C bonds). Ni(3,6-DBSQ)$_2$ is a monomeric centrosymmetric square-planar complex (Scheme 14) of divalent nickel with d^8 configuration (X-ray).

Ni(3,6-DBSQ)$_2$ is diamagnetic over a wide temperature interval from 77 to 470 K (in contrast to other nickel semiquinone complexes described in literature [1,32]). The antiferromagnetic ligand–ligand coupling is so strong that the triplet state of the complex is inaccessible even at 400 K. Tetrameric complexes [Ni(3,5-DBSQ)$_2$]$_4$ and [Ni(9,10-phenSQ)$_2$]$_4$ were investigated in the same manner as cobalt analogues [Co(3,5-DBSQ)$_2$]$_4$ and [Co(9,10-PhenSQ)$_2$]$_4$ [4]. Nickel tetramers contain four nickel(II) centers with $S_{Ni} = 1$ and eight radical centers with $S_{rad} = 1/2$. The exchange interactions in the tetramer are weak.

An unusual six-coordinate nickel complex Ni(3,6-DBSQ)$_2$(3,6-DBBQ) (Scheme 14) was obtained using the reaction of excess 3,6-DBBQ with nickel carbonyl Ni(CO)$_4$ [76]. The complex molecule consists of nickel(II) with ligands in different oxidation states (X-ray). Ni(3,6-DBSQ)$_2$(3,6-DBBQ) is strongly paramagnetic ($\mu_{eff} = 4.57\ \mu_B$).

6.3. Palladium and platinum

The palladium and platinum analogues of **43**–**45**, Pd(ISQ^{L1})$_2$ [6] (**46**) and Pt(ISQ^{L1})$_2$ [35] (**47**) are diamagnetic (ground state is $S = 0$) and square planar. The neutral palladium complex Pd(ISQ^{L4})$_2$ (**48**) and its mono-reduced and mono-/di-oxidized derivatives form a redox series [62]. Mono-oxidized tetrafluoroborate [Pd(ISQ^{L4})(IBQ^{L4})][BF_4] (**49**) and mono-reduced cobalticenium [Cp_2Co][Pd(ISQ^{L4})(AP^{L4})] (**50**) salts are paramagnetic with $S = 1/2$. In both cases, the magnetic moment is temperature-independent at 1.7 μ_B. X-band EPR spectrum of the monocation [Pd(ISQ^{L4})(IBQ^{L4})]$^+$ in **49** (CH_2Cl_2, 10 K) is isotropic with $g_{iso} = 2.0007$ reflecting a ligand-based unpaired electron without any sizeable metal character. However, the monoanion [Pd(ISQ^{L4})(AP^{L4})]$^-$ in **50** has a rhombic signal with

$g_1 = 2.0715$, $g_2 = 2.0167$, and $g_3 = 1.974$ (Table S4). This situation is typical for a number of square planar monocations $[ML_2]^+$ and monoanions $[ML_2]^-$ [72] and can be rationalized in terms of the nature of the redox-active MOs. DFT calculations have shown that the magnetic features of such complexes can be interpreted using a model involving two molecular orbitals which are basically the symmetric and antisymmetric combination of the SOMO of the free radical ligand (Chart 3) [35,62,72]. As it was mentioned above (Section 6.2), the SOMO of the monocation is "ungerade" and cannot mix with metal d-AO causing only a small *g*-shift and reflecting clear organic radical character. The SOMO of monoanion is "gerade" and can mix with the d_{xz} and d_{yz} orbitals. In this case, the spin-orbit coupling of excited states with the ground state is efficient, *g*-shift is large, HFC with metal atom is observed [35,72].

The neutral complexes **46**–**48** display very intense LLCT band (with maxima at 875, 813 and 871 nm, respectively) (Chart 4). The expected LLIVCT for monocationic **49** and monoanionic **50** complexes ($\sim 2.5 \times 10^4\ M^{-1}\ cm^{-1}$) are observed at 1996 and 1547 nm, respectively. Moreover, an intraligand transition of the O,N-coordinated IBQ ligand in **49** was found at 504 nm while O,N-coordinated AP ligand in **50** gives rise to absorption at <360 nm. This clearly shows the presence of neutral IBQ ligand in **49** and dianionic AP ligand in **50**.

The geometrical characteristics of complexes **48**–**50** (X-ray) (C–O, C–N, C–C, Pd–O and Pd–N bonds etc.) clearly establish the oxidation level of the O,N-chelated ligands in these complexes (Table 3). Noteworthy, ligands in monocation compound **49** have different parameters allowing one to determine the oxidation level of each ligand. For monoanion **50**, bond lengths C–O, C–N, C–C in O,N-chelated ligands are quite close and can be considered to be identical within experimental error (±0.01 Å). Values of the C–O, C–N and C–C bond distances in **50** are average between the expected lengths of radical–anion ISQ and dianion AP ligands indicating delocalization of the unpaired electron over two ligands.

The crystal structure of dication derivative $[Pd^{II}(IBQ^{L4})_2]_3(BF_4)_4\{(BF_4)_2H\}_2$ (**51**) is more complicated. The unit cell of **51** contains four BF_4^- anions and two $\{(BF_4)_2H\}^-$ monoanions and four molecules of crystallization CH_2Cl_2 per three $[Pd^{II}(IBQ^{L4})_2]^{2+}$ dications. Two crystallographically independent $[Pd^{II}(IBQ^{L4})_2]^{2+}$ dications differ in the position of CF_3-groups. In first dication CF_3-groups are located on different sides of planar dication moiety (as in neutral $[Pd^{II}(ISQ^{L4})_2]$ **48**), while they are on the same side in the second dication (as in monocation **49** and monoanion **50**). Distances C–O and C–N are in average 1.252(5) and 1.301(5) Å – the shortest bonds among such type of bond in homoleptic *o*-iminobenzoquinonato type complexes. These and other ligand characteristics clearly show the neutral *o*-iminobenzoquinonato coordination mode. The complex is diamagnetic and does not show any LLIVCT bands above 630 nm.

6.4. Copper

The square planar bis-*o*-iminobenzosemiquinonato copper complex $Cu(ISQ^{L1})_2$ (**52**) (Scheme 15) was synthesized by the reaction of 4,6-di-*tert*-butyl-*N*-phenyl-*o*-aminophenol with anhydrous CuCl in CH_3CN solution in the presence of air and triethylamine [6]. The geometrical parameters (Table 3) in **52** are close to those in mono-ISQ type complexes (Section 3.2) and other *o*-iminobenzosemiquinonato complexes.

The temperature dependence of μ_{eff} (Table S5) indicates a $S = 1/2$ ground state and the occupancy of an excited state with higher spin multiplicity. The copper-ligand exchange coupling is ferromagnetic (due to the orthogonality of $(d_{x2-y2})^1$ mag-

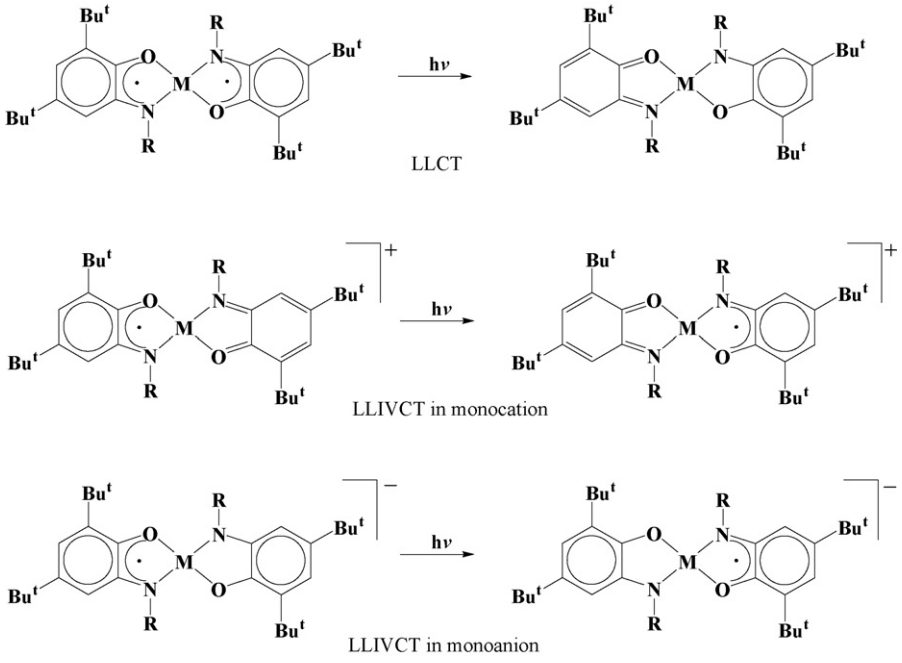

Chart 4. LLCT in square-planar complexes of $M(ISQ)_2$ type. Modified from ref. [62].

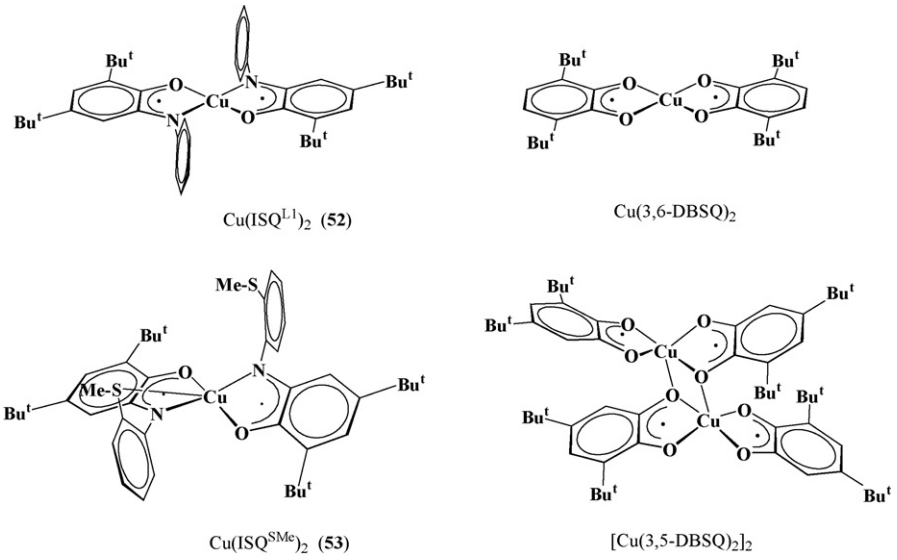

Scheme 15. Structures of copper *o*-iminosemiquinonato **52**, **53** and *o*-semiquinonato complexes [6,77,78].

netic orbital of copper(II) and the π*-MO of radical) while ligand–ligand coupling is strongly antiferromagnetic [6] (see the qualitative Chart 5).

Another bis-*o*-iminobenzosemiquinonato copper complex **53** was non-planar [78] containing two chelating 4,6-di-*tert*-butyl-*N*-(2-methyltiophenyl)-*o*-iminobenzosemiquinolate radical–anion ligands (Scheme 15). The dihedral angle between chelate planes is 32.20(9)°. Additional methylthio-groups of the *N*-aryls are located on one side of the hypothetical complex plane. Supplemental weak coordination of one sulfur to copper is observed (this distance is 3.198(1) Å while the second one is 3.475(1) Å).

The variable-temperature magnetic susceptibility measurements show a doublet ground state of **53** with an antiferromagnetic spin interaction (as in planar copper complex **52**). However, the two situations are different for **52** and **53**. The X-band EPR spectrum of **52** in frozen solvent (CH_2Cl_2 or THF) shows an axial symmetric *g*-factor anisotropy with slight rhombic distortions ($\Delta g = 0.17$, Table S4) with $g_z > g_x$, g_y [6] indicative of dominant antiferromagnetic coupling between radical ligands leading to substantial copper(II) character of the unpaired electron.

In the case of **53**, the X-band EPR spectrum in CH_2Cl_2 solution represents a radical–type spectrum with $g_{iso} = 2.0012$ (Table S4). In frozen state, *g*-anisotropy ($\Delta g = 0.093$, Table S4) is less pronounced than that in **52**. So, EPR data signify the lowest spin state of **53** to be of predominant ligand character in contrast to that one in **52**. As the result, the copper–ligand interaction is strongly antiferromagnetic with $J = -414\ cm^{-1}$, and ligand–ligand exchange J_{12} is also antiferromagnetic but much weaker ($J_{12} = -114\ cm^{-1}$). The remarkable difference in spin interactions of **52** and **53** is probably caused by the non-planar configuration of **53** (contrary to **52**) and, as a consequence, decreasing ligand–ligand and increasing metal–ligand exchange in **53**.

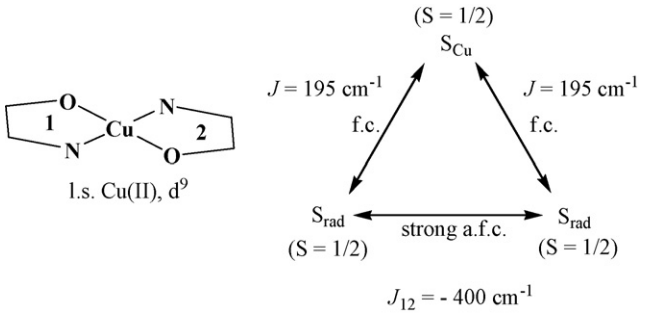

Chart 5. The qualitative scheme of magnetic exchange interactions in **52**.

A mononuclear bis-ligand *o*-benzosemiquinonato copper(II) complex Cu(3,6-DBSQ)$_2$ was described in ref. [69]. This complex is an isostructural analogue of nickel complex Ni(3,6-DBSQ)$_2$ according to cell parameters measurements and space group determination. From the temperature dependence of μ_{eff}, the calculated coupling constants for Cu(3,6-DBSQ)$_2$ are J(SQ-SQ) = $-179\ cm^{-1}$ and J(Cu-SQ) = $100\ cm^{-1}$ [69]. Thus, magnetic features of Cu(ISQ^{L1})$_2$ (**52**) and its SQ analogue Cu(3,6-DBSQ)$_2$ are the same but all exchange interactions in **52** are more substantial.

The copper complex with 3,5-DBSQ is a centrosymmetric dimer [Cu(3,5-DBSQ)$_2$]$_2$ [77] (Scheme 15) where the copper atom lies in a strongly distorted square-planar environment. Two Cu(3,5-DBSQ)$_2$ fragments are coupled into a dimer by bridge oxygen atoms which occupy axial sites towards the hypothetical CuO_4 plane of each fragment. The copper-bridge oxygen distance is 2.416 Å and the C–O bonds in the ligands are typical for the semiquinone form (1.290–1.296 Å). This is formally a bridged dimeric bis-semiquinonato copper(II) complex whose magnetic properties were interpreted in ref. [79]. The ground state of the Cu(3,5-DBSQ)$_2$ moiety is a doublet like the mononuclear analogue Cu(3,6-DBSQ)$_2$. The interaction between the Cu(SQ)$_2$ fragments in the dimer is weak antiferromagnetic.

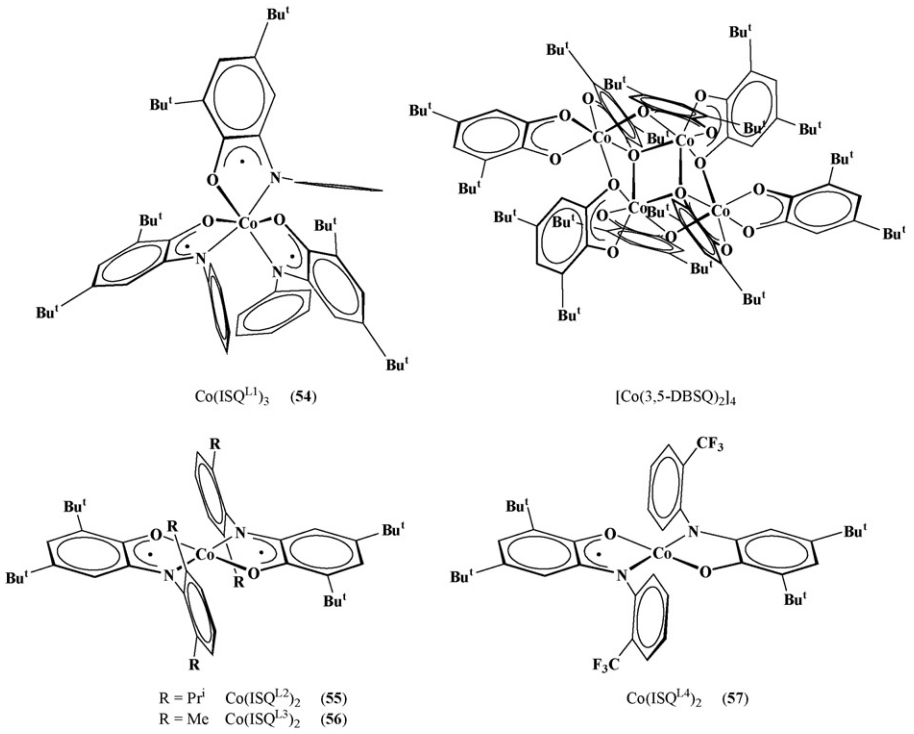

Scheme 16. Structures of *o*-iminobenzosemiquinonato **54**–**57** and *o*-benzosemiquinonato $[Co(3,5\text{-}DBSQ)_2]_4$ cobalt complexes [53,60,65,67].

6.5. Cobalt

Wieghardt and co-workers reported [65] X-ray data and magnetochemistry for the first tris-ligand complex with *o*-iminobenzoquinone ligands tris-(4,6-di-*tert*-butyl-*N*-phenyl-*o*-iminobenzosemiquinonato)cobalt(III) $Co(ISQ^{L1})_3$ (**54**). Cobalt(III) is bound to three 4,6-di-*tert*-butyl-*N*-phenyl-*o*-iminobenzosemiquinone radicals ISQ^{L1} in a distorted octahedral fashion (Scheme 16). Selected bond distances for this complex and other homoleptic *o*-iminobenzoquinonato complexes are listed in Table 3. The C–N bonds of the chelate ring are significantly shorter than C_{phenyl}–N (1.420 ± 0.005 Å). Average C–O distances are also shorter than expected for catecholates [1,32]. Six C–C distances of the *o*-quinone part show distortion of quinoid type while C–C bonds of *N*-phenyl substituent are identical within experimental error (1.39 ± 0.01 Å). The Co–O bonds and Co–N bonds indicate a low-spin configuration of Co(III) (d^6, $S_{Co} = 0$).

The low-temperature value of μ_{eff} for **54** (3.71 μ_B at 15 K) is close to expected for a $S = 3/2$ ground state where three ISQ radical–anions are ferromagnetically coupled. The ferromagnetic coupling is caused by the orthogonality of three π*-magnetic orbitals in octahedral geometry (see the qualitative Chart 6). The nonequivalence of the *J* values is justified by the difference in dihedral angles between the chelate ring planes: while the first one is 92.7° (the closest to 90°, clear orthogonality), the other two are 79.4° and 82.8° giving rise to antiferromagnetic contribution to the overall coupling.

The literature data on *o*-quinone cobalt complexes cover the coordination chemistry of 3,5-DBBQ, 3,6-DBBQ and 9,10-PhenQ.

The mononuclear tris-ligand octahedral cobalt complex $Co(3,6\text{-}DBSQ)_3$ is formed in the case of 3,6-*tert*-butyl-*o*-benzoquinone 3,6-DBBQ [80]. The Co–O, C–O and C–C bond distances of the chelate rings allow us to interpret this complex as a tris-semiquinonato cobalt(III) complex. An EPR spectrum of $Co(3,6\text{-}DBSQ)_3$ in solution is not observed. The temperature dependence of μ_{eff} for $Co(3,6\text{-}DBSQ)_3$ (1.82 μ_B (5 K), that is close to 1.73 μ_B of $S = 1/2$, and 3.04 μ_B (350 K) near the value 3 μ_B expected for three noninteracting $S = 1/2$ centers) indicate an $S = 3/2$ system at higher temperature. An EPR spectrum of $Co(3,6\text{-}DBSQ)_3$ powder is a broadened line with $g = 2.108$ without HFC with ^{59}Co ($I = 7/2$, 100%). The line broadening increases with temperature from values of ~500 G (at 100 K) to ~2000 G (at 260 K), the integral intensity decreases over this temperature range. The temperature dependence of μ_{eff} for $Co(3,6\text{-}DBSQ)_3$ indicates a doublet ground state with a weak antiferromagnetic exchange between three equivalent radical SQ ligands mediated by low-spin cobalt(III).

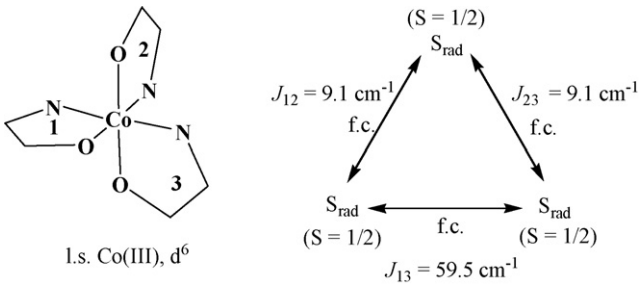

Chart 6. The qualitative scheme of magnetic exchange interactions in **54**.

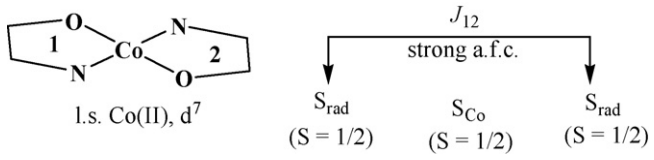

Chart 7. The qualitative scheme of magnetic exchange interactions in **55**, **56**.

Fifteen years prior to the publication of results on Co(3,6-DBSQ)$_3$, the same authors [67] demonstrated that the bis-semiquinonato complexes Co(3,5-DBSQ)$_2$ and Ni(3,5-DBSQ)$_2$ are more structurally complicated. Note that 3,5-di-*tert*-butyl-*o*-benzoquinone is the closest *o*-quinone analogue of 4,6-di-*tert*-butyl-*N*-phenyl-*o*-iminobenzoquinone IBQ^{L1}. The X-ray structural analysis was made for Co(3,5-DBSQ)$_2$.

Co(3,5-DBSQ)$_2$ is a centrosymmetric tetramer [Co(3,5-DBSQ)$_2$]$_4$ (Scheme 16). The cobalt atom lies in a strongly distorted environment consisting of ordinary chelate-bonded *o*-semiquinonato ligands and bridge ligands connecting two and three metallic centers. The C–O groups with bridging oxygen do not have adjacent *tert*-butyl substituents. The C–O and C–C bond distances in the chelate ring are typical for a radical semiquinone form. The exception, the C–O bond with the oxygen bound to three cobalt centers (1.328 Å), is rationalized to be a consequence of charge redistribution in the quinone fragment for the bonding provision of one oxygen with three metal atoms. The average Co–O bond distances are in good agreement with high-spin cobalt(II) in octahedral environment. The magnetic features were interpreted in ref. [4].

As shown above, cobalt(II, III) usually form six-coordinate compounds. However, the use of *N*-aryls in *o*-iminobenzoquinones allow us to reduce the coordination number and synthesize complexes of other structures.

In the case of 4,6-di-*tert*-butyl-*N*-(2,6-dialkylphenyl)-*o*-iminobenzoquinones (where alkyl is *iso*-propyl or methyl), the cobalt complexes formed are four-coordinated bis-ligand Co(ISQ)$_2$ species (Scheme 16) [53]. Complexes Co(ISQ^{L2})$_2$ (**55**) and Co(ISQ^{L3})$_2$ (**56**) have square-planar geometry (X-ray) with *trans*-orientation of ligands and consist of low-spin cobalt(II) (d^7, $S_{Co} = 1/2$) and two *o*-iminobenzosemiquinones ($S_{rad} = 1/2$) (magnetochemistry, IR and UV spectroscopy). The intraligand bonds lengths in **55** (Table 3) lie in the upper limit of the range typical for *o*-iminobenzosemiquinone – radical–anion coordination mode and seem to be intermediate between the ISQ and AP coordination mode. This situation resembles the case of nickel, palladium and platinum complexes **44**–**48**. All complexes show strong antiferromagnetic ligand–ligand coupling.

According to EPR spectroscopy (Table S4) and magnetic susceptibility data (Table S5) the complexes possess a metal-localized $S = 1/2$ ground state. This situation is the result of the strong antiferromagnetic coupling, known in literature [6,35,81], between two unpaired electrons on π*-MO of two ligands mediated by the metal 3d$_\pi$ and 4p$_z$ orbitals (see the qualitative Chart 7).

Another *o*-iminoquinone ligand contains a 2-trifluoromethylphenyl substituent at the nitrogen atom [60]. Complex Co(ISQ^{L4})$_2$ (**57**) also has a planar configuration (Scheme 16). The ligands are equivalent with geometrical parameters similar to those in Co(ISQ^{L2})$_2$ (**55**) with only minor lengthening of the C–O and C–N bonds (see Table 3). However based on X-ray and EPR the authors proposed the charge distribution of complex **57** to be [Co^{III}(ISQ^{L4})(AP^{L4})]. Complex **57** has a rhombic X-band EPR spectrum in frozen CH_2Cl_2 solution (Table S4) with no observable ^{59}Co hyperfine splitting. The magnetic moment of **57** is 2.35 μ_B in the temperature range of 80–298 K [60].

However, the description of **57** as [Co^{III}(ISQ^{L4})(AP^{L4})] is not incontrovertible. The second possible description of **57** may be [Co^{II}(ISQ^{L4})$_2$]. Theoretically, [Co^{III}(ISQ^{L4})(AP^{L4})] should have a ligand-centered unpaired electron and, as a consequence, a normal EPR spectrum with small anisotropy and $g \sim 2.00$. But this is not the case (see above). For explanation of the large *g*-anisotropy, the authors suppose the possibility of antiferromagnetic exchange between cobalt(III) with $S = 1$ local spin state and ISQ radical with $S_{rad} = 1/2$ leading to a metal centered doublet state. However, in the square-planar geometry of cobalt(III) with $S = 1$, the unpaired electrons occupy MOs with d$_{x^2-y^2}$ and d$_{z^2}$ character whose symmetry does not allow them to interact with ligand π-MOs. Thus there is reason to doubt the possibility of such a supposition.

The square planar Co(ISQ)$_2$ complexes **55**, **56** display very intense LLCT absorption in the ~900 nm region. This LLCT with $\varepsilon \sim (1–7)\ 10^4\ M^{-1}\ cm^{-1}$ is typical for all M(ISQ)$_2$ type complexes but it is shifted to long-wave region (1200–2000 nm) in mixed-valence M(ISQ)(AP) species. Complex **57** also displays this LLCT at 916 nm ($\varepsilon = 2.5 \times 10^4\ M^{-1}\ cm^{-1}$), but also exhibits weak and broad absorption at 1600 nm ($\varepsilon = 2.5 \times 10^3\ M^{-1}\ cm^{-1}$). Thus, it is possible that **57** is [Co^{II}(ISQ^{L4})$_2$] rather than [Co^{III}(ISQ^{L4})(AP^{L4})].

Wieghardt and co-workers also reported the reduced derivative [Co^{III}(AP^{L4})$_2$]$^-$[CoCp$_2$]$^+$ (**57a**) where [CoCp$_2$]$^+$ is the cobaltocenium cation [60] characterized by X-ray analysis. As shown in Table 3, the C–N and C–O bond lengths in the monoanion unit [Co^{III}(AP^{L4})$_2$]$^-$ of **57a,** possessing an $S = 1$ ground state, are slightly (0.011–0.015 Å) longer than those in neutral complex **57**. Six C–C bonds are equidistant at 1.40 Å within experimental error. Thus, the geometric characteristics of ligands in **57a** indicate the presence of two dianionic (AP^{L4})$^{2-}$ ligands.

6.6. Iron

The tris-*o*-iminobenzosemiquinonato iron complexes Fe(ISQ^{L1})$_3$ (**58**) [7], Fe(ISQ^{L5F})$_3$ (**59**) and Fe(ISQ^{L5tBu})$_3$ (**60**) [66] resemble the cobalt analogue **54** [65] in their structures (Scheme 17). As one can expect, the *o*-iminobenzosemiquinone part of O,N-coordinated ligands exhibits different C–C bond distances in the ring indicating a typical quinoid pattern (Table 3). Additionally, the average C–O and C–N bond lengths, at 1.28–1.30 Å and 1.33–1.35 Å, respectively, are significantly shorter than the corresponding single C–O and C–N bonds, and they lie in the typical range for radical–anions with one-and-half C–O and C–N bonds. Thus, the structural parameters of ligands (Table 3) in **58**–**60** are typical for *o*-iminobenzosemiquinonato radical–anion ligands.

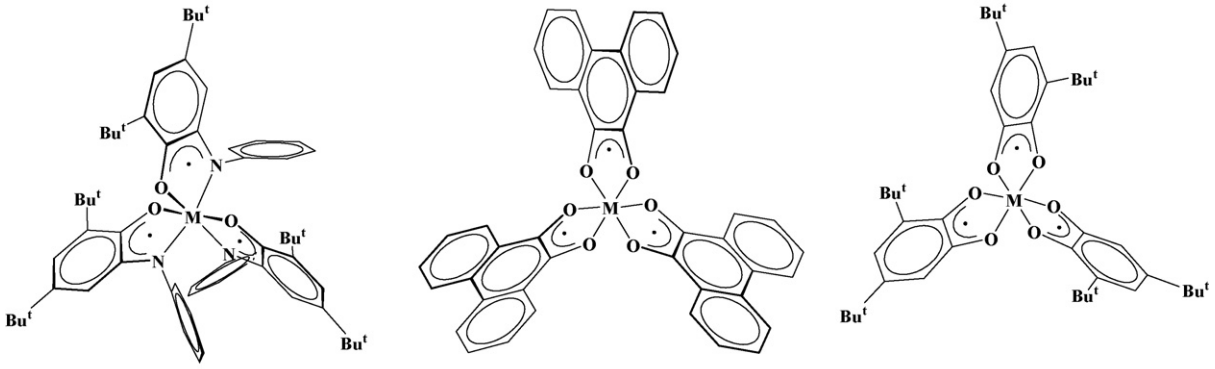

Scheme 17. Structures of *o*-iminobenzosemiquinonato **58**, **61** and *o*-benzosemiquinonato complexes of iron and chromium [7,82].

The Fe–O and Fe–N distances observed for **58**–**60** reveal remarkable differences. The Fe–O and Fe–N bonds for **58** and **59** at 100 K, and for **60** at 293 K (see Table 3) are in good agreement with a high-spin Fe(III) assignment, but these bonds for **60** at 100 K are significantly shorter supporting the presence of low-spin Fe(III) ion in **60** at 100 K. Thus, the authors [66] suppose that the spin state of iron in **60** changes from $S = 5/2$ at 293 K to $S = 1/2$ at lower temperatures.

Magnetic susceptibility measurements and Mössbauer spectroscopic studies performed for these iron complexes have made clear this point. Low-temperature values of μ_{eff} for Fe(ISQ^{L1})$_3$ (**58**) and Fe(ISQ^{L5F})$_3$ (**59**) (Table S5) are close to spin-only value of system with two unpaired electrons on one center ($S = 1$, 2.83 μ_B). The increasing μ_B with temperature rise indicates the onset of thermal population of excited spin manifolds. The antiferromagnetic exchange between π*-MO unpaired electrons of three ISQ radical–anions and d_π-electrons of high-spin Fe(III) (d^5, $S = 5/2$) in **58** and **59** causes the $S = 1$ ground state (see the qualitative Chart 8, top) [7,66].

A significantly different situation takes place in the case of the iron complex Fe(ISQ^{L5tBu})$_3$ (**60**). The weak paramagnetism of this complex at low temperature ($\mu_{eff} \approx 1\ \mu_B$ at 10–120 K) was determined to be the result of a paramagnetic impurity (3% of $S = 5/2$) [66]. Above 130 K, the μ_{eff} increases rapidly reaching 2.83 μ_B at about 250 K. The magnetic behavior of **60** reveals the presence of a phase transition in the solid sample at approximately 175 K, corroborating the spin crossover assumed earlier for the central iron(III) of **60** basing on the X-ray diffraction data at high and low temperatures.

The zero-field Mössbauer spectra of solid **58** and **59** recorded at 80 K are quite similar and typical for octahedral high-spin iron(III) complexes (isomer shift $\delta = 0.54$ mm s^{-1} for both complexes, quadrupole splitting $\Delta E_Q = 1.035$ for **58** and 0.88 mm s^{-1} for **59**). Mössbauer spectroscopic data for **60** were collected in the temperature range of 4.2–297 K. At low temperature (4.2–160 K), isomer shift is small ($\delta = 0.13$–0.12 mm s^{-1}) with large quadrupole splitting ($|\Delta E_Q| = 1.34$–1.37 mm s^{-1}). At higher temperature (240–297 K), the isomer shift increases ($\delta = 0.38$–0.40 mm s^{-1}) while the quadrupole splitting parameter decreases ($|\Delta E_Q| = 0.75$–0.92 mm s^{-1}). The low-temperature Mössbauer parameters of **60** indicate the presence of low-spin iron(III) with $S_{Fe} = 1/2$. In the high-temperature (above 250 K), the Mössbauer parameters of **60** are close to those of complexes **58** and **59** (at 290 K, $\delta = 0.40$ mm s^{-1}, $\Delta E_Q = 0.89$ mm s^{-1}), evidence of high-spin state $S_{Fe} = 5/2$. In summary, the Mössbauer spectroscopic data confirm the presence of the typical high-spin Fe(III) ↔ low-spin Fe(III) equilibrium for compound **60** with fast spin crossover mechanism [66]. The singlet ground state observed at low temperatures arises from the competing antiferromagnetic interactions of the low-spin iron(III) (t_{2g}^5, $S_{Fe} = 1/2$) and the three equivalent radicals ($S_{rad} = 1/2$) and super-exchange interaction between the ligand radicals (Chart 8, bottom). This singlet ground state owes its origin to the condition $|J'| > 1/3$

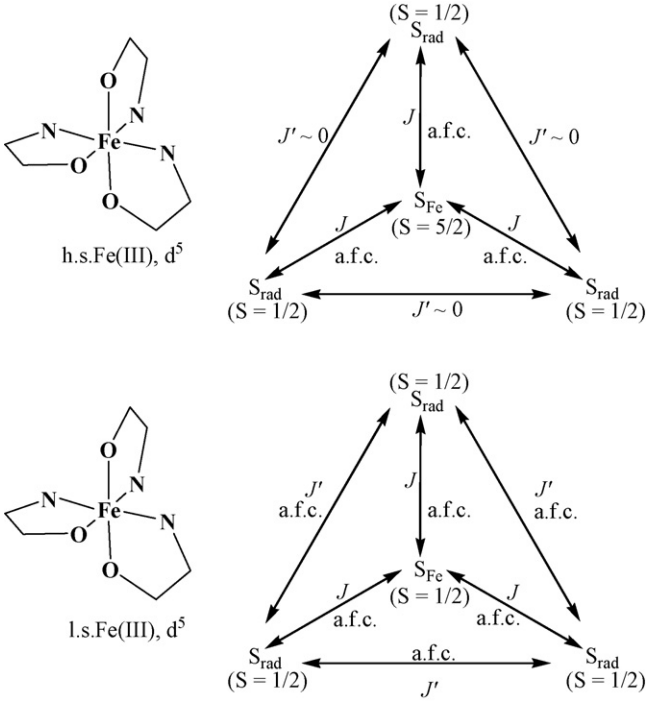

Chart 8. The qualitative scheme of magnetic exchange interactions in **58**, **59** (top) and **60** (bottom).

$|J|$, where J' represents the radical–radical coupling and J is the antiferromagnetic iron–radical coupling.

The electronic spectra of these complexes show intense LMCT transitions at 420–440 nm ($\varepsilon \sim 6$–$7 \times 10^3\ M^{-1}\ cm^{-1}$) and LLCT at 740–750 nm ($\varepsilon \sim 9 \times 10^3\ M^{-1}\ cm^{-1}$), common for this type of complex ($M(ISQ)_n$).

What about iron *o*-benzosemiquinone complexes? According to [82], Fe(9,10-PhenSQ)$_3$ also has a distorted octahedral structure and includes three *o*-semiquinonato radical–anions bound to iron(III). The Mössbauer spectra of complexes Fe(9,10-PhenSQ)$_3$, Fe(*o*-Cl$_4$SQ)$_3$ and Fe(3,5-DBSQ)$_3$ show the high-spin state of iron(III) ($S_{Fe} = 5/2$). In complexes of Fe(SQ)$_3$ type, the antiferromagnetic metal–ligand coupling (with J(Fe-SQ) $< -100\ cm^{-1}$) [82] leads to a triplet ground state.

In addition to the mononuclear iron complex Fe(3,5-DBSQ)$_3$, 3,5-di-*tert*-butyl-*o*-benzoquinone also forms a tetranuclear compound [Fe(3,5-DBSQ)(3,5-DBCat)]$_4$ [83] with a tetrameric structure like its cobalt and nickel analogues but each FeL_2 moiety contains ligands in different oxidation states (radical–anion *o*-semiquinone and dianion catecholate).

6.7. Chromium

The tris-*o*-iminobenzosemiquinonato chromium Cr(ISQ^{L1})$_3$ (**61**) complex [7] resembles cobalt **54** and iron **58**–**60** analogues in their structures (Scheme 17) (X-ray studies) [7,65,66]. Selected bond lengths in **61** are listed in Table 3. Strong antiferromagnetic coupling of three ISQ radical–anions with the singly occupied d_π-AO of high-spin Cr(III) (d^3) in **61** leads to the observed $S = 0$ ground state for the chromium complex. Calculated values of the metal–ligand antiferromagnetic coupling constant are given in Table S5. The electronic spectrum of **61** is dominated by an intense sharp band at ~520 nm (with $\varepsilon = 1.7 \times 10^3\ M^{-1}\ cm^{-1}$) assigned to a spin forbidden transition of a spin flip in the ground state [84] intensified due to the strong antiferromagnetic exchange coupling between the Cr(III) and the three ISQ radicals. The same electronic spectroscopic features were observed in [Cr(CTH)(3,5-DBSQ)]$_2$Cl(PF$_6$)$_3$, [Cr(CTH)(*o*-Cl$_4$SQ)](PF$_6$) [85] and in the Cr(SQ)$_3$ series [86–88]. The corresponding LLCT band is observed at ~750 nm. These results resemble closely those of *o*-semiquinone chromium complexes.

Tris-ligand chromium complexes of the Cr(SQ)$_3$ type are among early examples of polysemiquinone complexes [86]. X-ray data for Cr(3,5-DBSQ)$_3$ [87] and Cr(*o*-Cl$_4$SQ)$_3$ [88] show these compounds to be monomeric with octahedral structures. The C–O bonds average 1.28(1) Å and are typical for the radical–anion form of the ligands. Noteworthy, these bonds are shorter than the C–O bond in the molybdenum complex [Mo(*o*-Cl$_4$Cat)$_3$]$_2$ which is a dimer [89] with the tetrachloro-*o*-catecholate dianion. Complex Cr(9,10-PhenSQ)$_3$ was also characterized structurally (Scheme 17) [1].

The variable-temperature magnetic susceptibility measurements for chromium *o*-semiquinone complexes are reported in ref. [82,90], theoretical studies of semiquinonato chromium complexes made in ref. [91]. Complex Cr(3,5-DBSQ)$_3$ is diamagnetic, complexes Cr(*o*-Cl$_4$SQ)$_3$ and Cr(9,10-PhenSQ)$_3$ exhibit weak paramagnetism (1.08 μ_B and 1.15 μ_B respectively at 285 K; 0.38 μ_B and 0.30 μ_B at 4.2 K).

Thus, Cr(ISQ)$_3$ and Cr(SQ)$_3$ complexes contain chromium(III) ($S_{Cr} = 3/2$) bound to three paramagnetic radical ligands with strong antiferromagnetic metal–ligand coupling.

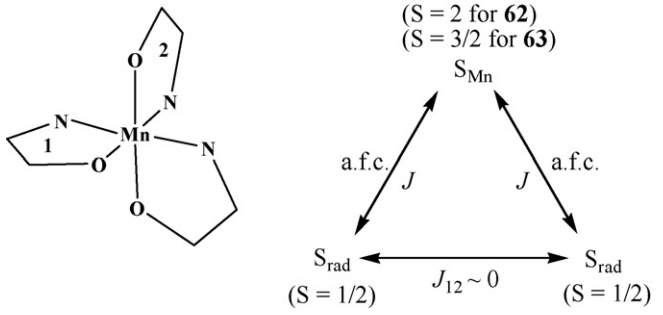

Chart 9. The qualitative scheme of magnetic exchange interactions in **62** and **63**.

6.8. Manganese

Wieghardt and co-workers [92] have reported two, distorted octahedral, *o*-iminobenzoquinonato manganese MnL_3 complexes with different oxidation levels of metal and ligands.

The first complex (**62**) is Mn^{III}(ISQ^{L1})$_2$(APH^{L1}) containing two *o*-iminobenzosemiquinonato radical–anions (ISQ^{L1}) and one *o*-aminophenolato anion (APH^{L1}) as shown on Scheme 18. The geometrical characteristics of the first two ligands lie in ranges characteristic for ISQ (Table 3). The third ligand contains the protonated nitrogen atom (sp^3 hybridization), with C–O (1.34 Å) and C–N (1.42 Å) bonds typical of phenolates and aromatic amines respectively. Furthermore, the C–C bonds of the aminophenolato are equal (1.39 ± 0.015 Å).

The second (**63**) also contains two O,N-coordinated *o*-iminobenzosemiquinonato ligands which reveal the same structural features as the ISQ ligands in **62** [92]. However, unlike Mn^{III}(ISQ^{L1})$_2$(APH^{L1}) (**62**), the third ligand in **63** is not protonated at nitrogen, rather the N atom has sp^2 hybridization (the sum of angles at nitrogen is 355.5°). Six C–C distances of the carbon cycle of third ligand are almost equal (on average, 1.40 ± 0.015 Å), the C–O and C–N bonds are typical for an O,N-coordinated *o*-amidophenolato dianion (Table 3). The observed Mn–O and Mn–N distances confirm an oxidation level of manganese Mn(IV), d^3; they are shorter than those in **62**. Thus, the molecular structure of **63** can be assigned as Mn^{IV}(ISQ^{L1})$_2$(AP^{L1}) (Scheme 18).

The magnetic moments μ_{eff} (Table S5) indicate that the ground states of **62** and **63** are a triplet ($S = 1$) and doublet ($S = 1/2$) respectively. The ligand–ligand exchange constant J_{12} is close to zero for both complexes while metal–ligand exchange coupling was calculated to be strong for both complexes (Chart 9, Table S5).

A solution of **63** in CH_2Cl_2 at 298 K reveals an isotropic EPR spectrum with $g_{iso} = 1.983$ and HFS on one ^{55}Mn and on three nitrogen atoms ^{14}N (Table S4) confirming a metal-centered

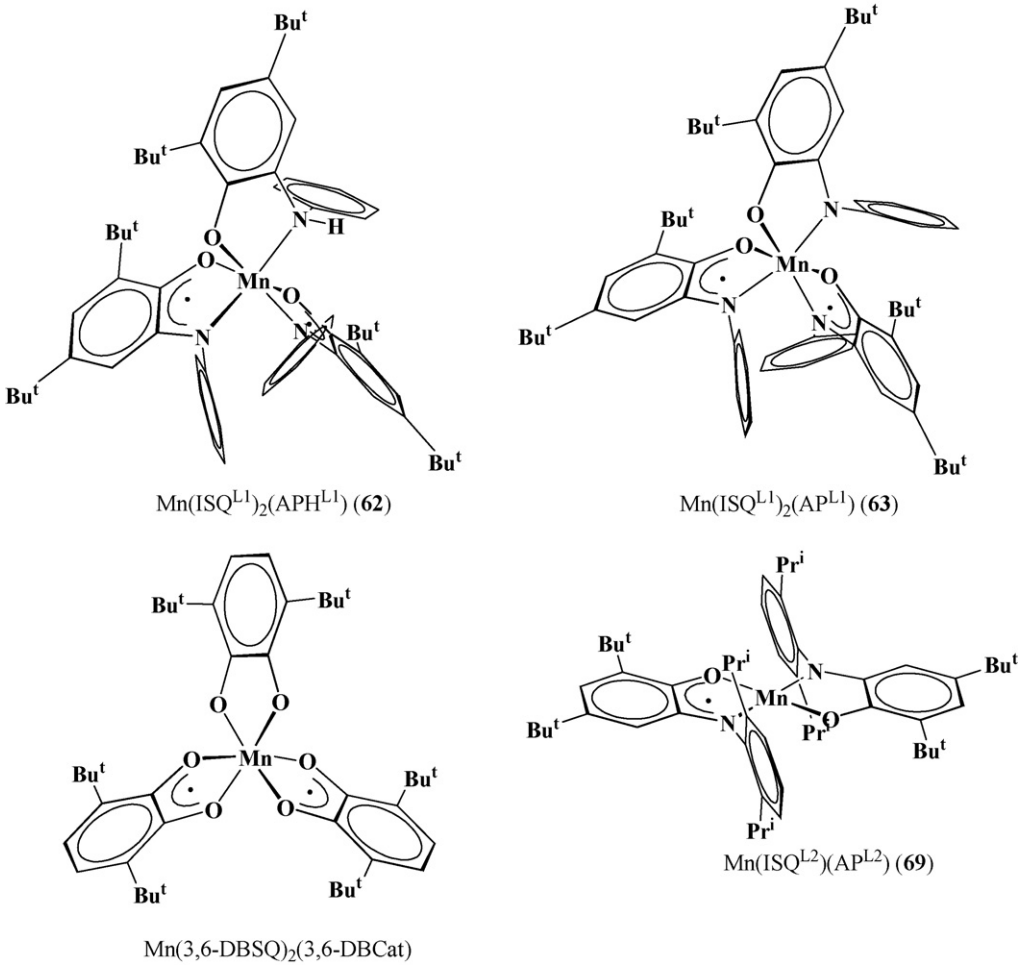

Scheme 18. The structures of *o*-iminobenzosemiquinonato **62**, **63**, **69** and *o*-benzosemiquinonato Mn(3,6-DBSQ)$_2$(3,6-DBCat) manganese complexes [61,92,93].

ground state $S = 1/2$ for **63**. At 10 K, the EPR spectrum of the frozen solution displays rhombic symmetry. These results are close to EPR spectroscopic data for the *o*-quinonato analogue Mn^{IV}(3,6-DBSQ)$_2$(3,6-DBCat) mentioned below [93].

The principal differences between the similar structured *o*-iminoquinonato **63** and *o*-quinonato complexes [$Mn^{IV}(ISQ^{L1})_2(AP^{L1})$ and Mn^{IV}(3,6-DBSQ)$_2$(3,6-DBCat)] can be deduced from NIR studies. The NIR spectrum of the *o*-quinonato complex contains a broad charge transfer band with maximum at 2300 nm which intensifies with decrease of temperature. This was explained as the result of valence tautomerism between the redox-isomers Mn^{IV}(3,6-DBSQ)$_2$(3,6-DBCat) and Mn^{III}(3,6-DBSQ)$_3$ in the solid. In contrast to the latter, the *o*-iminobenzoquinonato complex $Mn^{IV}(ISQ^{L1})_2(AP^{L1})$ (**63**) has no corresponding temperature dependent absorption band in the region of 1100–2500 nm. In other words, there is no charge redistribution. The oxidation levels of the ligands (two *o*-iminobenzosemiquinones and one *o*-amidophenolate) and Mn(IV) remain fully localized in the 2–300 K temperature range. The antiferromagnetic interactions between radical ligands and central Mn(IV) ion in the *o*-iminobenzoquinonato complex **63** are significantly stronger than in its *o*-benzoquinonato analogue. This is explained [92] by greater covalency of the Mn–N bonds in $Mn^{IV}(ISQ^{L1})_2(AP^{L1})$ (**63**) as compared with corresponding Mn–O bonds in Mn^{IV}(3,6-DBSQ)$_2$(3,6-DBCat).

A series of manganese(III) complexes **64–68,** identical with **63,** is described in ref [68]. All these complexes contain the (3,5-disubstituted-*N*-aryl)-4,6-di-*tert*-butyl-*o*-iminobenzoquinonato type ligand derived from APH_2^{L5X} (X = Bu^t, Me, OMe, CF_3, Cl) and can be described as $Mn(ISQ^{L5X})_2(AP^{L5X})$ complexes.

Application of the more sterically hindered 4,6-di-*tert*-butyl-*N*-(2,6-di-*iso*-propylphenyl)-*o*-iminobenzoquinone IBQ^{L2} generates the unusual four-coordinate manganese complex $Mn(ISQ^{L2})(AP^{L2})$ (**69**) (Scheme 18) [61]. The complex was obtained by the reaction of $Mn_2(CO)_{10}$ with the neutral *o*-iminobenzoquinone in a non-polar solvent (toluene) to avoid the formation of manganese complexes with solvent in the coordination sphere. According to spectroscopic data, the complex consists of manganese(III) and ligands in different oxidation states. One ligand is *o*-iminobenzosemiquinolate ISQ^{L2} while the second one is the dianionic *o*-amidophenolate AP^{L2}. The NIR spectrum of **69** contains a broad LLCT band with maximum at 1640 nm (6100 cm^{-1}). In the case of mixed valent complexes containing both mono- and di-anion, similar bands at 2000–2500 nm are attributed to ligand–ligand charge transfer

[72,81]. In solution, complex **69** has no EPR spectrum. However, the solid **69** at low temperature (120 K) has an EPR spectrum (Table S4) which is typical for manganese(III) systems with an $S = 3/2$ state [94]. At this temperature, the effective magnetic moment of **69** μ_{eff} is 3.08 μ_B. At 5 K μ_{eff} is 1.96 μ_B indicating a doublet ground state. Such behavior can be rationalized by the occupancy of an excited state with higher spin multiplicity at increasing temperature.

X-ray studies of **69** give interesting results. It is centrosymmetric square-planar molecule. The chelate ring bond lengths which may indicate the valence state of the ligand are an average between radical–anionic *o*-iminobenzosemiquinones and dianionic *o*-amidophenolates: the C–O and C–N bond lengths are 1.326(4) and 1.368(3) Å respectively. The two ligands in **69** are crystallographically identical. The six-membered carbon rings in the quinone part of ligands display quinoid distortion but it is feebly marked in comparison with typical *o*-iminosemiquinones; the C–C bond length varies in the range 1.383(3)–1.421(3) Å (Table 3). In typical radical–anions ISQ, this range is 1.36–1.43 Å, in dianions AP^{2-} 1.39–1.42 Å [6,7,35,53,92]. The structural equivalence is explained by the formation of a molecular orbital delocalizing over both ligands. The structure of **69** may be described as the combination of two resonance forms:

$$(ISQ^{L2})Mn^{III}(AP^{L2}) \leftrightarrow (AP^{L2})Mn^{III}(ISQ^{L2}).$$

As in the case of cobalt and nickel, the reaction of $Mn_2(CO)_{10}$ with different kind of quinones (3,5- or 3,6-DBBQ) yields different products. A tetrameric manganese(II) complex $[Mn^{II}(3,5\text{-DBSQ})_2]_4$ was isolated [5] with structure similar to those of the cobalt and nickel analogues. Magnetochemical studies have shown the antiferromagnetic metal–ligand exchange therein.

With 3,6-DBBQ, the monomeric tris-ligand complex $Mn^{IV}(3,6\text{-DBSQ})_2(3,6\text{-DBCat})$ was isolated [93] (Scheme 18). X-ray data show this complex to be of weakly distorted structure. The short interatomic distances Mn–O and geometrical parameters of the organic ligands indicate the formation of a manganese(IV) complex containing ligands in different oxidation states.

As mentioned above, a temperature-dependent LLCT band for $Mn^{IV}(3,6\text{-DBSQ})_2(3,6\text{-DBCat})$ is observed in the NIR at 2300 nm (this band would not be observed in the case of formation of a manganese(III) complex $Mn^{III}(3,6\text{-DBSQ})_3$). This fact was interpreted by authors as the shift of charge distribution to formation of the manganese(III) redox-isomer:

$$Mn^{IV}(3,6\text{-DBSQ})_2(3,6\text{-DBCat}) \rightleftarrows Mn^{III}(3,6\text{-DBSQ})_3$$

The ground state of $Mn^{IV}(3,6\text{-DBSQ})_2(3,6\text{-DBCat})$ is a doublet ($S = 1/2$) with a metal localized unpaired electron according to anisotropic EPR spectroscopic data. A similar type of redox-isomerism was found for bis-quinone manganese complexes with donor nitrogen ligands [95].

6.9. Vanadium

There are two homoleptic vanadium(V) complexes containing *o*-iminobenzoquinonato ligands [7] forming complexes containing *o*-iminobenzoquinone ligands in different oxidation states similar to the complexes of Mn. The first compound is $V(AP^{L1})_2(ISQ^{L1})$ (**70**) synthesized from $VCl_3{\cdot}(THF)_3$ and *o*-aminophenol $APH_2{}^{L1}$ (molar ratio was 1:3) in acetonitrile in the presence of Et_3N and air (yield 55%). An X-ray study of **70** has shown the presence of two ligands with identical oxidation level and another which is distinct. This third ligand has C–O and C–N bonds which are shorter than the corresponding bonds in the other two ligands and has the quinoid type distortion typical for the *o*-iminosemiquinonato form of the ligand. The two identical ligands have geometrical parameters close to those expected for an O,N-coordinated dianion *o*-amidophenolate $(AP^{L1})^{2-}$.

The second complex – $V(AP^{L1})_2(APH^{L1})$ (**71**) was prepared by the reaction of *o*-aminophenol with $VO(SO_4)$ $5H_2O$ also in acetonitrile in the presence of Et_3N and air (yield 26%). The presence, in this complex, of the *o*-aminophenolato ligand APH was determined from the sp^3 hybridized nitrogen atom with bound hydrogen (Scheme 19).

The ground state of complex **70** is doublet ($S = 1/2$) (Table S5), with an isotropic EPR spectrum in frozen CH_2Cl_2 solution at 60 K (Table S4) showing the localization of the unpaired electron on the organic ligand with diamagnetic vanadium(V), corroborating the formulation of the complex as $V(AP^{L1})_2(ISQ^{L1})$. In contrast to $V(AP^{L1})_2(ISQ^{L1})$ (**70**), complex $V(AP^{L1})_2(APH^{L1})$ (**71**) is diamagnetic (ground state $S = 0$); it has a resolved ^1H NMR spectrum.

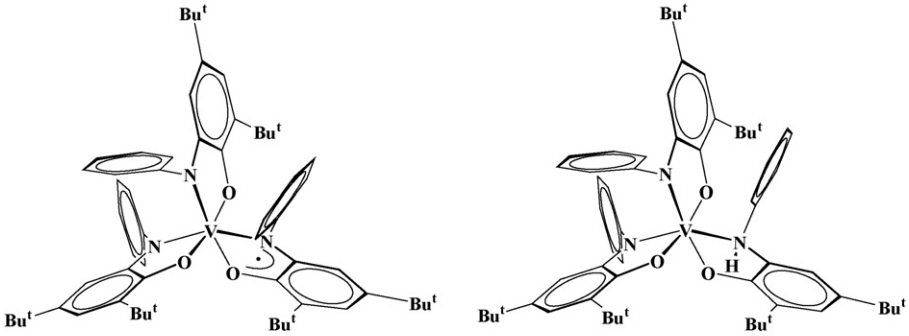

Scheme 19. The structure of vanadium complexes **70** and **71** [7].

We have not found the structurally characterized homoleptic vanadium complexes with *o*-quinone ligands. In [90] the vanadium complex with tetrachloro-*o*-benzoquinonato ligands was described to be a tris-semiquinonato complex of V(III), V(*o*-$Cl_4SQ)_3$, with doublet spin state. The EPR spectrum of this complex in Et_2O solution at ambient temperature consists of eight HFS components with $g_{iso} = 2.0079$ and HFS constant $A_i(^{51}V) = 4.1$ G (^{51}V, $I = 7/2$, 99.8%). Based on the comparison of its EPR and EPR of tris-ligand vanadium complexes with chelating ligands (the HFC on vanadium, with metal-localized unpaired electron, usually lies in the range 60–80 G, for example the EPR spectroscopic parameters of $V(bipy)_3$ [96] and V(1,2-dithiolene)$_3$ [97] are: $g_{iso} = 1.9831$, $A_i(^{51}V) = 84$ G and $g_{iso} = 1.9960$, $A_i(^{51}V) = 61.5$ G, respectively) the authors concluded that the doublet ground state is attained through antiferromagnetic exchange of two unpaired electrons on t_{2g} subshell of V(III), d^2, with two *o*-semiquinone unpaired electrons. In this case, the third SQ ligand causes a $S = 1/2$ state, where the unpaired electron is localized on the organic fragment (*o*-semiquinone). However, two different descriptions of this complex are also possible: V^{IV}(*o*-$Cl_4SQ)_2$(*o*-Cl_4Cat) and V^{V}(*o*-Cl_4SQ)(*o*-$Cl_4Cat)_2$. In both cases the unpaired electron will be a SQ-localized. In the case of V(IV) complex, it requires antiferromagnetic coupling of unpaired electrons of V(IV), d^1, and one SQ ligand. It is difficult to choose between these three descriptions.

7. Coordination compounds of other *o*-iminobenzoquinone derivatives

The chemistry of *N*-aryl-*o*-iminobenzoquinonato complexes based on $APH_2{}^{L1}$-$APH_2{}^{L7}$ and $(AP\text{-}AP)H_3{}^{L9}$ is the most developed in the literature. The coordination chemistry of 4,6-di-*tert*-butyl-*o*-aminophenol $APH_2{}^{L8}$ is less widely presented. However, this ligand was also reported as a good ligand for the complexation of transition elements [98–103] including tris-ligand complexes [98,99] which resemble complexes of $M(SQ)_3$ and $M(ISQ)_3$. Mono-*o*-aminophenolato complexes of this ligand include the four-coordinate complexes $Ir(AP^{L8})(NO)(PPh_3)$ (**72**), $Pt(AP^{L8})X$ (**73**), where X – oxalate, malonate, formate, acetate etc., and $Pt(AP^{L8})(PPh_3)_2$ (**74**) [103] (Scheme 20).

The tridentate ligands $(AP\text{-}AP)H_3{}^{L9}$ and $APH_2{}^{L10}$ form hexacoordinate bis-ligand products. For example, the neutral complex $Mn^{IV}(AP^{L10})_2$ (**75**) (Scheme 21), complex cation $[Mn^{IV}(AP^{L10})(ISQ^{L10})]^+$ in complex $[Mn^{IV}(AP^{L10})(ISQ^{L10})](PF_6)\cdot CH_2Cl_2$ (**76**), and iron complex $[Fe^{III}(ISQ^{L10})_2](ClO_4)\cdot 0.5H_2O$ (**77**) [104].

The quadruplet ground state of $Mn^{IV}(AP^{L10})_2$ (**75**) is caused by high-spin manganese(III) (d^3, $S_{Mn} = 3/2$) with diamagnetic AP ligands (Table S6 of Supplementary information). In the case of $[Mn^{IV}(AP^{L10})(ISQ^{L10})](PF_6)\cdot CH_2Cl_2$ (**76**), one t_{2g} electron of high-spin manganese(III) (d^3, $S_{Mn} = 3/2$) and the unpaired electron of the π*-MO of the O,N,N-coordinated radical–anion ISQ^{L10} ($S_{rad} = 1/2$) are coupled strongly antiferromagnetically producing an $S = 1$ ground state [104].

The EPR spectrum of a frozen solution of $[Fe^{III}(ISQ^{L10})_2](ClO_4)\cdot 0.5H_2O$ (**77**) in CH_2Cl_2 at 10 K with $g = 1.9905$ is evidence of an unpaired electron localized on an organic ligand MO with a weak contribution of metal orbitals. The magnetic and EPR data suggest antiferromagnetic exchange between a t_{2g} unpaired electron of low-spin iron(III), (d^5, $S_{Fe} = 1/2$), and unpaired electrons of two radical ligands yielding ground state $S = 1/2$ of **77**. Mössbauer spectrum of **77** is typical for octahedral low spin ferric ion (the isomer shift $\delta = 0.14$ mm s^{-1}, quadrupole splitting $\Delta E_Q = 1.70$ mm s^{-1}).

Complexes with $(AP\text{-}AP)H_3{}^{L9}$ type ligand have been prepared for such metals as Ni (**78**), Fe (**79**), Co (**80**), Mn (**81**), Ti (**82**), V (**83**) [105–109] (Scheme 21). In Scheme 21, ligand ($AP\text{-}AP^{L9}$) is a trianion, ($AP\text{-}ISQ^{L9}$) is a dianion–radical and ($AP\text{-}IBQ^{L9}$) is a monoanion. The manganese (**81**) and cobalt (**80**) complexes are the most interesting. Two possible electronic configurations of manganese complex **81,** possessing a doublet ground state [106,109], were discussed in ref. [110]. The first is the configuration $Mn^{II}(AP\text{-}IBQ^{L9})_2$ of low-spin manganese(II) (d^5, $S_{Mn} = 1/2$), with two monoanionic diamagnetic ligands like the nickel complex. The second one is the configuration $Mn^{IV}(AP\text{-}ISQ^{L9})_2$ of high-spin manganese(IV) (d^3, $S_{Mn} = 3/2$), with two radical–dianions $[AP\text{-}ISQ^{L9}]^{2-}$ ($S_{rad} = 1/2$) and strong antiferromagnetic metal–ligand exchange. Based on X-ray [106] and EPR data analysis, **81** can be described [110] as intermediate between $Mn^{II}(AP\text{-}IBQ^{L9})_2$ and $Mn^{IV}(AP\text{-}ISQ^{L9})_2$ states.

The electronic structure and behavior of cobalt complex $Co(AP\text{-}IBQ^{L9})(AP\text{-}ISQ^{L9})$ (**80**) was described in a number of ref. [106,107,109,111,112]. Evidently, this cobalt(III) complex is in an equilibrium with a form of cobalt(II) (valence tautomerism) [111] in non-polar solvents (toluene, *sim*-dichloroethane): $Co^{III}(AP\text{-}IBQ^{L9})(AP\text{-}ISQ^{L9}) \leftrightarrow Co^{II}(AP\text{-}IBQ^{L9})_2$.

The titanium complex $Ti^{IV}(AP\text{-}ISQ^{L9})_2$ (**82**) contains two $S = 1/2$ radical centers with negligible spin–spin interaction (Table S6). However, low-temperature value of the μ_{eff} indicates the ferromagnetic ligand–ligand coupling leading to an $S = 1$ ground state [108]. An EPR spectrum of frozen toluene-CH_2Cl_2 solution of **82** at 4 K is also consistent with triplet ground state.

The vanadium complex **83** has an EPR signal with $g = 1.99$ without hyperfine splitting both in solid and in frozen solution at 4.2 K; and reveals a nearly temperature-independent magnetic moment with value of 1.71 μ_B at room temperature [108]. Geometrical characteristics of ligands in **83** are consistent with $V^{IV}(AP\text{-}ISQ^{L9})_2$ formulation. In this case, the observed doublet ground state of complex **83** requires an antiferromagnetic exchange between vanadium(IV) (d^1, $S = 1/2$) and one radical ligand. An alternative assignment of **83** is $V^{V}(AP\text{-}AP^{L9})(AP\text{-}ISQ^{L9})$ consistent with the spectroscopic data, EPR in particular. In this case there is no need for the antiferromagnetic metal–ligand exchange. Authors conclude that the formulation of **83** may be intermediate between $V^{IV}(AP\text{-}ISQ^{L9})_2$ and $V^{V}(AP\text{-}AP^{L9})(AP\text{-}ISQ^{L9})$.

Iron complex **79** contains iron(III) coordinated by anion $(AP\text{-}IBQ^{L9})^-$ and dianion–radical $(AP\text{-}ISQ^{L9})^{2-}$ ligands. No structural difference was found between ligands suggesting charge delocalization over the entire organic region

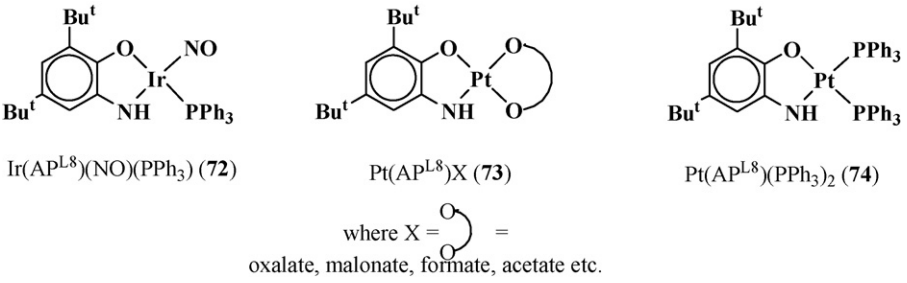

Scheme 20. *o*-Amidophenolato iridium and platinum complexes **72–74** [103].

of the molecule [109]. The Complex has an $S=2$ ground state ($\mu_{eff}=5.25\,\mu_B$ at room temperature) which is a result of antiferromagnetic coupling between the $S=5/2$ iron(III) ($\delta=0.4164(5)$ mm s^{-1} and $\Delta E_Q=0.479(1)$ mm s^{-1} in Mössbauer spectrum) and the $S=1/2$ radical ligand.

Complexes containing one tridentate ligand based on (AP-AP)$H_3{}^{L9}$, namely, cobalt Co(tpy)(AP-ISQ^{L9})Y, where Y = PF_6 (**84**) or BPh_4 (**85**), and nickel Ni(tpy)(AP-ISQ^{L9})PF_6 (**86**) are reported in ref. [113] (tpy = 2,2′:6′,2″-terpyridine). In species **85**, the [Co(tpy)(AP-ISQ^{L9})]$^+$ cation is pseudo octahedral (X-ray) and the structural characteristics are close to those for M(AP-ISQ^{L9})$_2$ complexes [108,109]. A valence tautomeric equilibrium [Co^{III}(tpy)(AP-ISQ^{L9})]$^+$ ↔ [Co^{II}(tpy)(AP-IBQ^{L9})]$^+$ is apparently present. The nickel complex **86** has a triplet ground state.

In the binuclear manganese(IV) complex Mn_2(ISQ-AP^{L11})$_2$(ISQ-ISQ^{L11}) (**87**), two of the three tetradentate ligands of APH_2-$APH_2{}^{L11}$ type are in radical–trianion form (Scheme 22) while third ligand is diradical–dianion [68]. There are two organic radical centers and high-spin manganese(IV), d^3 ($S_{Mn}=3/2$) in complex **87** molecule in each side of three *m*-phenylene fragments. The strong antiferromagnetic exchange between manganese and radical fragments' unpaired electrons gives rise to one $S=1/2$ center on each of two metallic fragment which suffer a weak antiferromagnetic interaction (Table S6) (Chart 10).

The data on similar tris-ligand complexes M_2(ISQ-ISQ^{L11})$_3$ of other metals (M = Fe (**88**), Co (**89**), Cr (**90**)), and also binuclear bis-ligand complexes of M_2(ISQ-ISQ^{L11})$_2$ composition (M = Cu (**91**), Ni (**92**)) are collected in ref. [114]. The cobalt **88** and iron **89** complexes are reported in [115]. All complexes **88–92** contain ISQ radical–anion fragments connected by *m*-phenylene bridges.

The zero-field Mössbauer spectrum of **88** at 80 K ($\delta=0.56$ mm s^{-1} and $\Delta E_Q=1.011$ mm s^{-1}) indicates high-spin iron(III). For cobalt complex **89**, the exchange between organic radical centers in each M(ISQ)$_3$ fragment is weak antiferromagnetic while coupling of two of these fragments is weak ferromagnetic (Table S6, Chart 10). Chromium (**90**) and nickel (**92**) complexes are diamagnetic. Copper compound **91** (Scheme 22) contains two uncoupled copper(II) centers [114]. Two different exchange mechanisms take place in manganese **87** and cobalt **89** complexes: weak antiferromagnetic exchange J_{12} between two MnL_3 fragments in **87** but weak ferromagnetic exchange between two CoL_3 fragments in **89**. It can be due to differences in geometry of ML_3 fragments and the ML_3-ML_3 units – the different dihedral angles between the planes containing the next-neighbor rings (the iminosemiquinonato rings with

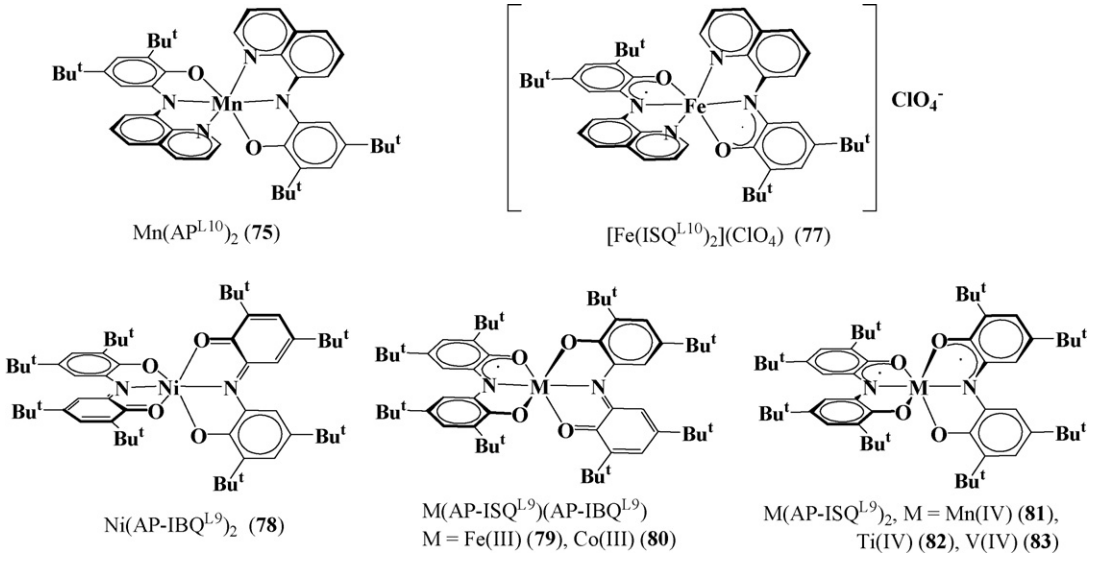

Scheme 21. Complexes **75**, **77** [104], **78–83** [105–110].

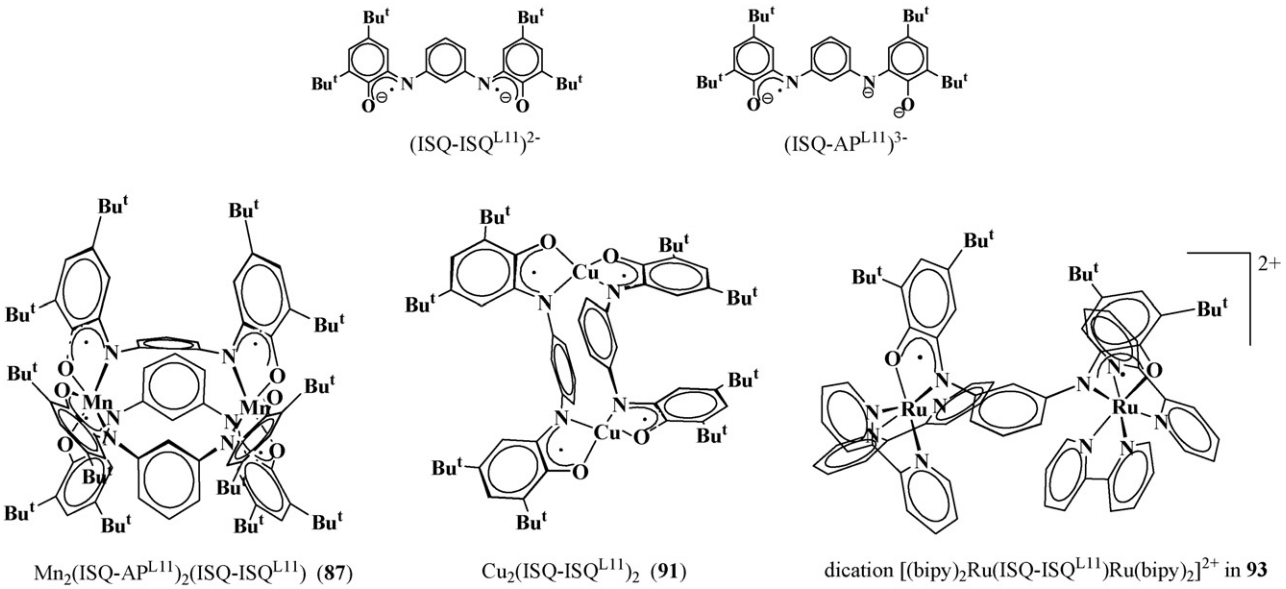

Scheme 22. Diradical dianion, (ISQ-ISQ^{L11})$^{2-}$, and monoradical three-anion, (ISQ-AP^{L11})$^{3-}$, forms of ligand (top) and binuclear manganese (**87**), copper (**91**) and ruthenium (**93**) complexes [68,114,37].

respect to the linker *m*-phenylene rings). Each ligand has two different values of this dihedral angle: in the cobalt complex **89** they are in the range of 66.8–72.1° and 83.3–88.1° (close to orthogonal providing a ferromagnetic coupling mechanism), while in the manganese complex **87** they are 61.6–72.8° and 79.5–83.3° causing a greater antiferromagnetic contribution to the resulting exchange.

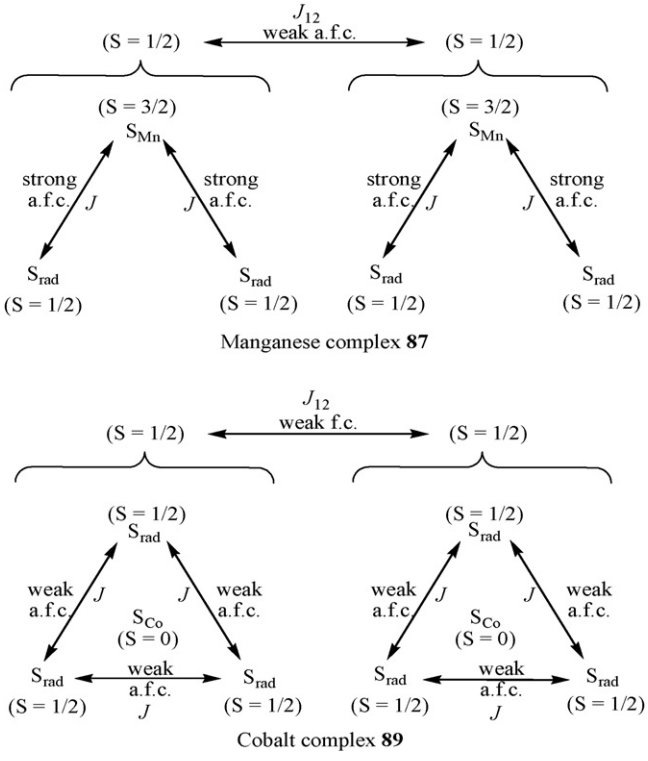

Chart 10. The qualitative scheme of magnetic coupling in binuclear complexes **87** and **89**.

The dinuclear and spin triplet ruthenium(II) complex [(bipy)$_2$Ru(ISQ-ISQ^{L11})Ru(bipy)$_2$](PF$_6$)$_2$ (**93**), Scheme 22, contains iminobenzosemiquinonato fragments [L$_2$Ru(ISQ)]$^+$ which are intramolecularly ferromagnetically coupled ($J = 85\ cm^{-1}$) as established by EPR and variable-temperature magnetic susceptibility measurements [37]. Definitely, ferromagnetic exchange in this case is provided by the orthogonality of *m*-phenylene and *o*-iminobenzosemiquinone rings of ISQ-ISQ^{L11} ligand.

The complexes based on analogous APH$_2$-APH$_2$^{L12} type ligand are limited by copper and zinc derivatives [116]. Both complexes are mononuclear and contain one tetradentate organic ligand in the dianion form – diiminodiphenolate (IP-IP^{L12})$^{2-}$ (Scheme 23). In copper complex Cu(IP-IP^{L12}) (**94**), the divalent copper is coordinated by the ligand in a nearly square-planar coordination polyhedron (also true for the zinc analogue; in the accordance with X-ray data the sum of bond angles around Zn is 361.5°).

The complex **94** was prepared by the reaction of APH$_2$-APH$_2$^{L12} with [Cu^I(MeCN)$_4$](ClO$_4$) in dry methanol in the presence of air. Reaction of the same ligand APH$_2$-APH$_2$^{L12} with Cu^{II}(ClO$_4$)$_2$·6H$_2$O (1:1) in dry methanol under an argon atmosphere with 2 equivalent of NEt$_3$ leads to the neutral complex Cu^{II}(APH-APH^{L12}) (**95**). On the other hand, oxidation of neutral complex **94** in dry CH$_2$Cl$_2$ with ferrocenium hexafluorophosphate [Fc]PF$_6$ (1:1) produces the ionic complex [Cu^{II}(IBQ-ISQ^{L12})]$^+$(PF$_6$)$^-$ (**96**). The oxidation of **94** with the stronger one-electron oxidant [Ni^{III}(tacn)$_2$](ClO$_4$)$_3$ (where tacn is 1,4,7-triazacyclononane) in molar ratio 1:2 generates another ionic complex [Cu(IBQ-IBQ^{L12})]$^{2+}$(ClO$_4$$^-$)$_2$ (**97**) [116]. Complexes **94**, **95** and **97** exhibit temperature-independent magnetic

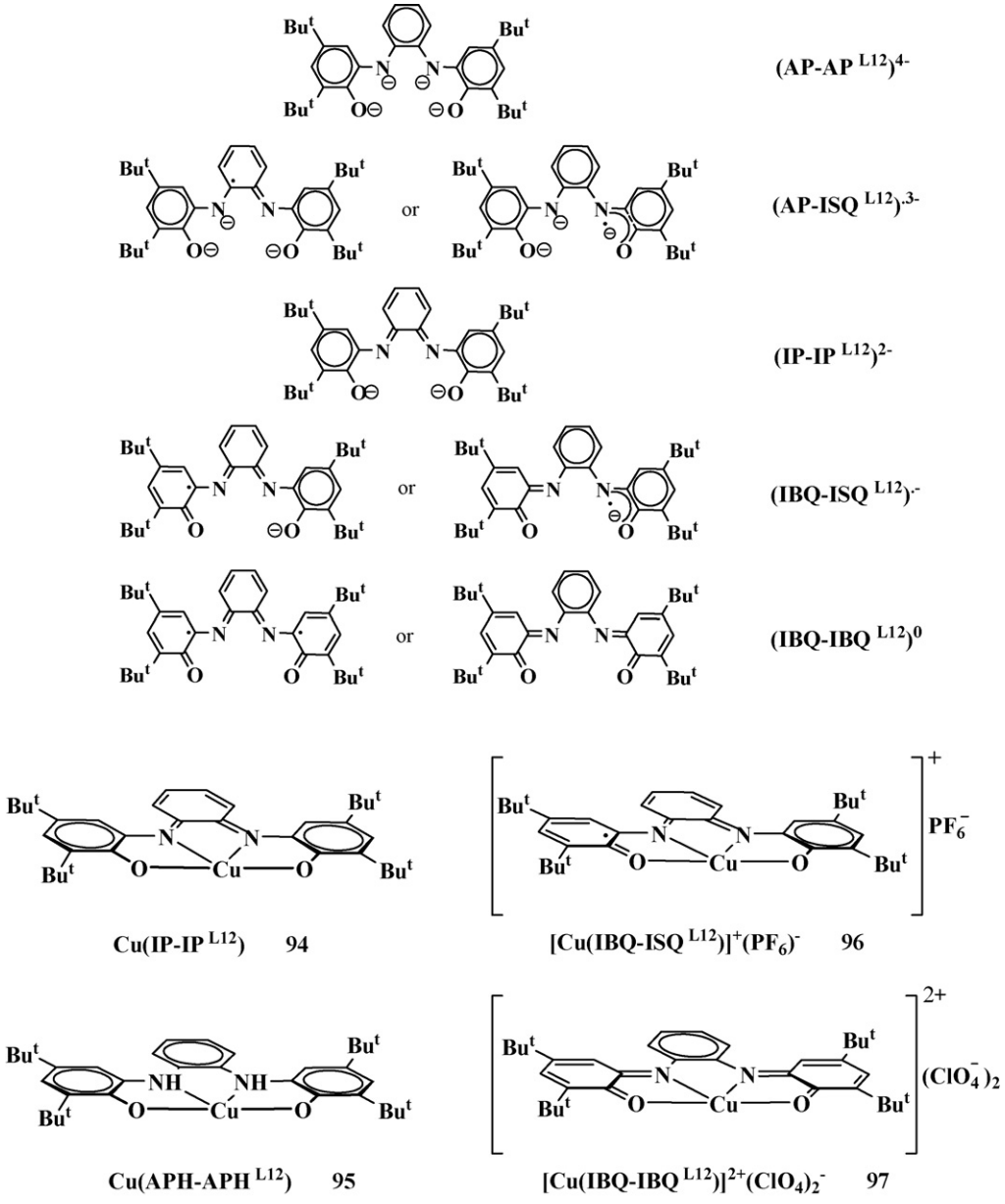

Scheme 23. Ligands derived from APH_2-APH_2^{L12} and its copper complexes **94–97** [116].

moments typical for a copper(II) ion, d^9, with diamagnetic ligands (Table S6). On the other hand, complex $[Cu^{II}(IBQ\text{-}ISQ^{L12})]^+(PF_6)^-$ (**96**) has a temperature-dependent magnetic moment μ_{eff} of 0.45 μ_B at 5 K and 2.4 μ_B at 290 K. Modeling the temperature dependence reveals the antiferromagnetic coupling constant $J = -48.5\ cm^{-1}$ [116]. Resulting ground state of **96** is $S = 0$. The EPR spectrum of **96** at 50 K in CH_2Cl_2 appears at $g = 2.0$ with a typical half-field signal of an $S = 1$ system with $g = 4.0$. Decreasing temperature leads to the disappearance of the latter signal (with $g = 4.0$). Based on the analysis of temperature dependence of $\Delta m_s = 2$ transition in a half field in EPR (from this temperature dependence, an antiferromagnetic coupling constant $J = -7\ cm^{-1}$ was evaluated) the authors suggested that this coupling constant J does not represent intramolecular spin exchange between the organic radical and the Cu^{II} because coupling is inter- rather than intramolecular in nature. However, stronger intermolecular than intramolecular exchange seems unlikely. The magnetic behavior may be rationalized by the usual copper(II)-ISQ coupling process and the occupancy of an excited state with higher spin multiplicity ($S = 1$).

Complexes **94**, **95** and **97** display EPR spectra typical for square planar Cu(II) complexes with copper hyperfine structure [116].

An unusual vanadium(V) complex with the pentadentate ligand APH_2-NH-APH_2^{L13}, containing two *o*-iminoquinonato fragments has been reported in [7]. Diamagnetic complex $[V^VO\{(APH)\text{-}NH\text{-}(AP)\}^{L13}]$ (**98**) was prepared by the reaction of APH_2-NH-APH_2^{L13} with vanadyl salt $[NEt_4][VOBr_4]$ in acetonitrile solution in the presence of Et_3N. Vanadium has a distorted octahedral environment, V = O bond length is 1.65 Å, one of O,N-coordinated fragments contains protonated nitrogen atom (APH) (Scheme 24).

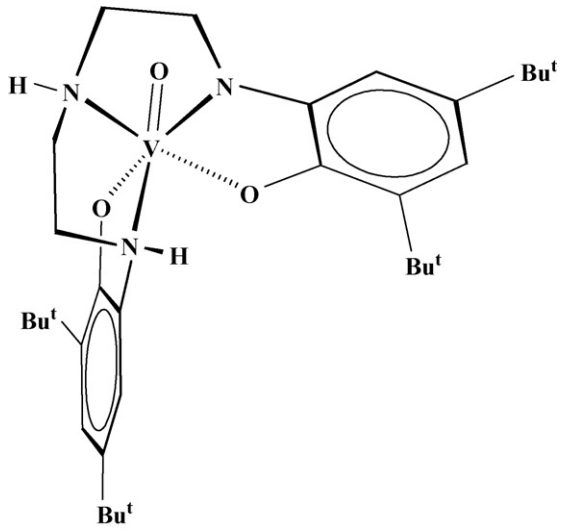

Scheme 24. Vanadium complex [$V^{V}O\{(APH)\text{-}NH\text{-}(AP)\}^{L13}$] (**98**) [7].

A number of bis-*o*-iminobenzosemiquinonato nickel, palladium and copper complexes (Scheme 25) derived from the tetradentate ligands $APH_2\text{-}APH_2^{L14}$ and $APH_2\text{-}APH_2^{L15}$ are reported in ref. [117]. Nickel(II) complexes $Ni(APH_2\text{-}APH^{L14})_2$ (**99**) and $Ni(IP\text{-}IPH^{L14})_2$ (**100**) reveal a distorted octahedral environment of nickel(II) bound with two tridentate ligands, namely O,N,N′-coordinated *o*-aminophenol-*o*-aminophenolate $(APH_2\text{-}APH^{L14})^{-}$ and *o*-iminophenol-*o*-iminophenolate $(IP\text{-}IPH^{L14})^{-}$ monoanions correspondingly. Both complexes are paramagnetic with an $S = 1$ ground state (Table S6).

The diamagnetic nickel(II) and palladium(II) derivatives, complexes **101** and **102**, contain the organic ligand in the form $ISQ\text{-}ISQ^{L15}$ where the two components are radical–anions *o*-iminobenzosemiquinones [117]. The copper complex **103** has also been prepared containing the *o*-iminophenolate-*o*-iminophenolate dianion $(IP\text{-}IP^{L15})^{2-}$ – the oxidized diimine derivative of $APH_2\text{-}APH_2^{L15}$. Central atoms in **101** and **102** are in square-planar environment while copper(II) in **103** was additionally coordinated with a water molecule.

The palladium complex **104** is a dimer due to four N–H···O hydrogen bonds between two tetradentate *o*-aminophenolate-*o*-aminophenolate $(APH\text{-}APH^{L15})^{2-}$ ligands (Scheme 25). The intramolecular Pd–Pd distance is 3.0846(4) Å. The two ligand halves are clearly aromatic and two nitrogen atoms are sp^3 hybridized in the dimer **104**. The geometrical features are the same with those of O,N-coordinated APH^{L1} ligands in, for instance, $[Mn^{III}(APH^{L1})(ISQ^{L1})_2]$ [92].

Turning back to the ligand derived from APH_2^{L10}, there is a diamagnetic, binuclear cobalt complex $Co_2(NCS)_2(AP^{L10})_2(AQ)$ (**105**) (Scheme 26) [104] where AQ is 8-aminoquinoline. The *o*-amidophenolate dianion ligands $(AP^{L10})^{2-}$ bridge between two cobalt(III) centers. The authors were not able to report a rational synthetic path to **105**. This complex was obtained as a byproduct (with 2% yield) of another complex with the APH_2^{L10} ligand

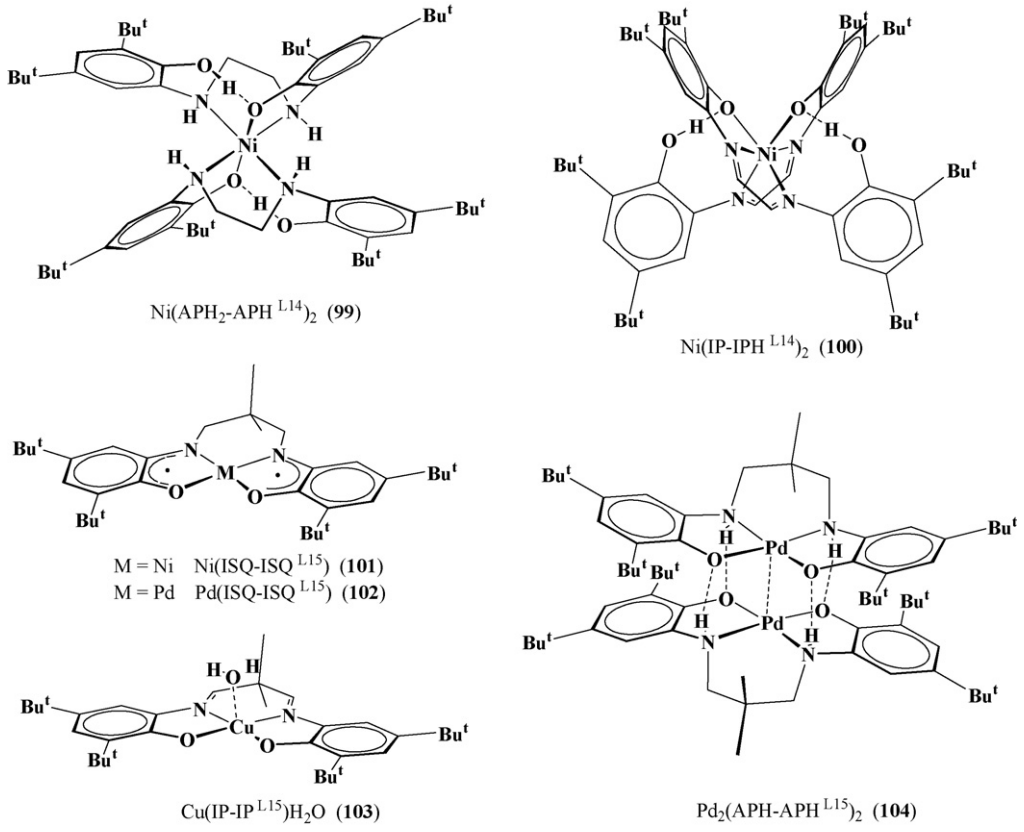

Scheme 25. Structures of nickel, palladium and copper complexes of tetradentate ligands derived from $APH_2\text{-}APH_2^{L14}$ and $APH_2\text{-}APH_2^{L15}$ [117].

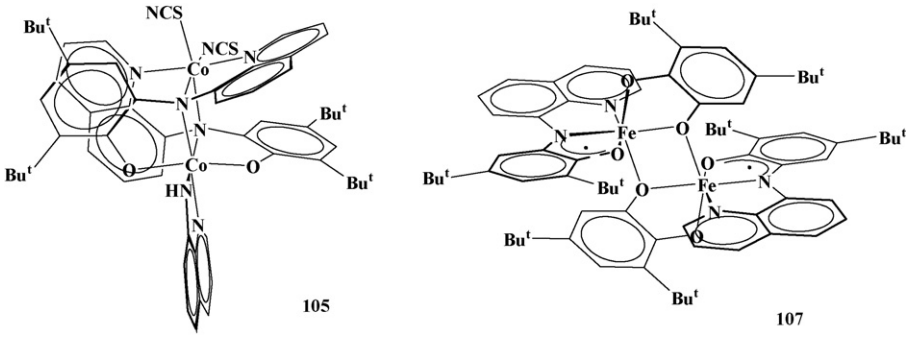

Scheme 26. Dinuclear complexes $Co_2(NCS)_2(AP^{L10})_2(AQ)$ (**105**) and $[Fe(ISQ^{L10})(3,5\text{-DBCat})]_2$ (**107**) [104].

–$K[Co^{II}(ISQ^{L10})(IBQ^{L10})](NCS)_2$ (**106**) – by the reaction of KSCN, $Co(ClO_4)_2{\cdot}6H_2O$, ligand $APH_2{}^{L10}$ (5:1:1) in the presence of air and an excess Et_3N. 8-Aminoquinoline, AQ, is present as a ~2% impurity in the starting ligand $APH_2{}^{L10}$ [104]. The cobalt complex **106** contains ligands in different oxidation states (one is a radical–anion *o*-iminobenzosemiquinone ISQ^{L10} and the other is a neutral *o*-iminobenzoquinone IBQ^{L10}) according to magnetic data. Complex **106** possesses an $S = 1$ ground state resulting from a strong antiferromagnetic exchange between the high-spin cobalt(II) (d^7, $S_{Co} = 3/2$) and a radical ligand.

The interesting dinuclear iron complex $[Fe(ISQ^{L10})(3,5\text{-DBCat})]_2$ (**107**) consists of two moieties $Fe^{III}(ISQ)(Cat)$, where iron(III) is bound with the radical–anion *o*-iminobenzosemiquinone, ISQ^{L10}, and dianion 3,5-di-*tert*-butyl-catecholate, 3,5-DBCat (Scheme 26). The isomer shift $\delta = 0.51\,mm\,s^{-1}$ and Mössbauer quadrupole splitting $\Delta E_Q = 0.99\,mm\,s^{-1}$ for **107** are typical for an octahedral high-spin Fe(III) ion [104].

The insertion of $–CH_2OH$ group (group with a potential valence) into the 2-position of *N*-phenyl in $APH_2{}^{L1}$ results in a new redox-active ligand $APH_2(CH_2OH)^{L16}$ (Scheme 27) [118]. An unique trinuclear manganese complex $[Mn^{II}Mn^{III}M^{IV}(AP(CH_2O^-)^{L16})(ISQ(CH_2O^-)L^{16})_2(IBQ(CH_2O^-)L^{16})Cl]$ (**108**) containing manganese(II), manganese(III) and manganese(IV) was prepared by the reaction of $MnCl_2$ with ligand $APH_3{}^{L16}$ in 1:1 molar ratio. The X-ray structure of **108** clearly shows the oxidation levels of the central metals. In Scheme 27, pentacoordinate Mn(1) is Mn(III), Mn(2) is Mn(II) and Mn(3) is Mn(IV). Manganese atoms are connected to each other by two μ-alkoxo ($–CH_2OH$) groups. High-spin manganese(IV) (Mn(3) in Scheme 27) is bound

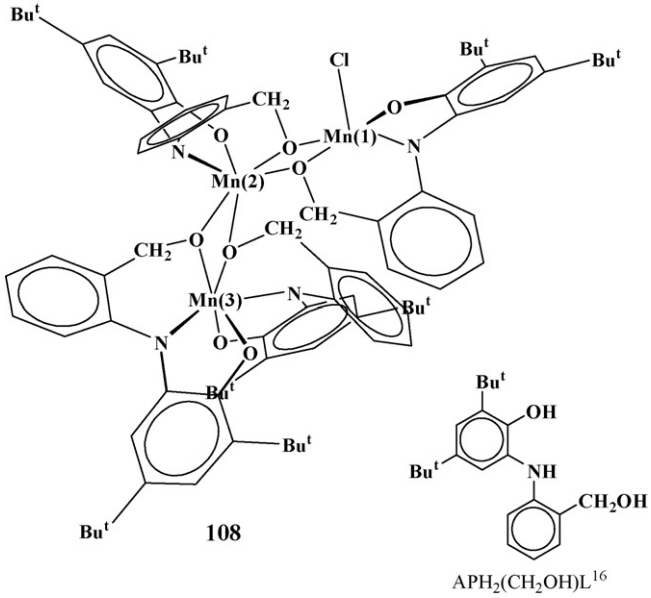

Scheme 27. Trinuclear manganese complex $[Mn^{II}Mn^{III}M^{IV}(AP(CH_2O^-)^{L16})(ISQ(CH_2O^-)L^{16})_2(IBQ(CH_2O^-)L^{16})Cl]$ (**108**) [118].

with *o*-amidophenolate and *o*-iminobenzosemiquinone in an octahedral fashion. The coordination environment of high-spin manganese(II), Mn(2), consists of the O,N-coordinated *o*-iminobenzoquinone ligand IBQ and four μ-alkoxo groups. Square–pyramidal geometry of high-spin manganese(III), Mn(1), is formed by radical–anion *o*-iminobenzosemiquinone and two μ-alkoxo bridges in the base of pyramid and chloride ion in apical position. The effective magnetic moment increases from 5.8 μ_B at 2 K to a maximum of 8.48 μ_B at 10 K and then it slowly decreases to 7.6 μ_B at 300 K. Authors have

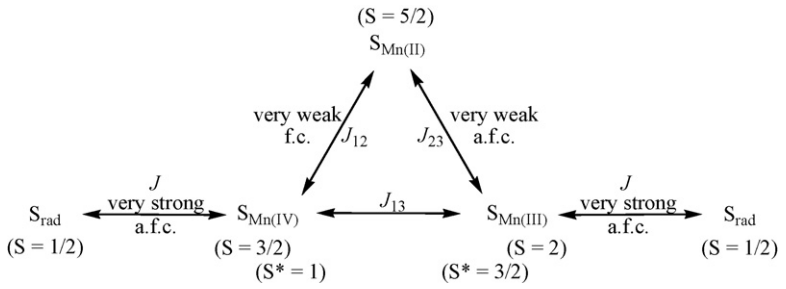

Chart 11. The qualitative scheme of magnetic coupling in trinuclear manganese complex **108**.

proposed that the magnetic exchange manganese(III)–ISQ and manganese(IV)–ISQ interactions have a strong antiferromagnetic nature ($-J > 200$–$300\,cm^{-1}$) leading to effective spin states $S^* = 1$ for the high-spin Mn(IV)-center and $S^* = 3/2$ for high-spin Mn(III) center (see Chart 11). The simulation of magnetic data (variable-temperature magnetic susceptibility measurements and variable-temperature variable-field magnetization measurements) gave the exchange parameters $J_{12} = 2.6$–$2.7\,cm^{-1}$, $J_{23} = -(0.1$–$0.3)\ cm^{-1}$, $g_1 = g_2 = g_3 = 2.05$ and D (for Mn(III)) $= 8.0\,cm^{-1}$.

8. Some conclusions

At the present time the chemistry of *o*-semiquinonato and related transition metal complexes forms an independent field of research and has many interesting aspects. One of them is represented by their unique magnetic properties. Because of the possibility of designing of a hetero-spin multicenter system where the magnetic centers are the metal ions and radical *o*-semiquinones and related ligands, interest in the investigation of such complexes has greatly increased. Remarkable contributions to modeling and directed synthesis of high- and low-spin molecules, and investigation of their physical properties was made by the scientific groups of A.L. Balch; F. Brito; R.M. Buchanan and C.W. Lange; A. Dei and D. Gatteschi; D.N. Hendrickson and M.W. Lynch; W. Kaim; A.B.P. Lever; J.K. McCusker; C.G. Pierpont, A. I. Prokof'ev, N.N. Bubnov and S.P. Solodovnikov; D.A. Shultz; K. Wieghardt; M.D. Ward.

A large number of *o*-iminobenzoquinonato type complexes have been synthesized and their structural features and magnetic properties have been investigated in detail. Thus far, it has been shown that the type of magnetic exchange interactions in *o*-iminobenzosemiquinonato complexes is very strictly determined by the molecular structure which determines the symmetry and relative position (and the overlap integral and the resonance integral, consequently) of interacting MOs of unpaired electrons, and by electronic structure of compounds which determines the electron and spin state of central metal and ligands.

o-Iminobenzoquinonate ligands are non-innocent in complexes formed from the viewpoint of their structural as well as magnetic properties. Bidentate *N*-phenyl-substituted *o*-iminobenzoquinonates form structural analogues of *o*-quinolates in most cases. The growth of steric shielding near the central metal atom leads to significant structural changes and consequently results in the appearance of remarkable magnetochemical features. The presence of an additional donor neutral group or a group with potential valence (in three-, tetra-, pentadentate ligands etc.) can be the cause of di-, three- and polynuclear complex formation. The more pronounced covalent character of metal-to-nitrogen bond in comparison with metal-to-oxygen bond gives rise to an increased ferro/antiferromagnetic exchange interaction between the magnetic centers of *o*-iminobenzoquinonato complexes. Different channels of exchange interactions appear depending on the nature and the oxidation level of a central metal atom(s) and ligands.

Thus, the many structural features and coordination capabilities of the *o*-iminobenzoquinonato ligands allow one to design a wide variety of complexes with interesting, rare and in some cases unique structural and magnetic properties. Sometimes magneto-structural correlations in *o*-iminosemiquinonato and *o*-semiquinonato complexes are strict and obvious to such an extent that Oliver Kahn has defined these ligands as "visual teaching" in one of his works [119].

o-Iminobenzoquinonato type complexes can serve as modeling objects and structural units in the design of molecular and supramolecular magnetic devices. On the other hand, many transition metal complexes with *o*-iminobenzoquinonato type ligands are active in different catalytic processes (this aspect is the subject of another special review), and to have potential relevance to biochemical processes modeling biochemical systems. Furthermore, *o*-iminobenzoquinonato complexes can be applied in the field of small molecule fixation/activation. The next decade of research will be likely connected with the application of known and new complexes to these prospective areas.

Acknowledgement

We would like to thank the President of the Russian Federation (grant MK-3523.2007.3) and Russian Science Support Foundation for financial support of this work.

Appendix A. Supplementary data

Supplementary data associated with this article can be found, in the online version, at doi:10.1016/j.ccr.2008.02.004.

References

[1] C.G. Pierpont, Coord. Chem. Rev. 219–221 (2001) 415.
[2] C.G. Pierpont, Coord. Chem. Rev. 216–217 (2001) 99.
[3] C. Roux, D.M. Adams, J.P. Itie, A. Polian, D.N. Hendrickson, M. Verdaguer, Inorg. Chem. 35 (1996) 2846.
[4] M.W. Lynch, R.M. Buchanan, C.G. Pierpont, D.N. Hendrickson, Inorg. Chem. 20 (1981) 1038.
[5] M.W. Lynch, D.N. Hendrickson, B.J. Fitzgerald, C.G. Pierpont, J. Am. Chem. Soc. 106 (1984) 2041.
[6] P. Chaudhuri, C.N. Verani, E. Bill, E. Bothe, T. Weyhermüller, K. Wieghardt, J. Am. Chem. Soc. 123 (2001) 2213.
[7] H. Chun, C.N. Verani, P. Chaudhuri, E. Bothe, E. Bill, T. Weyhermüller, K. Wieghardt, Inorg. Chem. 40 (2001) 4157.
[8] A.Y. Girgis, Y.S. Sohn, A.L. Balch, Inorg. Chem. 14 (1975) 2327.
[9] A. Mederos, S. Dominguez, R. Hernandez-Molina, J. Sanchiz, F. Brito, Coord. Chem. Rev. 193–195 (1999) 913.
[10] S. Ghumaan, B. Sarkar, S. Patra, J. van Slageren, J. Fiedler, W. Kaim, G.K. Lahiri, Inorg. Chem. 44 (2005) 3210.
[11] S. Ye, B. Sarkar, C. Duboc, J. Fiedler, W. Kaim, Inorg. Chem. 44 (2005) 2843.
[12] W. Kaim, Dalton Trans. (2003) 761.
[13] A.M. Barthram, Z.R. Reeves, J.C. Jeffery, M.D. Ward, J. Chem. Soc. Dalton Trans. (2000) 3162.
[14] A.K. Ghosh, S.-M. Peng, R.L. Paul, M.D. Ward, S. Goswami, J. Chem. Soc. Dalton Trans. (2001) 336.
[15] A.B.P. Lever, P.R. Auburn, E.S. Dodsworth, Haga Masa-aki, W. Liu, M. Melnik, W.A. Nevin, J. Am. Chem. Soc. 110 (1988) 8076.
[16] H. Masui, A.B.P. Lever, P.R. Auburn, Inorg. Chem. 30 (1991) 2402.

[17] J. Rusanova, E. Rusanov, S.I. Gorelsky, D. Christendat, R. Popescu, A.A. Farah, R. Beaulac, C. Reber, A.B.P. Lever, Inorg. Chem. 45 (2006) 6246.
[18] G.A. Abakumov, V.I. Nevodchikov, Dokl. Akad. Nauk SSSR 266 (1982) 1407.
[19] G.A. Abakumov, V.K. Cherkasov, M.P. Bubnov, O.G. Ellert, Z.B. Dobrokhotova, L.N. Zakharov, Y.T. Struchkov, Dokl. Akad. Nauk 328 (1993) 12.
[20] A. Caneschi, A. Dei, H. Lee, D.A. Shultz, L. Sorace, Inorg. Chem. 40 (2001) 408.
[21] A. Caneschi, A. Dei, C.P. Mussari, D.A. Shultz, L. Sorace, K.E. Vostrikova, Inorg. Chem. 41 (2002) 1086.
[22] J.H. Rodriguez, D.E. Wheeler, J.K. McCusker, J. Am. Chem. Soc. 120 (1998) 12051.
[23] D.E. Wheeler, J.K. McCusker, Inorg. Chem. 37 (1998) 2296.
[24] D.E. Wheeler, J.H. Rodriguez, J.K. McCusker, J. Phys. Chem. A 103 (1999) 4101.
[25] J.A. McCleverty, Prog. Inorg. Chem. 10 (1968) 49.
[26] S.-I. Ohnishi, H.M. McConnell, J. Am. Chem. Soc. 87 (1965) 2293.
[27] V.I. Nevodchikov, G.A. Abakumov, V.K. Cherkasov, G.A. Razuvaev, J. Organomet. Chem. 214 (1981) 119.
[28] G.A. Razuvaev, V.K. Cherkasov, G.A. Abakumov, J. Organomet. Chem. 160 (1978) 361.
[29] W. Kaim, M. Wanner, A. Knodler, S. Zalis, Inorg. Chim. Acta 337 (2002) 163.
[30] J. Rall, M. Wanner, M. Albrecht, F.M. Hornung, W. Kaim, Chem. Eur. J. 5 (1999) 2802.
[31] A. Rockenbauer, M. Gyor, G. Speier, Z. Tueklar, Inorg. Chem. 26 (1987) 3293.
[32] C.G. Pierpont, R.M. Buchanan, Coord. Chem. Rev. 38 (1981) 45.
[33] C.G. Pierpont, H.H. Downs, Inorg. Chem. 16 (1977) 2970.
[34] K.S. Min, T. Weyhermüller, K. Wieghardt, J. Chem. Soc. Dalton Trans. (2003) 1126.
[35] X. Sun, H. Chun, K. Hildenbrand, E. Bothe, T. Weyhermüller, F. Neese, K. Wieghardt, Inorg. Chem. 41 (2002) 4295.
[36] S.-L. Kokatam, P. Chaudhuri, T. Weyhermüller, K. Wieghardt, Dalton Trans. (2007) 373.
[37] F.F. De Biani, A. Dei, C. Sangregoriob, L. Soraceb, Dalton Trans. (2005) 3868.
[38] A.I. Poddel'sky, G.A. Abakumov, M.P. Bubnov, V.K. Cherkasov, L.G. Abakumova, Russ. Chem. Bull. Int. Ed. 53 (2004) 1189.
[39] A.I. Poddel'sky, V.K. Cherkasov, M.P. Bubnov, L.G. Abakumova, G.A. Abakumov, J. Organomet. Chem. 690 (2005) 145.
[40] K.N. Mitra, S.-M. Peng, S. Goswami, Chem. Commun. (1998) 1685.
[41] R.B. Salmonsen, A. Abelleira, M.J. Clarke, Inorg. Chem. 23 (1984) 387.
[42] S. Patra, B. Sarkar, S.M. Mobin, W. Kaim, G.K. Lahiri, Inorg. Chem. 42 (2003) 6469.
[43] M. Haga, E.S. Dodsworth, A.B.P. Lever, Inorg. Chem. 25 (1986) 447.
[44] E. Waldhor, B. Schwederski, W. Kaim, J. Chem. Soc. Perkin Trans. 2 (1993) 2109.
[45] S. Ernst, P. Hanel, J. Jordanov, W. Kaim, V. Kasack, E. Roth, J. Am. Chem. Soc. 111 (1989) 1733.
[46] S. Ernst, V. Kasack, C. Bessenbacher, W. Kaim, Z. Naturforsch. 42b (1987) 425.
[47] S.I. Gorelsky, E.S. Dodsworth, A.B.P. Lever, A.A. Vlcek, Coord. Chem. Rev. 174 (1998) 469.
[48] A.B.P. Lever, S.I. Gorelsky, Coord. Chem. Rev. 208 (2000) 153.
[49] C. Remenyi, M. Kaupp, J. Am. Chem. Soc. 127 (2005) 11399.
[50] M. Ebadi, A.B.P. Lever, Inorg. Chem. 38 (1999) 467 (and references therein).
[51] M. Haga, K. Isobe, S.R. Boone, C.G. Pierpont, Inorg. Chem. 29 (1990) 3795.
[52] K. Majumder, S.-M. Peng, S. Bhattacharya, J. Chem. Soc. Dalton Trans. (2001) 284.
[53] A.I. Poddel'sky, V.K. Cherkasov, G.K. Fukin, M.P. Bubnov, L.G. Abakumova, G.A. Abakumov, Inorg. Chim. Acta 357 (2004) 3632.
[54] D. Herebian, P. Ghosh, H. Chun, E. Bothe, T. Weyhermüller, K. Wieghardt, Eur. J. Inorg. Chem. (2002) 1957.
[55] G.A. Abakumov, V.K. Cherkasov, M.P. Bubnov, L.G. Abakumova, V.N. Ikorskii, G.V. Romanenko, A.I. Poddel'sky, Rus. Chem. Bull. 55 (2006) 44.
[56] H. Chun, T. Weyhermüller, E. Bill, K. Wieghardt, Angew. Chem. 113 (2001) 2552.
[57] H. Chun, E. Bill, T. Weyhermüller, K. Wieghardt, Inorg. Chem. 42 (2003) 5612.
[58] S. Mukherjee, T. Weyhermüller, K. Wieghardt, P. Chaudhuri, Dalton Trans. (2003) 3483.
[59] G.A. Abakumov, V.K. Cherkasov, A.I. Poddel'sky, M.P. Bubnov, L.G. Abakumova, G.K. Fukin, Dokl. Chem. 399 (2004) 207.
[60] E. Bill, E. Bothe, P. Chaudhuri, K. Chlopek, D. Herebian, S. Kokatam, K. Ray, T. Weyhermüller, F. Neese, K. Wieghardt, Chem. Eur. J. 11 (2005) 204.
[61] G.A. Abakumov, A.I. Poddel'sky, M.P. Bubnov, G.K. Fukin, L.G. Abakumova, V.N. Ikorskii, V.K. Cherkasov, Inorg. Chim. Acta 358 (2005) 3829.
[62] S. Kokatam, T. Weyhermüller, E. Bothe, P. Chaudhuri, K. Wieghardt, Inorg. Chem. 44 (2005) 3709.
[63] K.J. Blackmore, J.W. Ziller, A.F. Heyduk, Inorg. Chem. 44 (2005) 5559.
[64] M.R. Haneline, A.F. Heyduk, J. Am. Chem. Soc. 128 (2006) 8410.
[65] C.N. Verani, S. Gallert, E. Bill, T. Weyhermüller, K. Wieghardt, P. Chaudhuri, Chem. Commun. (1999) 1747.
[66] S. Mukherjee, T. Weyhermüller, E. Bill, K. Wieghardt, P. Chaudhuri, Inorg. Chem. 44 (2005) 7099.
[67] R.M. Buchanan, B.J. Fitzgerald, C.G. Pierpont, Inorg. Chem. 18 (1979) 3439.
[68] S. Mukherjee, T. Weyhermüller, E. Bothe, K. Wieghardt, P. Chaudhuri, Dalton Trans. (2004) 3842.
[69] G.A. Abakumov, V.K. Cherkasov, M.P. Bubnov, O.G. Ellert, Y.V. Rakitin, L.N. Zakharov, Y.T. Struchkov, Y.N. Saf'yanov, Bull. Russ. Acad. Sci. 41 (1992) 1813 (Translated from: Izv. Akad. Nauk Ser. Khim. 10 (1992) 2315).
[70] D. Herebian, K.E. Wieghardt, F. Neese, J. Am. Chem. Soc. 125 (2003) 10997.
[71] K. Ray, A. Begum, T. Weyhermuller, S. Piligkos, J. van Slageren, F. Neese, K. Wieghardt, J. Am. Chem. Soc. 127 (2005) 4403.
[72] D. Herebian, E. Bothe, F. Neese, T. Weyhermüller, K. Wieghardt, J. Am. Chem. Soc. 125 (2003) 9116.
[73] K. Ray, F. Neese, K. Wieghardt, Inorg. Chem. 44 (2005) 5345.
[74] H.-C. Chand, H. Myasaka, S. Kitagawa, Inorg. Chem. 40 (2001) 146.
[75] C. Benelli, A. Dei, D. Gatteschi, L. Pardi, Inorg. Chem. 27 (1988) 2831.
[76] C.G. Pierpont, C.W. Lange, Inorg. Chim. Acta 263 (1997) 219.
[77] J.S. Thompson, J.C. Calabrese, J. Am. Chem. Soc. 108 (1986) 1903.
[78] S. Ye, B. Sarkar, F. Lissner, T. Schleid, J. van Slageren, J. Fiedler, W. Kaim, Angew. Chem., Int. Ed. 44 (2005) 2103.
[79] O. Kahn, R. Prins, J. Peerdijk, J.S. Thompson, Inorg. Chem. 26 (1987) 3557.
[80] C.W. Lange, B.J. Couklin, C.G. Pierpont, Inorg. Chem. 33 (1994) 1276.
[81] V. Bachler, G. Olbrich, F. Neese, K. Wieghardt, Inorg. Chem. 41 (2002) 4179.
[82] R.M. Buchanan, S.C. Kessel, H.H. Downs, C.G. Pierpont, D.N. Hendrickson, J. Am. Chem. Soc. 100 (1978) 7894.
[83] S.R. Boone, G.H. Purser, H.-R. Chang, M.D. Lowery, D.N. Hendrickson, C.G. Pierpont, J. Am. Chem. Soc. 111 (1989) 2292.
[84] A.B.P. Lever, Inorganic Electronic Spectroscopy, 2nd ed., Elsevier, Amsterdam, 1984.
[85] C. Benelli, A. Dei, D. Catteschi, H.U. Giidel, L. Pardi, Inorg. Chem. 28 (1989) 3089.
[86] C.G. Pierpont, H.H. Downs, T.G. Rukavina, J. Am. Chem. Soc. 96 (1974) 5573.
[87] S.R. Sofen, D.C. Ware, S.R. Cooper, K.N. Raymond, Inorg. Chem. 18 (1979) 234.
[88] C.G. Pierpont, H.H. Downs, J. Am. Chem. Soc. 98 (1976) 4834.
[89] C.G. Pierpont, H.H. Downs, J. Am. Chem. Soc. 97 (1975) 2123.
[90] R.M. Buchanan, H.H. Downs, W.B. Shorthill, C.G. Pierpont, S.L. Kessel, D.N. Hendrickson, J. Am. Chem. Soc. 100 (1978) 4318.
[91] D.J. Gordon, R.F. Fenske, Inorg. Chem. 21 (1982) 2907.

[92] H. Chun, P. Chaudhuri, T. Weyhermüller, K. Wieghardt, Inorg. Chem. 41 (2002) 790.
[93] A.S. Attia, C.G. Pierpont, Inorg. Chem. 37 (1998) 3051.
[94] T. Weyhermüller, T.R. Paine, E. Bothe, E. Bill, P. Chaudhuri, Inorg. Chim. Acta 337 (2002) 344.
[95] A.S. Attia, C.G. Pierpont, Inorg. Chem. 34 (1995) 1172.
[96] E. Konig, Z. Naturforsch. A 19 (1964) 1139.
[97] J.A. McCleverty, Prog. Inorg. Chem. 32 (1970) 601.
[98] K.N. Raymond, S.S. Isied, L.D. Brown, F.R. Fronczek, J.H. Nibert, J. Am. Chem. Soc. 98 (1978) 1767.
[99] P.R. Shukla, J. Inorg. Nucl. Chem. 27 (1967) 1800.
[100] H.F. Bauer, W.C. Drinkard, J. Am. Chem. Soc. 82 (1960) 5031.
[101] G.W. Watt, J.F. Knifton, Inorg. Chem. 7 (1968) 1443.
[102] M. Ghedini, G. Dolcetti, B. Giovannitti, Trans. Metal. Chem. 4 (1979) 49.
[103] J.M. Clemente, C. Wong, P. Bhattacharyya, A.M.Z. Slawin, D.J. Williams, J.D. Woollins, Polyhedron 13 (1994) 261.
[104] K.S. Min, T. Weyhermüller, K. Wieghardt, Dalton Trans. (2004) 178.
[105] A.Y. Girgis, A.L. Balch, Inorg. Chem. 14 (1975) 2724.
[106] S.K. Larsen, C.G. Pierpont, J. Am. Chem. Soc. 110 (1988) 1827.
[107] C.L. Simpson, S.R. Boone, C.G. Pierpont, Inorg. Chem. 28 (1989) 4379.
[108] S. Bruni, A. Caneschi, F. Cariati, C. Delfs, A. Dei, D. Gatteschi, J. Am. Chem. Soc. 116 (1994) 1388.
[109] C.G. Pierpont, S.K. Larsen, S.R. Boone, Pure Appl. Chem. 60 (1988) 1331.
[110] G. Swamabala, M.V. Rajasekharan, S. Padhye, Chem. Phys. Lett. 267 (1997) 539.
[111] A. Caneschi, A. Cornia, A. Dei, Inorg. Chem. 37 (1998) 3419.
[112] D. Ruiz-Molina, J. Veciana, K. Wurst, D.N. Hendrickson, C. Rovira, Inorg. Chem. 39 (2000) 617.
[113] O. Cador, F. Chabre, A. Dei, C. Sangregorio, J. Van Slageren, M.G.F. Vaz, Inorg. Chem. 42 (2003) 6432.
[114] S. Mukherjee, E. Rentschler, T. Weyhermüller, K. Wieghardt, P. Chaudhuri, Chem. Comm. (2003) 1828.
[115] A. Dei, D. Gatteschi, C. Sangregorio, L. Sorace, M.G.F. Vaz, Inorg. Chem. 42 (2003) 1701.
[116] P. Chaudhuri, M. Hess, J. Muller, K. Hildenbrand, E. Bill, T. Weyhermüller, K. Wieghardt, J. Am. Chem. Soc. 121 (1999) 9599.
[117] Min Kil Sik, T. Weyhermüller, E. Bothe, K. Wieghardt, Inorg. Chem. 43 (2004) 2922.
[118] C. Mukherjee, T. Weyhermüller, K. Wieghardt, P. Chaudhuri, Dalton Trans. (2006) 2169.
[119] O. Kahn, Angew. Chem. Int. Ed. 24 (1985) 834.